STIMULATION AND RESERVOIR ENGINEERING OF GEOTHERMAL RESOURCES

Paul Kruger and Henry J. Ramey, Jr.
Co-Principal Investigators
Stanford University
Stanford, California

Progress Report No. 3

June, 1974

Grant No. GI-34925

to

Division of Advanced Energy Research and Technology
National Science Foundation
Washington, D.C.

TABLE OF CONTENTS

LIST OF TABLES

LIST OF FIGURES

INTRODUCTION

The Stanford University research program on the study of stimulation and reservoir engineering of geothermal resources commenced as an interdisciplinary program i.n September, 1972. The broad objectives of this program have been:

(1) the development of experimental and computational data to evaluate the optimum performance of fracture-stimulated geothermal reservoirs;

(2) the development of a geothermal reservoir model to evaluate important thermophysical, hydrodynamic, and chemical parameters based on fluid-energy-volume balances as part of standard reservoir engineering practice; and

(3) the construction of a laboratory model of an explosion-produced chimney to obtain experimental data on the processes of in-place boiling, moving flash fronts, and two-phase flow in porous and fractured hydrothermal reservoirs.

The project was initiated as a joint program between the Civil Engineering Department of the School of Engineering and the Petroleum Engineering Department of the School of Earth Sciences. During the present year, assistance was provided by the Mechanical Engineering Department of the School of Engineering. Personnel associated with the project who have contributed to the preparation of this progress report are:

Prof. Paul Kruger, Civil Engr. Dept., Co-Principal Investigator

Prof. Henry J. Ramey, Jr., Petroleum Engr. Dept., Co-Principal Investigator

Prof. William E. Brigham, Petroleum Engr. Dept., Faculty Associate

Prof. A. Louis London, Mechanical Engr. Dept., Faculty Associate

Mr. Norio Arihara,, Petroleum Engr. Dept. , Research Assistant

Mr. Paul Atkinson, Petroleum Engr. Dept., Research Assistant

Mr. Francis J. Casse, Petroleum Engr. Dept. , Research Assistant

Mr. Hsiu-Kuo Chen, Petroleum Engr. Dept., Research Assistant

Mr. Stephen D. Chicoine, Petroleum Engr. Dept., Research Assistant

Mr. Anstein Hunsbedt, Civil Engr. Dept., Research Assistant
Mr. James A. Liburdy, Civil Engr. Dept., Research Assistant
Mr. M.-C. Tom Kuo, Civil Engr. Dept., Research Assistant
Mr. Alan K. Stoker, Civil Engr. Dept,, Research Assistant

During the current annual period, rapid development of several aspects of the research program occurred simultaneously (in keeping with the objectives of the RANN program of the National Science Foundation) to bring research results to the attention of potential users. A Project Review Presentation to participants from industry, university, and government agencies was held during May 1974. Much of the results given in this progress report were described at: that meeting.

During the current annual period, both the geothermal chimney model and the two-phase boiling model were essentially completed and placed into operation. Also completed was a feasibility study of the potential of naturally-occurring radon as a tracer for reservoir characteristics. Experiments are being initiated in several related aspects of mass and heat transfer in fractured rock, and in-place boiling in porous media. Continued effort is underway in the development of the mathematical simulation model of geothermal reservoirs. These developments are described in this progress report. The several experiments that comprise the objectives of this interdisciplinary research program are being developed in parallel to accelerate the assimilation of the results into the emerging geothermal energy industry.

THE GEOTHERMAL CHIMNEY MODEL

Current Design of the Chimney Model

A description of the geothermal chimney model and an analysis of the design requirements for the major components were discussed in Progress Report No. 1. The major test objectives of the model were also described in Progress Report No. 1. In summary the model was designed to investigate the effectiveness of fracture stimulation of geothermal reservoirs to increase the extraction efficiency of geothermal energy. Experimental data are being obtained on the processes of in-place boiling, moving flash fronts, and two-phase flow in porous and fractured hydrothermal media. The general problems being examined include: (1) conditions for optimum energy extraction, (2) methods of cyclic and continuous recharge, (3) determination of heat transfer characteristics, (4) water quality aspects of produced geofluids, and (5) experimental data for mathematical models of stimulated reservoirs.

Analysis of the design requirements for the chimney model indicated that a maximum design temperature of 500°F and pressure of 800 psig would be an acceptable compromise between the desire to operate at the highest pressure and temperature conditions occurring in natural geothermal reservoirs and the need to minimize the thermal capacitance of the metal in the model. It was also deemed desirable that the chimney model have a quick opening device for easy access and loading of various rock types. However the availability of such devices for operation and use in California at the design conditions was unknown. Since safety considerations are of prime importance, it was decided to build the system to meet all State of California requirements on high pressure vessels and to obtain an operation permit from the State.

A major requirement of the model was a heatup system to establish the initial reservoir conditions of the rock-water hydrothermal system in the chimney. It was concluded that the most effective means of achieving this with acceptable heating times was to circulate hot water through the model at a relatively high rate using a circulation pump and

a high-power electric heater. To avoid flashing in the system, especially in the circulation pump and electric heater, pressurization with an inert gas during the heating transient was required. Provisions also had to be made for expansion of the water in the system. These conditions led to the use of accumulators with free surfaces above which an inert gas could be placed.

In the fluid production mode of operation, control is required with respect to: (1) chimney temperature and pressure, (2) rate of fluid recharge and temperature of recharged fluid, and (3) ability to condense and measure the produced fluid or recycle the condensed fluids.

The system code requirements were reviewed with the State of California agency in charge of pressure vessels. In order not to compromise the safe operation of the system the highest standards were applied. The ASME code requirements for the various components are summarized in Table 1.

Table 1

Summary of Chimney Model Code Requirements

Component	Code Requirements
Chimney Vessel Circulation Heater	ABLE Power Boiler Code, Section VIII, Division 1, Pressure Vessels. Specifically, quick opening device to satisfy paragraph UG35 of Section VIII.
Accumulators	ASME Power Boiler Code, Section 1.
Piping Valves	Installation according to ANSI standard B 31.1.0.
Safety Valves	ASME code stamped and rated.

Inspection by the state inspector is required on the completion of system construction and once a year thereafter. The system is under the supervision of and operated by trained individuals. However a power boiler operating permit is not required for this educational and research installation. Safety features built into the chimney model include a high-pressure safety relief system which will vent the high pressure

fluids to the atmosphere in case of accidental overpressurization, and an emergency blowdown system that can be operated manually from a remote location is included.

Although certain basic instrumentation requirements were readily apparent, the final instrumentation and accuracy required is being determined empirically by experience. Emphasis was therefore placed on acquiring only basic instrumentation and recording equipment at relatively low cost. Upon completion of initial test runs, the actual measurement accuracy obtained will be evaluated with respect to the requirements needed to ensure the objectives of the program. Improvements are envisioned in those areas where greater accuracy is required. The instrumentation for the basic parameters to be measured are summarized in Table 2.

Table 2

Instrumentation of the Chimney Model

	Quantity
Temperature	Terminal temperatures for chimney model, electric heater, condenser
	Water temperature distribution in chimney
	Rock temperature distribution
	Metal temperature distribtuion
Pressure Sensors	Chimney
	Accumulators
	Condenser
Flow Rate Meters	Circulation
	Injection
	Condenser cooling water
	Production flow rate (gravimetric measurement)

The initial efforts in the construction of the model were directed mainly towards getting the major components with long delivery times on

TABLE 3. SCHEDULE FOR CHIMNEY MODEL CONSTRUCTION AND SHAKE-DOWN

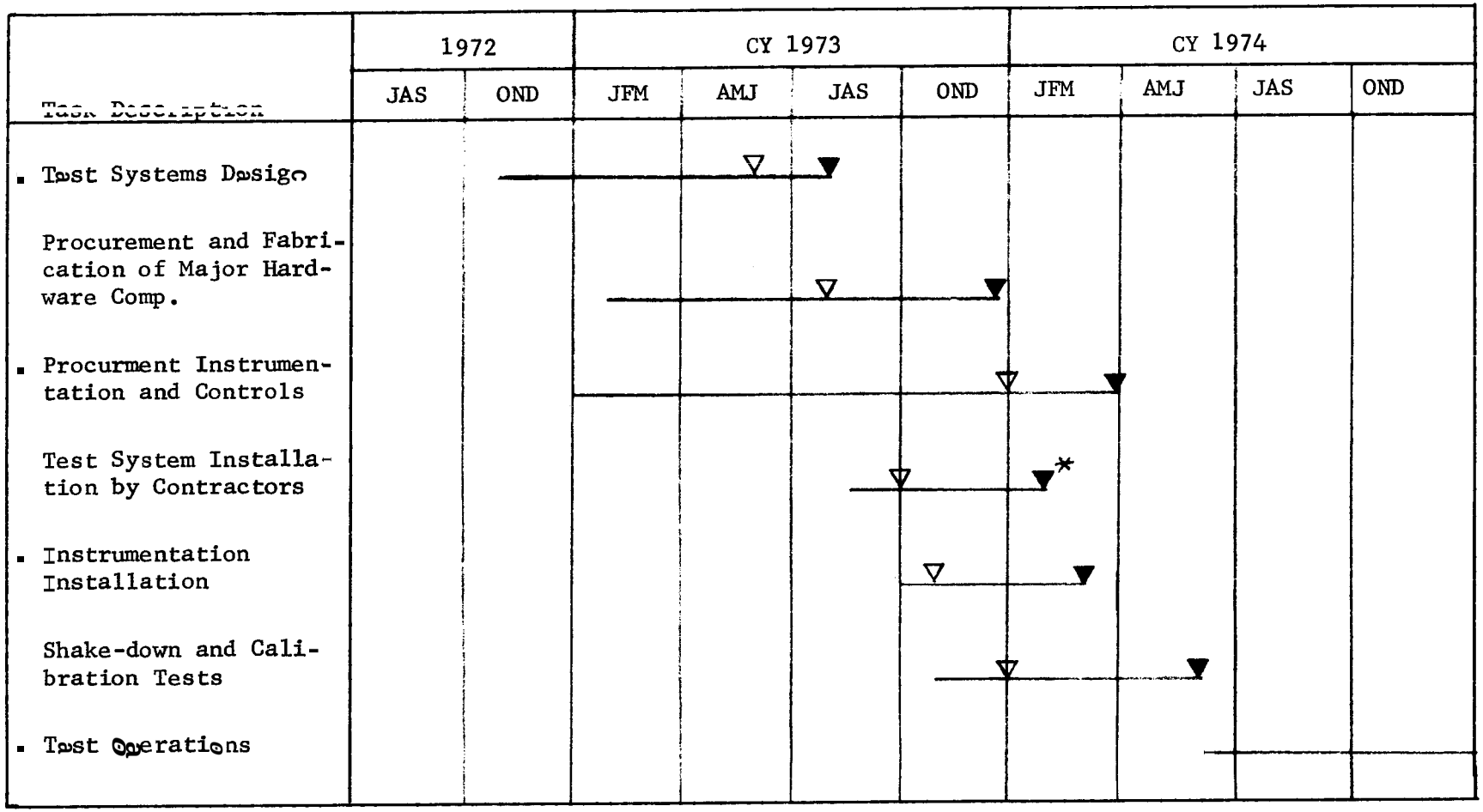

▽ Scheduled Completion

▼ Actual Completion

* Still not 100% completed

order at the earliest possible time. The projected and actual schedule for the various tasks involved in the construction project is summarized in Table 3. From the table it is apparent that delays in the delivery of the major hardware components (especially the electric heater) caused major delays in the project. Thus the starting date of useful test operations was delayed approximately 5 months (from January to June 1974).

Description of the Chimney Model

A photograph of the chimney model on construction completion is shown in Fig. 1. Figure 2 is a view of the auxillary system and operating controls. A schematic diagram of the chimney model system is given in Fig. 3. The operating parameters of the model are listed in Table 4.

Table 4
Chimney Model Operating Parameters

Operating pressure (max)	800 psig
Operating temperature (max)	500 ^{o}F
Chimney water/rock inventory	$\sim$15 ft^3
Total system water/rock inventory	$\sim$19 ft^3
Average heating rate	$\sim$40 ^{o}F/hr
Condenser cooling flow rate (max)	2 gpm
Circulation flow rate (during heatup (max)	15 gpm
Recharge flow rate (continuous)	0-1 gpm
Electric heater capacity	23 kW
Strap heater capacity (chimney)	4 kW
Strap heater capacity (water inlet)	2 kW

The system operates in two primary modes; the "heating mode" (see Fig. 4) which establishes the initial reservoir temperature and pressure conditions in a relatively short time, and the "fluid production mode" (see Fig. 5) during which production from a fractured geothermal system

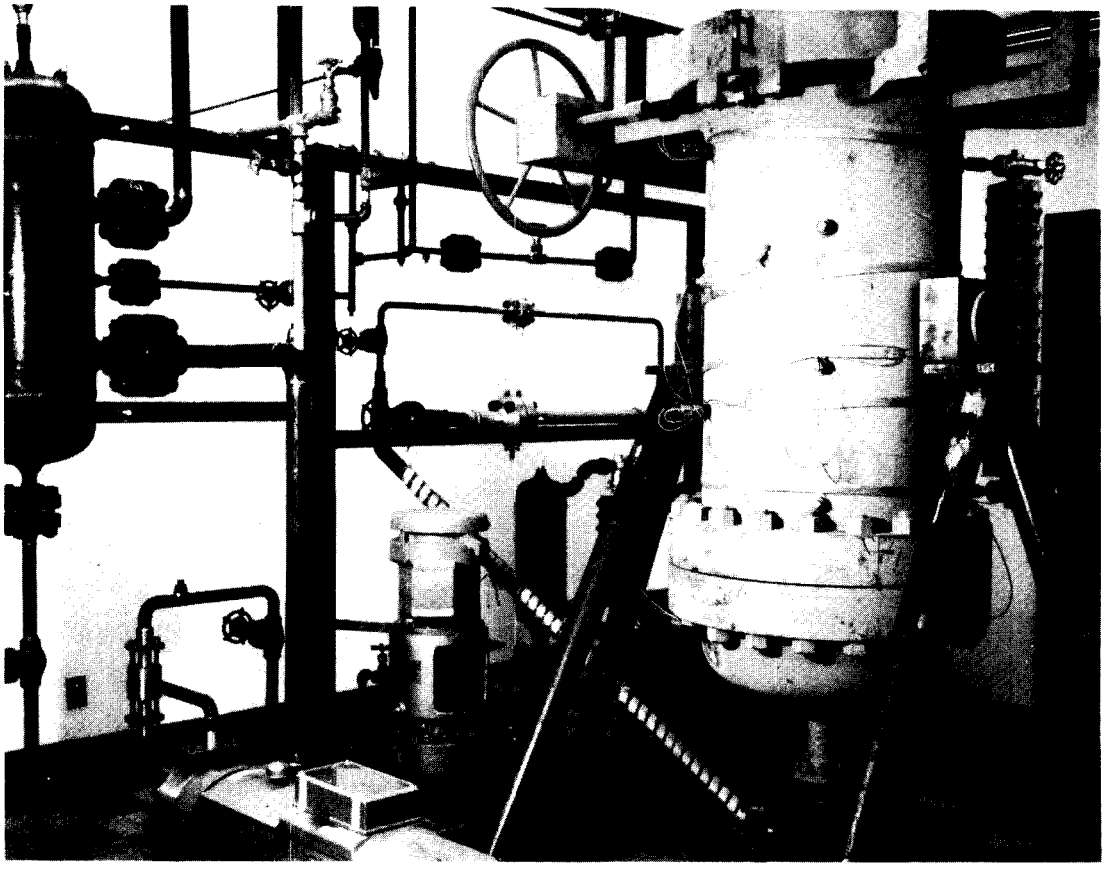

Figure 1. Photograph of Chimney Model Prior to Installation of Insulation.

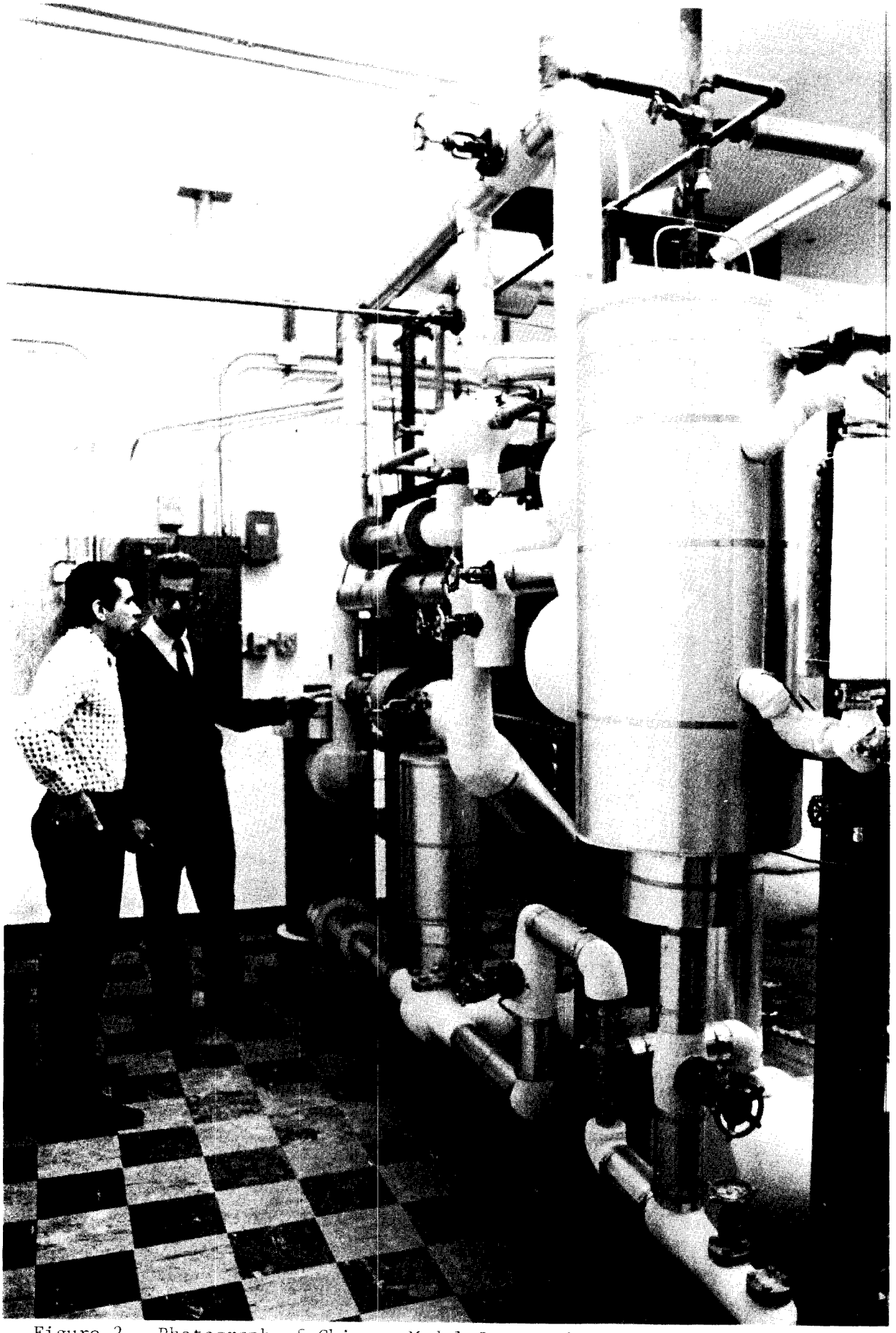

Figure 2. Photograph of Chimney Model System Showing Operating Controls.

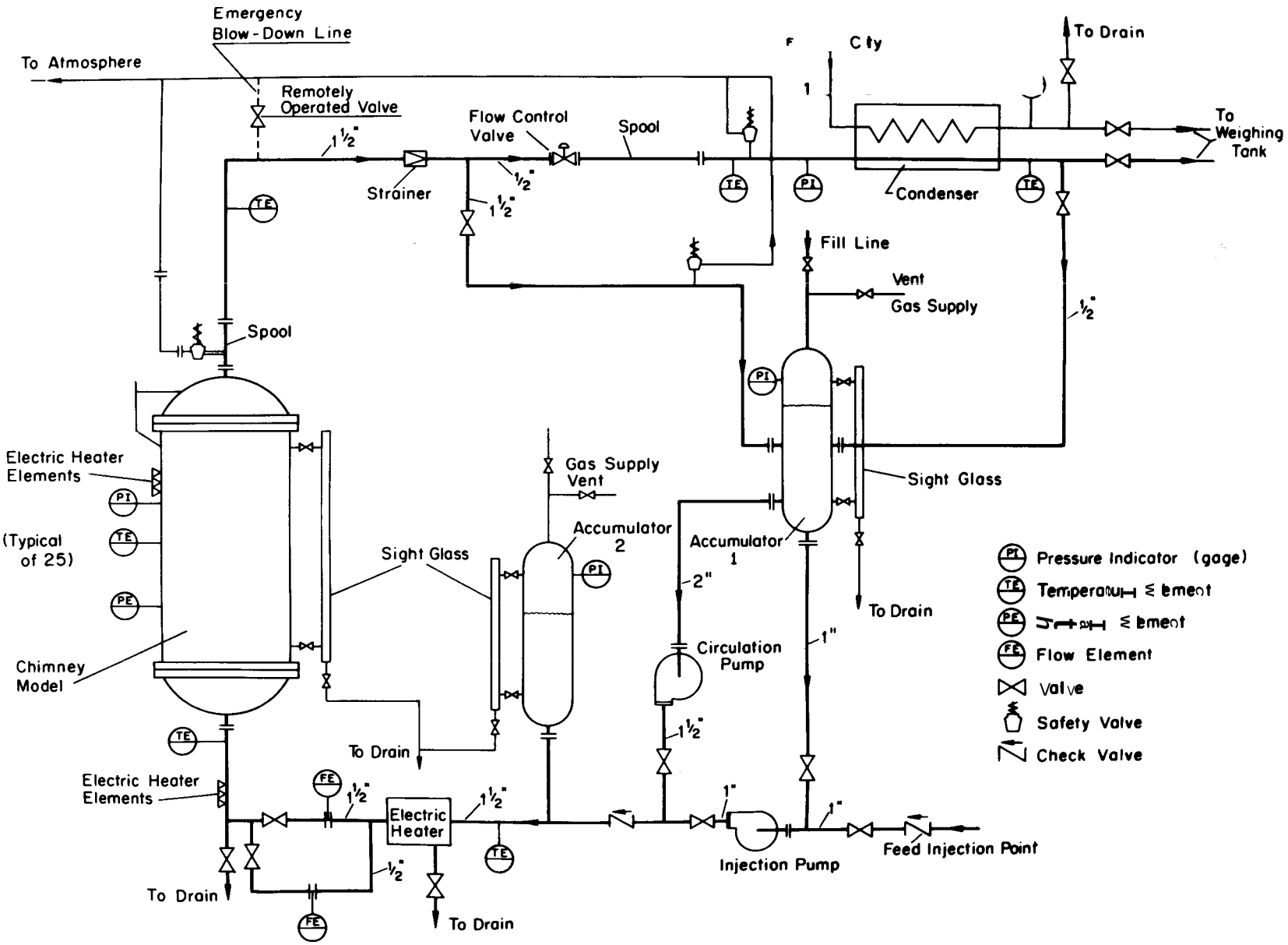

Figure 3. Piping and Instrumentation Diagram of the Chimney Model System.

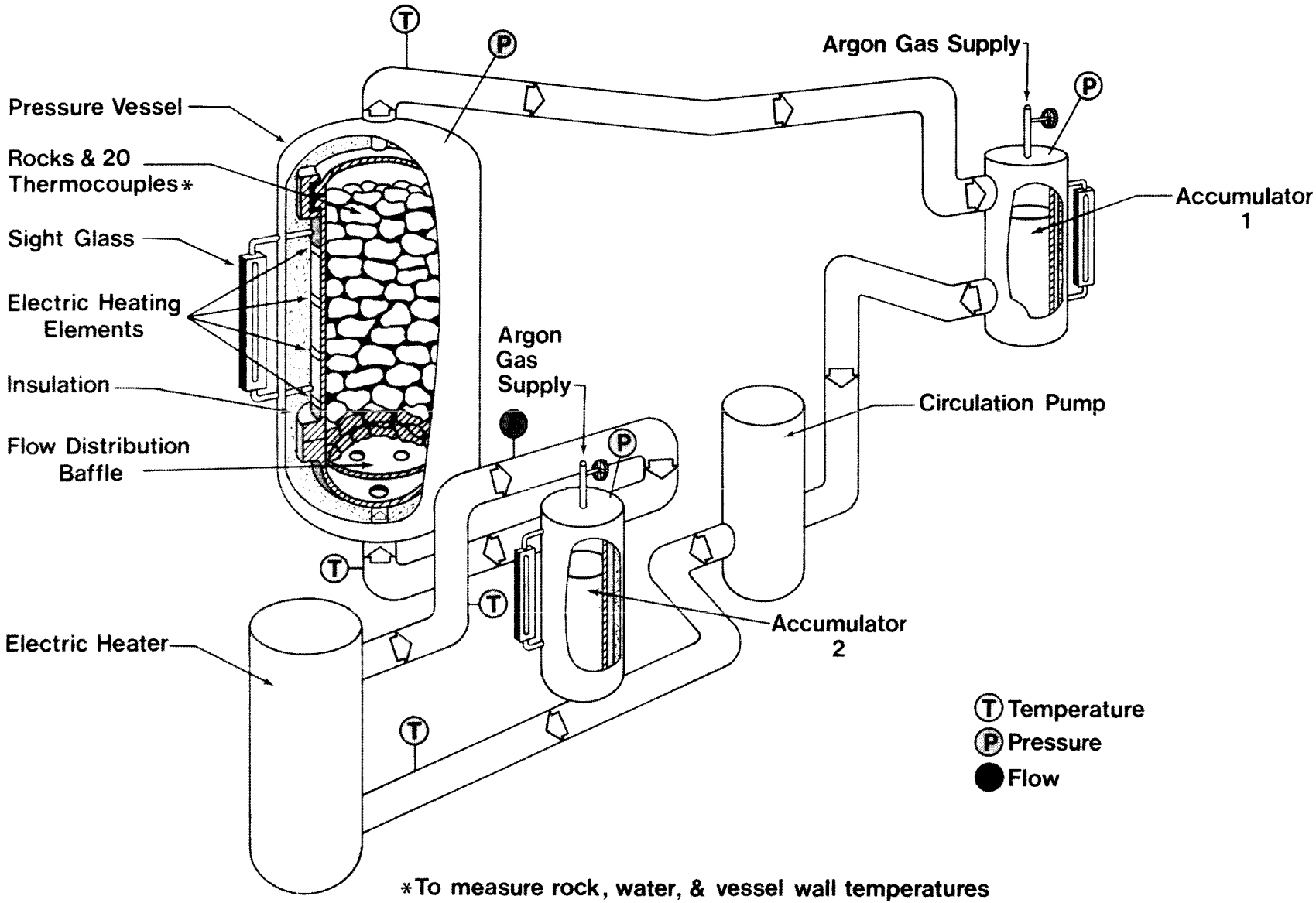

Figure 4. Heating Mode Operation of the Chimney Model System.

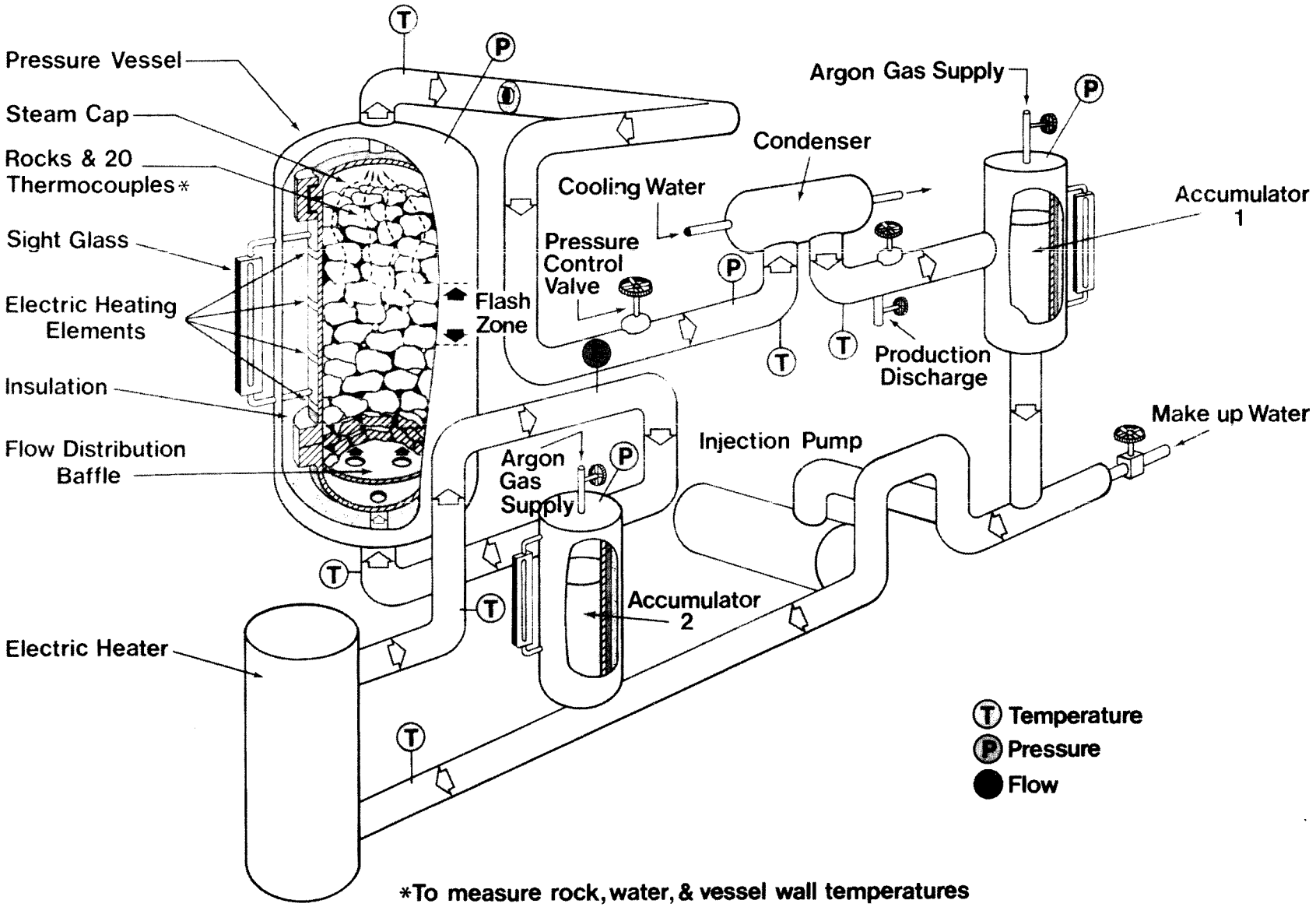

Figure 5. Fluid Production Mode Operation of the Chimney Model System.

is simulated.

A brief summary of the heatup and production mode operations is useful for a description of the system operation. The system is filled with water to desired levels through the make-up water line. Pressurization of the system to 100-200 psig is accomplished by addition of argon gas to accumulators 1 and 2. The circulation pump starts the flow of water through the electric heater where it acquires its thermal energy with an approximately 10^{o}F increase in temperature. The water from the heater circulates through the chimney where some of its energy is transferred to the vessel and the rock loading. Water at the chimney water mixture temperature is then returned via accumulator 1. The heatup process is continued until the desired temperature and pressure conditions are achieved and temperature equilibrium of the rock/water/metal system is established.

Fluid production is initiated by opening the pressure control valve. The produced fluids are passed through the condenser and subsequently either: (1) removed from the system through the production discharge line into a weighing system or, (2) returned through accumulator 1. Recharge of the system is accomplished by the injection pump which draws fluids from: (1) a make-up water line, or (2) accumulator 1, depending on the production operating scheme.

The recharge water is preheated in the electric heater to the desired recharge temperature and enters the chimney uniformly through the flow distribution baffle.

The steel vessel which simulates a fractured rock chimney produced by explosive, hydraulic, or thermal-stress fracturing is 2 feet I.D. and approximately 5 feet high. The lower head is connected to the vessel shell by standard bolted flanges while the closure at the top end is accomplished using a "quick opening" (Tube-Turn) closure. The vessel shell has numerous nozzles for instrumentation entry for measurement of chimney temperatures and pressures. A sight glass is installed on the shell to observe water/steam level movements during operation of the system.

The vessel is supported at its approximate center of gravity by cylindrical pivots which allow the vessel to be rotated from a vertical position

to a horizontal position after inlet and outlet piping, instrumentation connections, etc., are disconnected from the vessel. This provides easy access to the lower section of the vessel during loading and instrumentation of the rock loading. The vessel shell has strap heaters wrapped around the outside diameter presently, with heating power sufficient to make up for heat losses, or to apply energy to the water/rock system at a desired rate. The vessel is insulated with approximately 4 inches of insulation.

To assure adequate flow distribution at the lower end of the vessel (inlet), a flow distribution baffle is installed in the lower head (see Fig. 6). At a low recharge flow rate of 0-1 gpm, the flow is through about 50 holes each 1/32 inch in diameter. This yields a maximum pressure drop of approximately 0.3 psi. At a heatup flow rate of 15 gpm, the flow is mainly through the 4 check valves which open when the pressure difference exeeds 1/3 psi.

The circulation electric heater supplies the thermal energy to provide the initial temperature/pressure conditions of the chimney system in an acceptable length of time, and to preheat the recharge water to operating temperature conditions. The heater is controlled by an on/off thermostat at the present time. However, continuous automatic power range control is being installed which will enhance the utility of the heater.

The high capacity circulation pump is a centrifugal liquid water pump delivering a head of 9 feet at rated capacity of 15 gpm. The pump housing and parts in contact with water are made from stainless steel. The injection pump used to recharge the chimney is a positive displacement pump delivering a maximum head of 800 psi at maximum flow of 1 gpm. The flow rate can be controlled continuously by adjustment of the piston displacement in the range 0-1 gpm. The parts in contact with the water are also made from stainless steel.

The system has two accumulators fabricated from low carbon steel, each with a sight glass for water level observation (see Figs. 4 and 5). Accumulator 1 has a total volume of approximately 1.5 ft3 and its primary

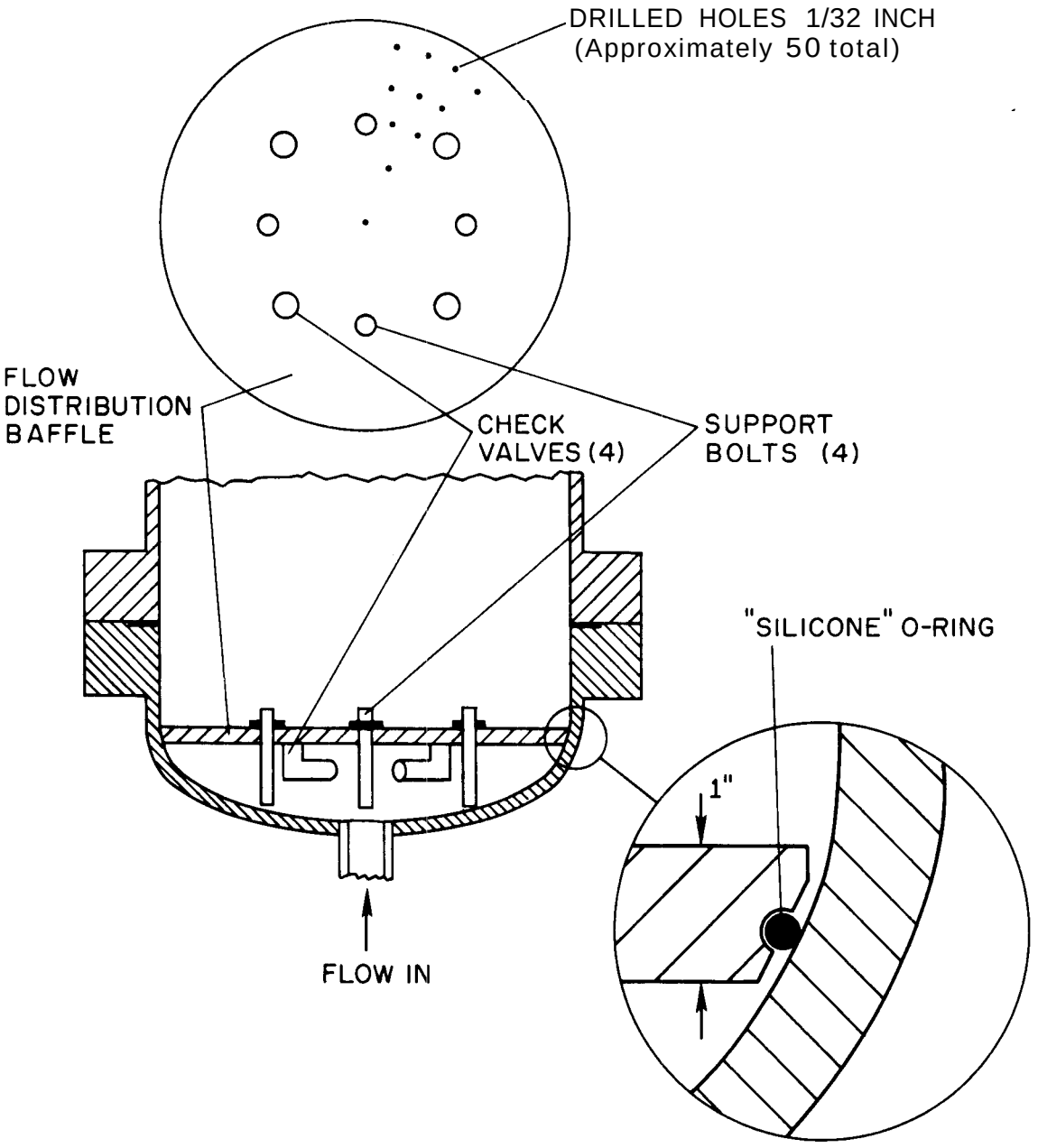

Figure 6. **Details of the Flow Distribution Baffle**

functions are to provide: (1) an expansion chamber during heatup, (2) a free gas surface for inert gas pressurization of system to avoid flashing during heatup, and *(3)* a head tank for the circulation and injection pumps. Accumulator 2 has a volume of approximately 0.5 ft^3. Its primary functions are to provide: (1) damping of pulses originating in the positive displacement injection pump, (2) inert gas pressurization of recharge water to avoid flashing in the electric heater during recharge, and *(3)* room for expansion of water during heatup.

The piping system is constructed from schedule 80 low carbon steel piping (sizes ½, 1, 1½ and 2 inch). Except for connections to chimney, pumps, electric heater and various other components, the system is an all-welded system (with a total of about 140 high pressure welds). The system can be emptied at two low points by the drain valves which drain approximately 99 per cent of the system fluids. The piping system, accumulators and other pertinent components are covered with 1½ to 2 inches ,of insulation.

The locations of the loop pressure, temperature and flow measurement sensors are indicated in Figs. *3*, *4*, and *5*. Pressure indicators are installed on components according to ASME code requirements, and are not designed to be used for experimental purposes. Sensors for acquiring experimental data are discussed individually in the following.

The thermocouples used for loop temperature measurement are all 1/8 inch diameter stainless steel sheathed (grounded) type J thermocouples. The positions of the thermocouples used to measure the chimney water, rock and metal conditions are shown in Fig. 7. All thermocouples are in the same vertical plane. The thermocouples used for water and rock temperature measurement are 1/16 inch in diameter and are of the J type. Holes are drilled in typically sized and shaped rocks to the approximate center of the rock, and the thermocouples are cemented in place with a high temperature porcelain-like cement. The water temperatures are measured adjacent to the "instrumented" rocks to obtain rock/water temperature differences, and at other points to obtain axial and radial profiles. All thermocouples are inserted through the vessel wall by

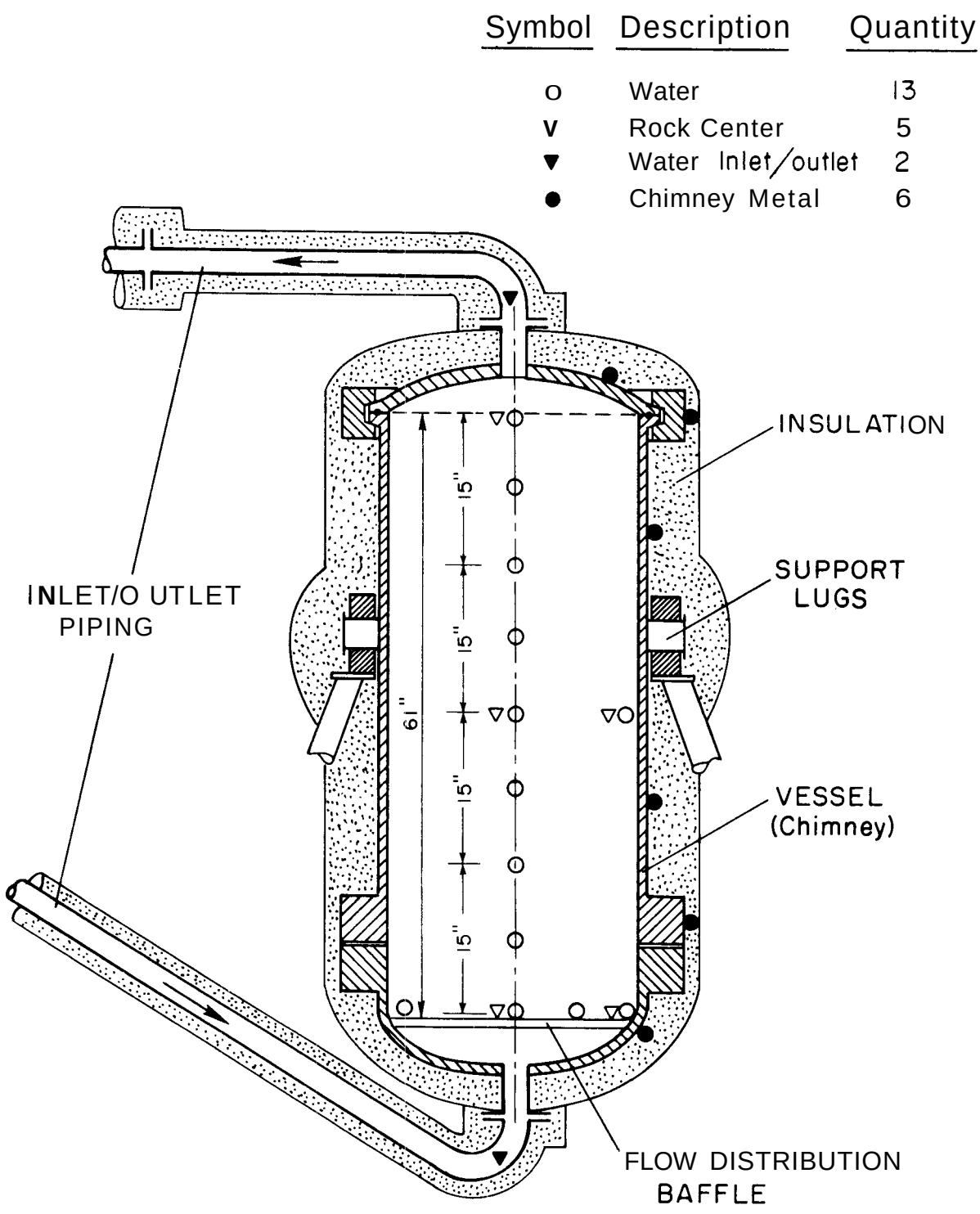

Figure 7. Diagram Showing Locations of Thermocouples for Measurement of Chimney Model Temperature Conditions.

Conax high pressure fittings. The metal temperatures are measured using unsheathed fine-gage type J thermocouples cemented to the metal surface with high temperature cement. All thermocouples are recorded on multipoint recorders. The loop metal temperatures are measured at accumulators 1 and 2. The pressure in the chimney is measured with an electronic pressure transmitter employing a Bourdon-tube as the primary sensing element.

The circulation flow rate during heating is measured using an orifice designed to ASME standards and installed in a 1½ inch line. The measured pressure difference is converted to an electrical signal by an electronic differential pressure transmitter which is fed to the multipoint recorders. The recharge flow is measured using another orifice installed in a ½ inch line. The condenser cooling flow rate is measured using an orifice installed in the 1 inch water line. The recording of the measurements is the same as for the circulation flow measurement. The produced fluid is collected in a tank and the weight is recorded as a function of time to measure the cumulative production and permit calculation of fluid production rate.

Initial Experiments

Initial experiments have been conducted to measure the heatup and cooldown transients of the geothermal chimney model. Analysis was made of the heating time required to bring the water/rock/vessel system to the desired initial reservoir conditions. A simplified "lumped parameter" analysis of the problem has been made in which the various masses of rock, water, and metal are considered to be at uniform temperature.

The lumped parameter approach assumes that all of the water is at uniform temperature and that the energy received from the electric heater is distributed uniformly to each water element.

In reality, the temperature rise across the heater is about 10^{o}F, and the hotter water requires a finite transport time before it reaches the chimney inlet where mixing is very good at the high flow rate. Experience has shown that the water contained in the chimney, accumulator 1, and loop ahead of heater inlet is essentially at uniform temperature to within 1 to 2^{o}F. An exception is the stagnant water in accumulator 2, which remains aibout 50^{o}F below the mean loop temperature.

The lumped parameter approach is generally considered to be adequate when the Biot number is small, i.e.,

$$Bi = \frac{hL}{k} < 0.1 \qquad (1)$$

where:

h = heat transfer coefficient (Btu/hr ft^2 ^{0}F)

L = characteristic length of body (ft)

k = thermal conductivity (Btu/hr ft ^{o}F)

For rocks with an equivalent diameter of 1 inch, the Biot number for typical chimney conditions is:

$$Bi \simeq \frac{(10)(1/12)}{(1)} \simeq 0.8$$

Although the Biot number for the rock appears to be larger than 0.1, experience has shown that during the relatively slow heating transient, the temperature difference between the water and the rock is sufficiently small (about 1^{o}F) so that the rock is practically at uniform temperature.

The lumped parameter approximation for the metal sections is valid because the Biot numbers for the metal portions of the vessel in contact with water are small. For example, the Biot number for the vessel wall is:

$$Bi \simeq \frac{(10)(0.75/12)}{(25)} = 0.025$$

and for the heavy lower flange it is:

$$Bi = \frac{(10)(4/12)}{(25)} = 0.13$$

An initial model was developed consisting of 4 lumped masses. The physical model is shown in the top sketch of Fig. 8. It was assumed that the water and rock are contained inside a tank whose walls were assumed to consist of two parts; one simulating the vessel metal and the other the metal contained in the circulation loop, piping, valves, pump, heater, etc. Electric energy was added to the water with instantaneous mixing,, The notation used for the various conductances between the masses as well as to the surroundings is also shown in Fig. 8. The "electrical analog" of this system is shown on the lower portion of Fig. 8. Energy balances on the various masses yield the following system of simultaneous first order ordinary differential equations in matrix form:

$$\frac{d\theta}{dt} = A\theta + F \qquad (2)$$

where

θ = $[\theta_1, \theta_2, \theta_3, \theta_4]$ temperature vector

$\theta_i = T_i - T_\infty$ (i = 1,..4) excess temperature (^oF)

T_i = temperature of i^{th} lump (^oF)

T_∞ = temperature of environment (^oF)

t = time (hr)

The coefficient matrix, A, is a 4 x 4 matrix where the elements contain various combinations of the heat: transfer conductances h_iA_i. The forcing function matrix is:

$$F = [S,0,0,0] \qquad (3)$$

where S is the rate of energy input by the electric heater.

A standard integration routine was used to solve (2) for the following estimated numerical values of the system parameters based on rock of equivalent: diameter of 1 inch:

Conductances

h_1A_1 = 63,000 (Btu/hr ^oF)

h_2A_2 = 1,000 "

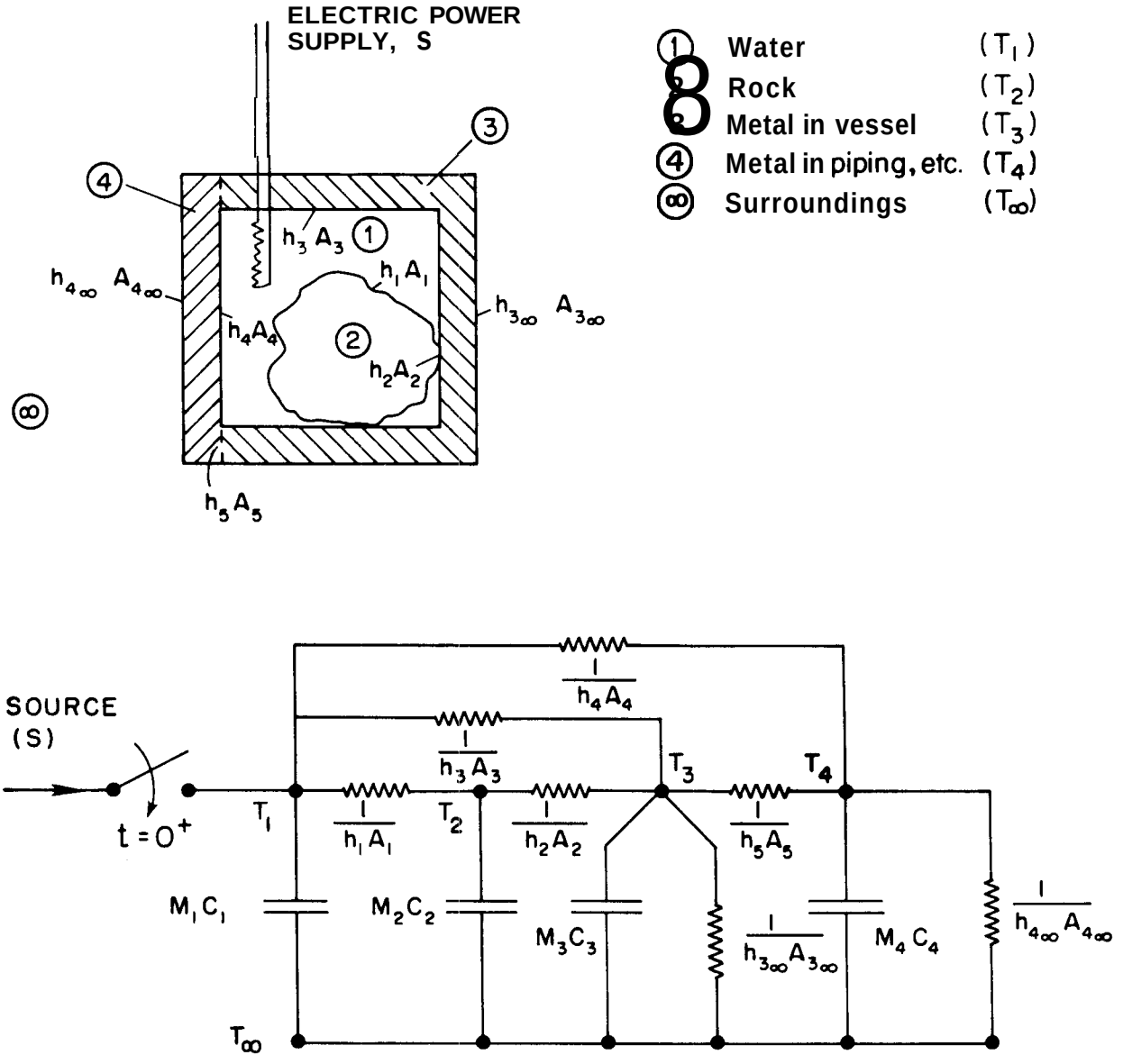

Figure 8. Four-Mass Lumped Parameter Model of the Chimney Model System

$$h_3A_3 = 3{,}500 \quad (\text{Btu/hr } ^{\circ}\text{F})$$

$$h_4A_4 = 1{,}200 \quad "$$

$$h_5A_5 = 100 \quad "$$

$$h_{3\infty}A_{3\infty} = 60 \quad "$$

$$h_{4\infty}A_{4\infty} = 50 \quad "$$

Capacitances

$$M_1C_1 = 350 \quad (\text{Btu}/^{\circ}\text{F})$$

$$M_2C_2 = 280 \quad "$$

$$M_3C_3 = 385 \quad "$$

$$M_4C_4 = 440 \quad "$$

Electric Heater Power (25 kW)

$$S = (25)(3413) = 85{,}300 \text{ (Btu/hr)}$$

Initial Conditions.

$$\theta_1 = \theta_2 = \theta_3 = \theta_4 = 0 \qquad (4)$$

The predicted heatup transient for these particular input parameters is shown in Fig. 9 (Curves 1, 2, 3 and 4). The results of these transient predictions show that the rock temperature will never be much different from the surrrounding water temperature for this slow transient. In fact, it was not possible to distinguish between the curves for the water and rock (Curves 1 and 2), and therefore only one curve was drawn. The reason for the predicted small temperature difference between water and rock is the large heat transfer conductance, h_1A_1, caused by the relatively large heat transfer coefficient and large rock surface area assumed for the small rock size. It can also be seen from Fig. 9 that the slope of the lines decreases with time. This is caused by increasing heat losses due to an increasing temperature difference between the system and its surroundings.

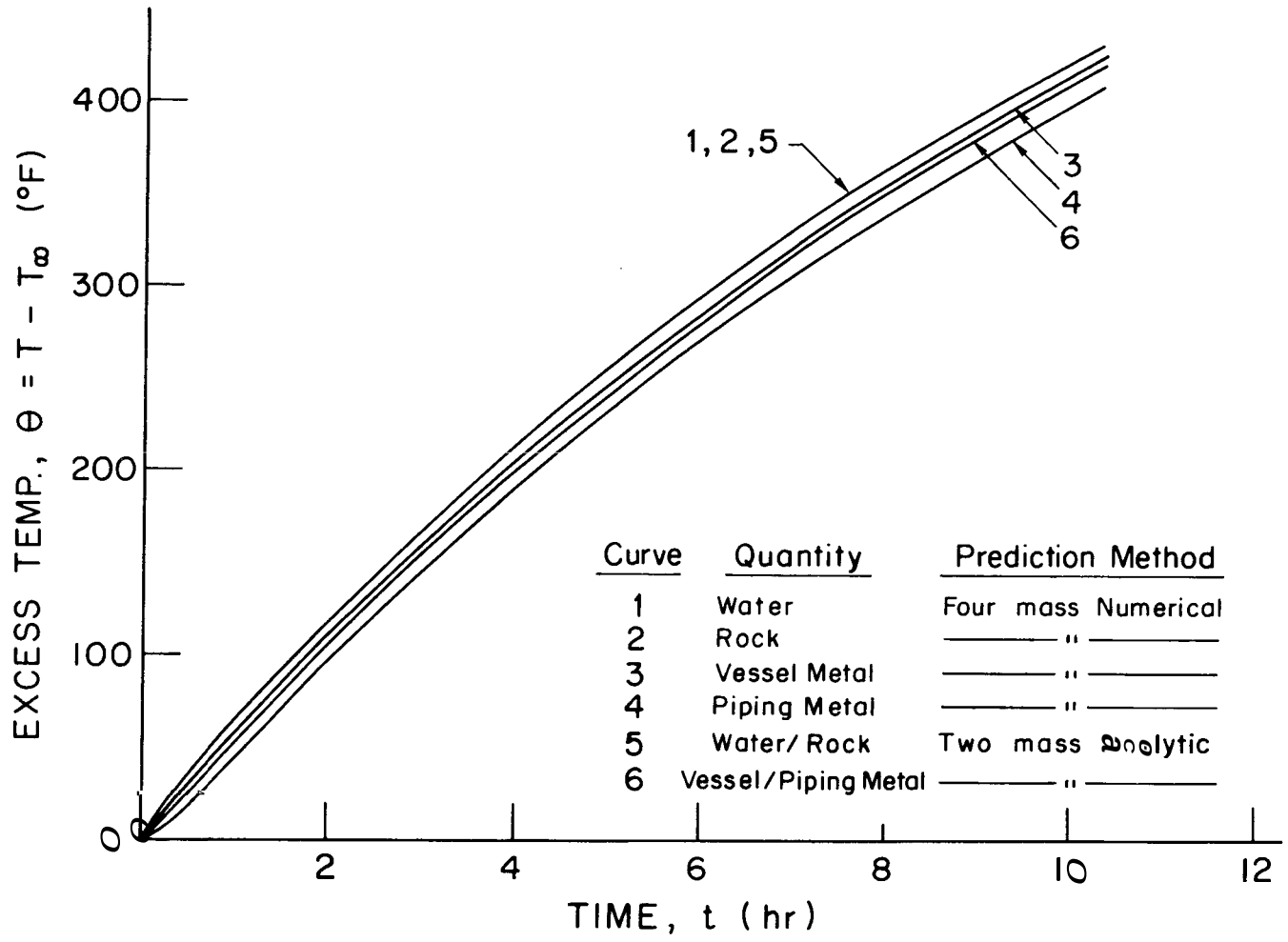

Figure 9. Predicted Heatup Transients Using the Four-Mass and Two Mass Models

Since the computer costs for the four-mass model transient runs were relatively high and it became apparent that the rock temperature was the same as the water temperature for these operating conditions, a simpler two-mass model, shown in Fig. 10, was devised for the system. The model consists of one mass for the water and rock at uniform temperature T_1 and a second mass at temperature T_2 for all of the metal in contact with hot water during the heatup process. The electric power is assumed to be supplied uniformly to the water/rock mass. The two simultaneous differential equations in $\theta_i = T_i - T_\infty$ are:

$$M_1C_1 \frac{d\theta_1}{dt} + h_1A_1(\theta_1 - \theta_2) = S \qquad (5)$$

$$M_2C_2 \frac{d\theta_2}{dt} + h_1A_1(\theta_2 - \theta_1) + h_2A_2\theta_2 = 0 \qquad (6)$$

where

H_1A_1 = heat transfer conductance from water/rock to metal (Btu/hr ^oF)

H_2A_2 = heat transfer conductance from metal to surroundings (Btu/hr ^oF)

M_1C_1 = heat capacitance of water/rock in chimney (Btu/^oF)

M_2C_2 = heat capacitance of metal in chimney (Btu/oF)

S = energy source (electric heater) (Btu/hr)

Let

$$a_1 = \frac{1A_1}{} \qquad a_2 = \frac{h_1A_1}{M_2C_2}, \quad a_3 = \frac{h_2A_2}{M_2C_2} \quad \text{and} \quad \bar{S} = S/M_1C_1 \qquad (7)$$

With initial conditions $\theta(0) = \theta(0) = 0$, and assuming constant coefficients and heat source, the solution to this problem is:

$$e, = \frac{\bar{S}(m_1 + a_2 it\text{-} a_3)}{(m_1 - m_2)m_1}(e^{m_1t} - 1) + \frac{\bar{S}(m_2 + a_2 + a_3)}{(m_2 - m_1)m_2}(e^{m_2t} - 1) \qquad (8)$$

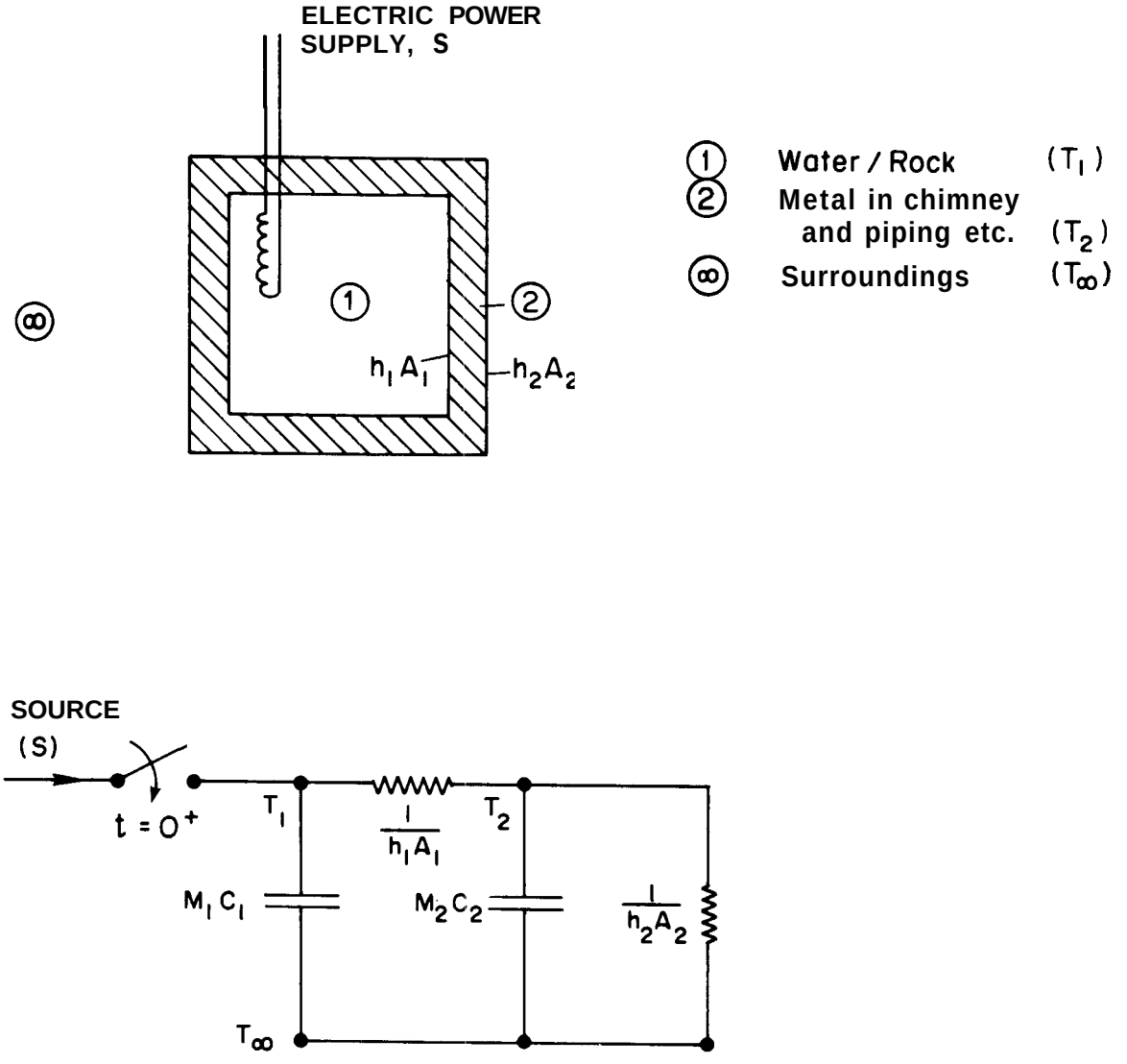

Figure 10. Two-Mass Lumped Parameter Model of the Chimney Model System.

$$\theta_2 = \frac{\bar{S}\, a_2}{m_1(m_1 - m_2)}(e^{m_1 t} - 1) + \frac{\bar{S}\, a_2}{m_2(m_2 - m_1)}(e^{m_2 t} - 1) \qquad (9)$$

where the inverse time constants m_1 and m_2 are given by:

$$m_{1,2} = \tfrac{1}{2}(a_1 + a_2 + a_3) \pm \tfrac{1}{2}[(a_1 + a_2 + a_3)^2 - 4a_1a_3]^{\frac{1}{2}} \qquad (10)$$

The system parameters for this problem are:

Conductances

$$h_1A_1 = 3{,}500 + 1{,}000 = 4{,}500 \quad (\text{Btu/hr } ^\circ\text{F})$$

$$h_2A_2 = 60 + 50 = 110 \quad "$$

Capacitances

$$M_1C_1 = 350 + 280 = 630 \quad (\text{Btu}/^\circ\text{F})$$

$$M_2C_2 = 385 + 440 = 825 \quad "$$

The predicted heatup transient using this model is also shown in Fig. 9 as Curves 5 and 6. The water/rock temperature curve (Curve 5) falls on Curves 1 and 2 from the four-mass solution which shows agreement between the two solutions. The temperature of the metal (Curve 6) lies between the curves obtained for the two separate metal masses.

It appears that the two-mass model is as good, and due to its simplicity may be even better for our purposes than the four-mass model. Thus the two-mass model has been used for heatup transient predictions. The two-mass model also makes it possible to study the relative effects of various parameters on the heatup transient. For example, the effect of changing the mean water to metal conductance is shown in Fig. 11 for otherwise identical conditions.[11] For small values of the water to metal conductance, relatively large water to metal temperature differences

[11] System parameters (such as magnitude of water and metal masses) were re-estimated for these runs. Since the first heatup experiments were made without rock loading, only water was assumed to be in the system.

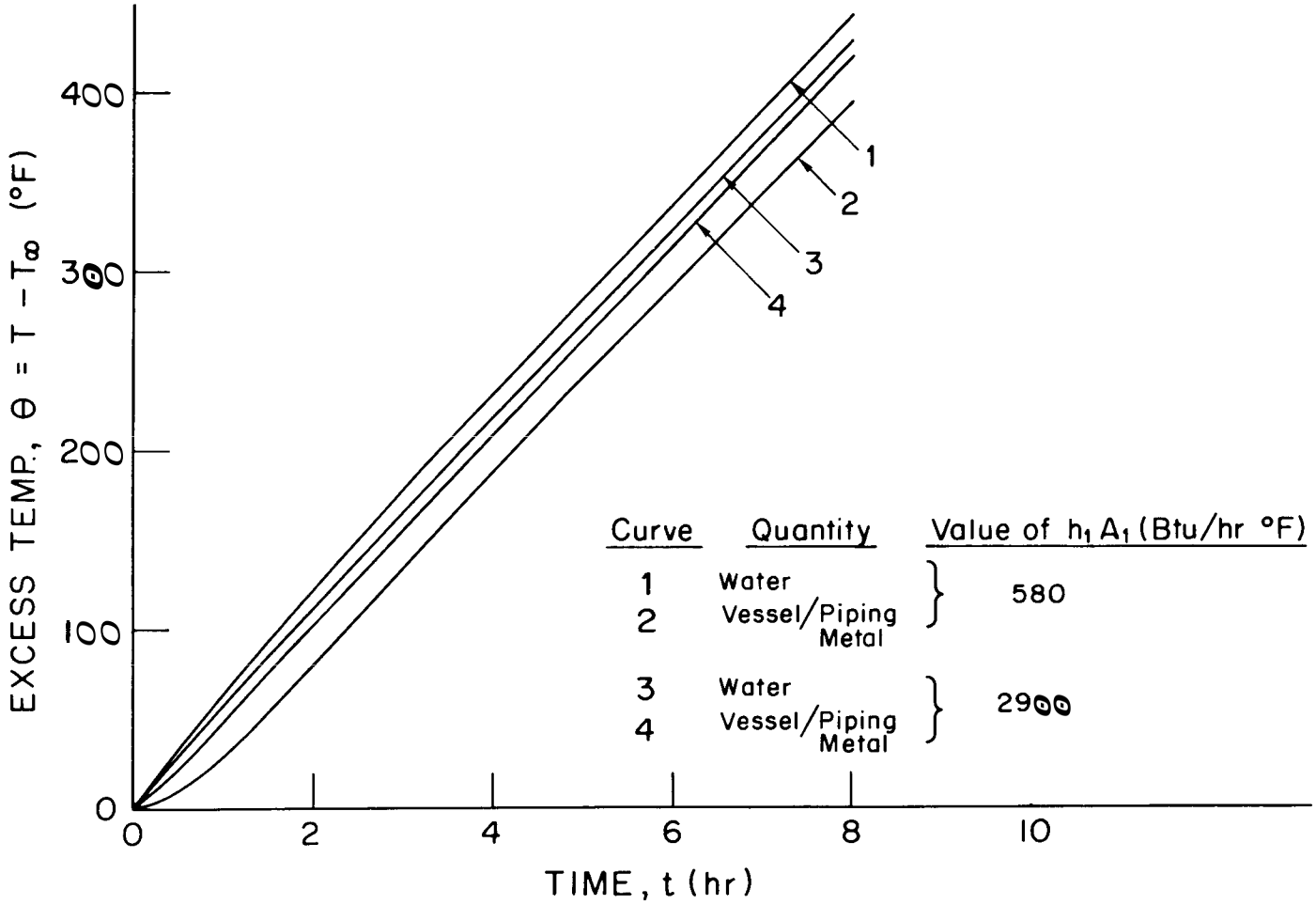

Figure 11. Predicted Heatup Transients Using the Two-Mass Model for $\dot{m}_{wo}$ Different Water to Metal Heat Transfer Conductances.

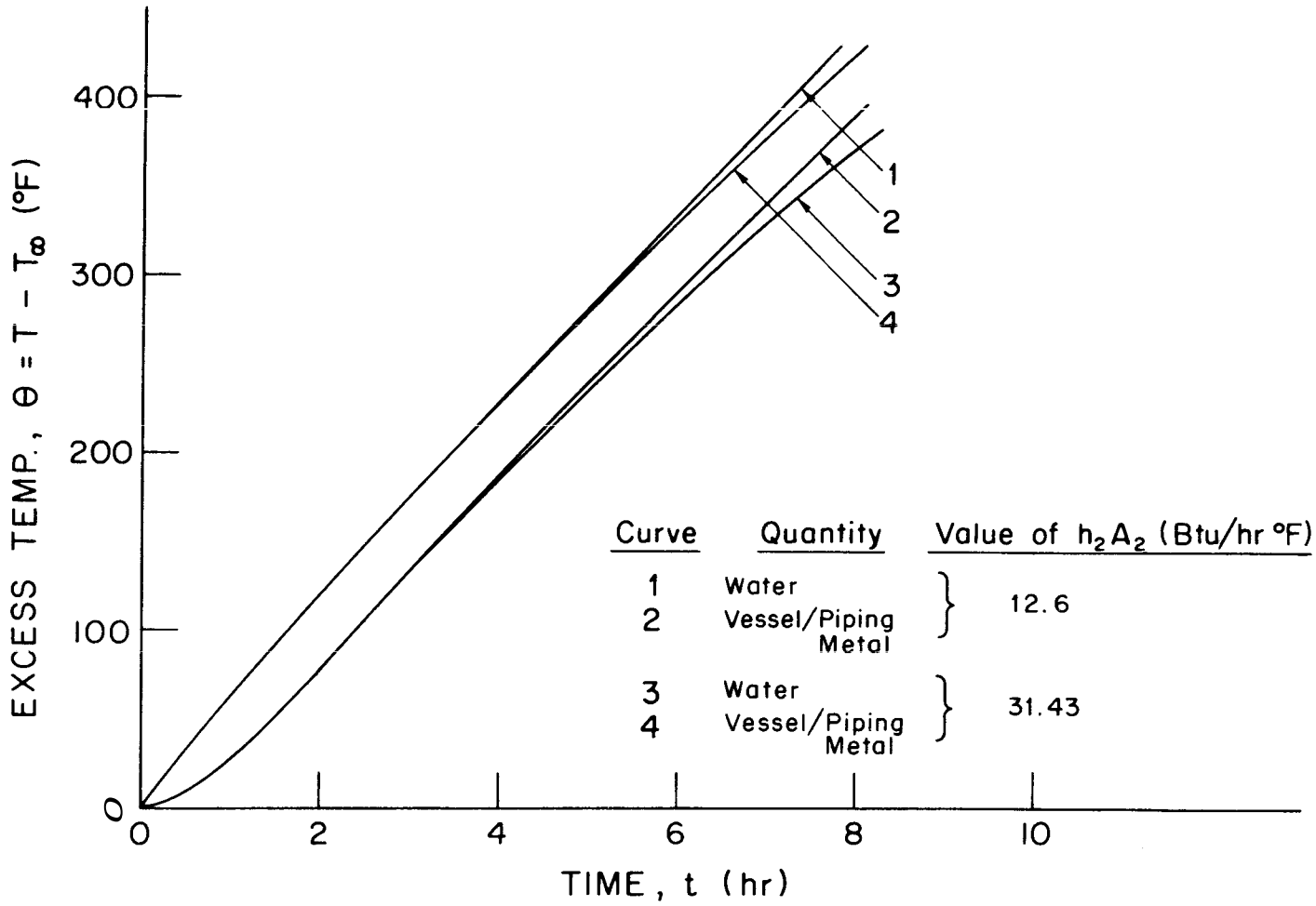

Figure 12. Predicted Heatup Transients Using the Two-Mass Model for Different Metal to Surrounding Heat Transfer Conductances (Heat Losses).

persist throughout the transient, while for large heat transfer conductance, relatively small temperature differences result. The true values of $h_1 A_1$ will be determined from calibration tests.

The effect of heat transfer conductance between metal to the surroundings (heat losses) are shown in Fig. 12. The temperature curves show the expected decreases in slope with increasing heat losses. The exact magnitude of the heat loss, however, needs to be evaluated.

The heat losses from the system to its surroundings are of major importance in determining the heat transfer from the rock media. The heat transfer problem is complex due to the irregular vessel shape, various insulation thicknesses, and fin effects from valves and other non-insulated objects. Since the heat loss cannot be predicted with sufficient accuracy, an experimental approach has been used in which the system is heated to an initial high temperature. During cooling, the temperature-time history is measured at various places in the system. The effective heat transfer conductance to the surroundings can then be evaluated from the slope of the water and metal mean temperature-time data. This results from the following analytic solution of the cool-down transient.

Since the chimney is isolated at the inlet and outlet during the cool-down transient, only the chimney and associated inlet and outlet piping between isolation valves are considered. The two-mass model adapted is essentially that of Fig. 10, with the switch opened at $t = 0^+$ (see electrical analog of Fig. 10). The system of equations to be solved are equations (5) and (6) with $S \equiv 0$ for this case.* With initial conditions:

$$\theta_1(0) = \theta_{10} \qquad \theta_1(0) = \theta_{20} \tag{11}$$

the solutions predicting the transients under similar restrictions as before become:

---

*Although the chimney is equipped with heating tapes, they are not being used during the initial cool-down tests.

$$\theta_1 = \left[\frac{\theta_{10}(m_1+a_2+a_3)+\theta_{20}a_1}{m_1 - m_2}\right]e^{m_1 t} - \left[\frac{\theta_{10}(m_2+a_2 f a_3)+\theta_{20}a_1}{m_1 - m_2}\right]e^{m_2 t} \qquad (12)$$

$$\theta_2 = \left[\frac{\theta_{20}(m_1+a_1)+ {}_{10}a_2}{m_1 - m_2}\right]e^{m_1 t} - \left[\frac{\theta_{20}(m_2+a_1)+\theta_{10}a_2}{m_1 - m_2}\right]e^{m_2 t} \qquad (13)$$

where m_1 and m_2 are given by equation (10). If realistic numbers are substituted one finds that $|m_2| >> |m_1|$ and are negative such that the last terms in equations (12) and *(13)* become relatively small after a short time. Thus θ_1 becomes approximately:

$$\theta_1 \simeq A_1 e^{m_1 t} \qquad t \geq 1 \text{ hr} \qquad (14)$$

Where A_1 is the first bracketed term in (12)

Taking the natural logarithm of equation *(14)* results in:

$$\ln \theta_1 = \ln A1 + m1t \qquad (15)$$

and evaluation at two points 1 and 2 gives the slope:

$$m_1 = \frac{(\ln \theta_1)_1 - (\ln \theta_1)_2}{t_1 - t_2} \qquad (16)$$

Thus, from data that plot approximately as a straight line on semilog paper the dominant inverse time constant, m_1, can be determined from the slope between two points in time,

Data from the first completed cool-down run (Run No. *032774)* are shown in Fig. 13. The system under consideration is now only the chimney and associated inlet and outlet piping with water in the chimney only. The measured water temperature did not differ by more than 1 or 2^{o}F from the top to the bottom of the chimney during the cool-down transient so the water temperatures plotted represent average water temperatures. However, the measured chimney metal temperatures differed by as much as 10 - 20^{o}F and therefore an averaging procedure was necessary. The metal temperature measurement points of the chimney are illustrated in Fig. 7. Each measurement was weighted according to its representative

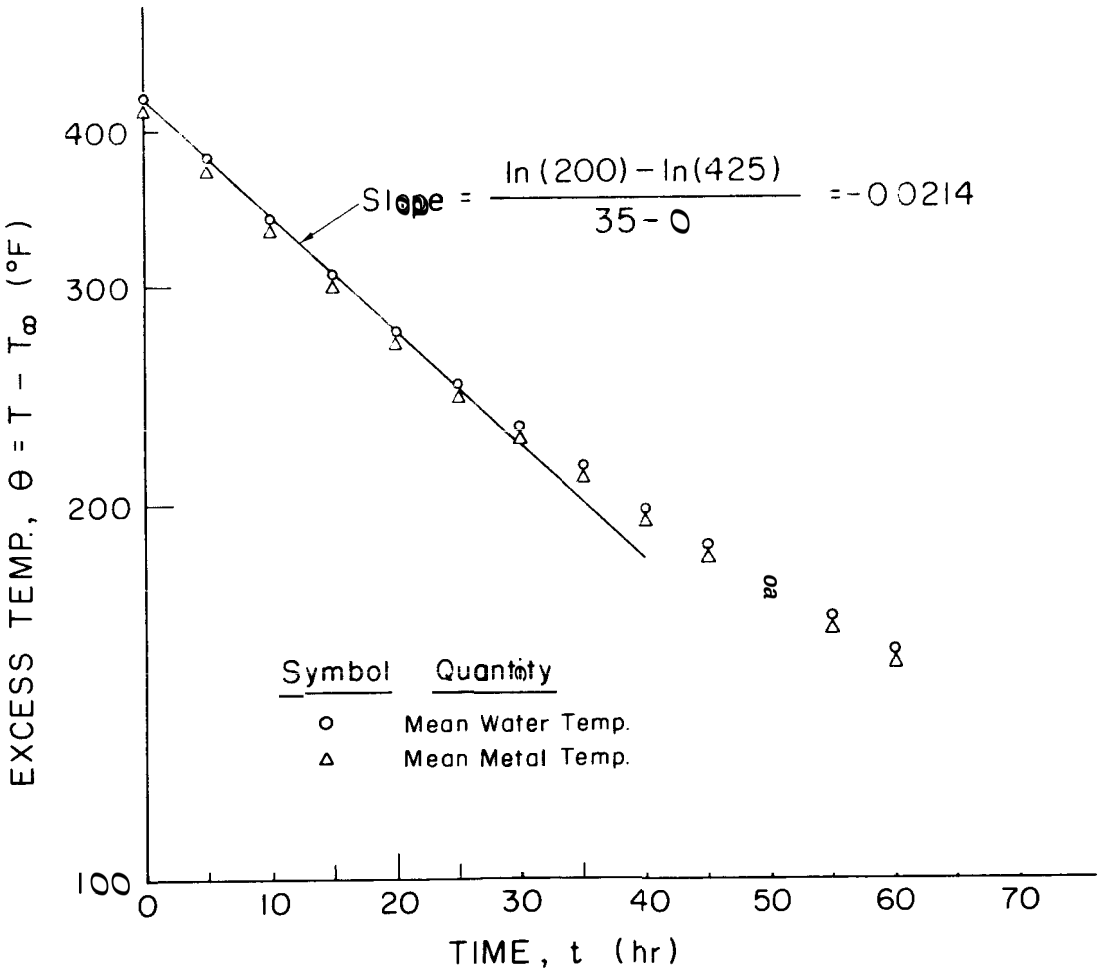

Figure 13. Experimental Cooldown Transient for Chimney Model Loaded with Water Only.

mass fraction to yield an average value. The best: estimate of chimney mass fractions are given in Table IS.

Table 5

Tabulation of Chimney Metal Mass Fractions

Section	Estimated Mass, M_{ic} (lb_m)	Mass Fraction M_{ic}/M_c
Lower heat and inlet piping to closest isolation value	248	0.0629
Lower flanges with bolts	1435	0.3637
Lower section of shell including ½ support structure plus ½ sight glass	*480*	0.1217
Upper section of shell including ½ support structure plus ½ sight glass	656	0.1664
Jock:; (closure device)	756	0.1916
Upper head and outlet piping to closest isolation value	370	0.0938
Total Mass	M_C = 3945 lb_m	

It can be seen from Fig. 13 that there appears to be a distinct break in the cooldown curve between 20 to 30 hours of cool-down time, in addition to a gradual change in slope with time., The last effect is believed to be caused by nonlinearities in the heat transfer coefficients, particularly the coefficient representing the heat loss from the system. The cause of the break in the curve, however, is not clear but may be related to changes in ambient temperature. Analysis of this effect will be made in future experiments. A line through the data in the range 0 to 25 hr yields the slope:

$$\text{Slope} = m_1 = -0.0214 \quad (1/hr)$$

Thus the time constant is:

$$\tau \triangleq \frac{1}{|m_1|} \simeq 48(\text{hr})$$

From the value of m_1 the effective heat transfer loss conductance, h_2A_2, can be derived. The expression for m_1 and m_2 (Equation 10) can be approximated using a binomial expansion of the square root term by the following expression:

$$m_1 \simeq -\frac{a_1 a_2}{(a_1 + a_2 + a_3)} \tag{17}$$

Substituting for a_1, a_2, and a_3 using the relations (7) one finds:

$$h_2A_2 \simeq -m_1(M_1C_1 - M_2C_2)$$

The best estimates of the capacitances are:

$$M_1C_1 = (16)(58)(0.998) = 925 \ (\text{Btu}/^{o}\text{F})$$

$$M_2C_2 = (3945)(0.11) = 443 \quad "$$

Thus, the best estimate of the heat loss conductance for the chimney is:

$$h_2A_2 = 29.3 \quad (\text{Btu/hr}\ ^{o}\text{F})$$

The complexity of the system, parts of which are not insulated, makes it difficult to estimate the effective mass of the system. Experimental heatup transient data can be of some help in this respect. The heatup transient for Run No. 032274 with only water in the system is shown in Fig. 14. The measured metal temperatures are weighted using the system mass fractions shown in Table 6. With the heatup transient data, approximate system mass can be determined. An energy balance on the total system yields:

$$(\text{Out}) - (\text{In}) + \frac{\Delta(\text{Storage})}{\Delta t} = 0 \tag{18}$$

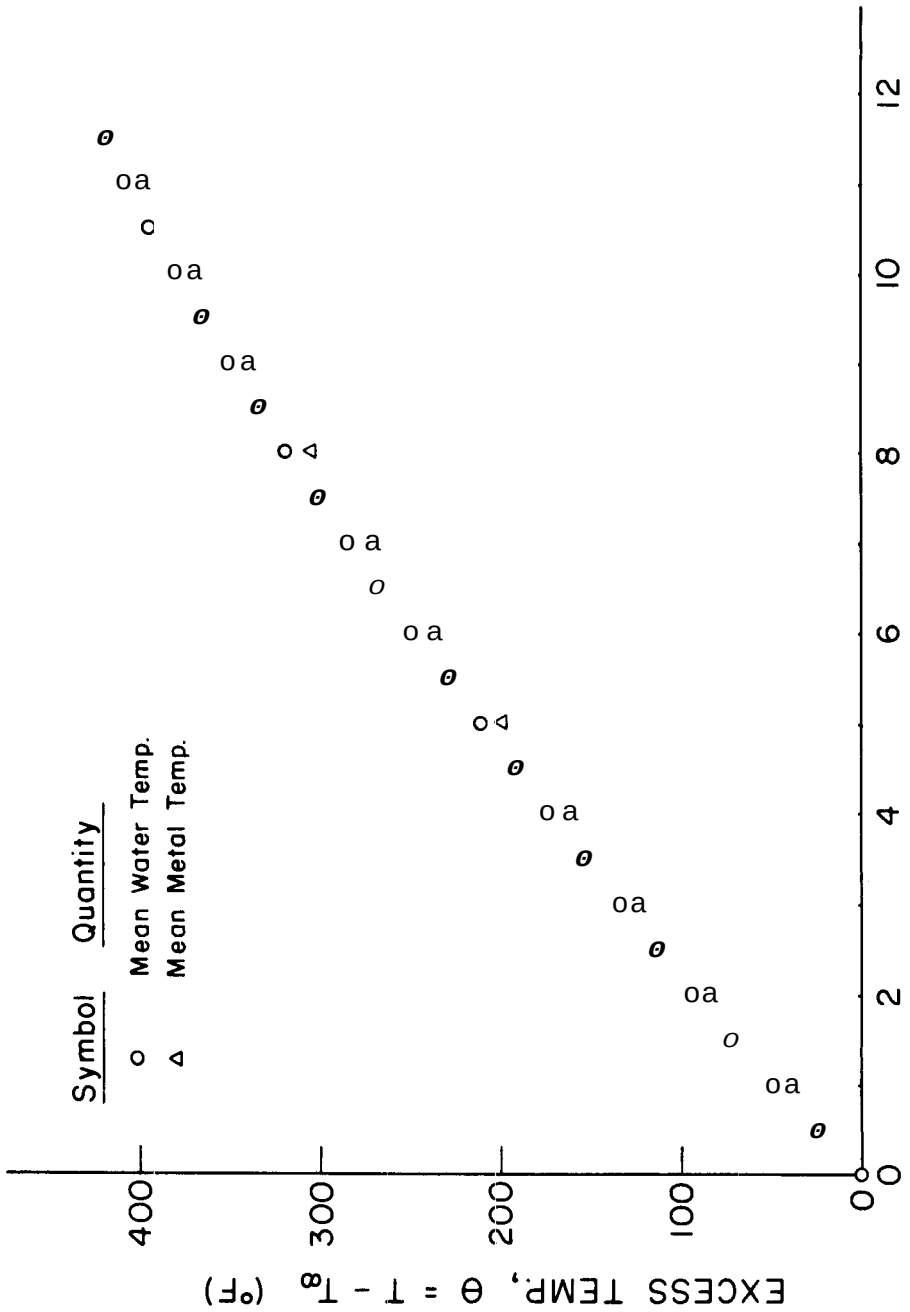

Figure 14. Experimental Heatup Transient with Water Only in the Chimney Model.

Table 6

Tabulation of System Metal Mass Fractions

Section	Estimated Mass, M_i (lb_m)	Mass Fraction M_i/M
Chimney including inlet and outlet pipe sections (M_C)	3945	0.7543
Accumulator 1, connecting piping, and circulation pump	690	0.1319
Accumulator 2 and connecting piping	165	0.0315
Electric heater and connecting piping	430	0.0822
Total system mass	$M = 5230\ lb_m$	

The outflow term is the heat loss term:

$$Q_L = hA\theta \quad (Btu/hr) \tag{19}$$

where hA is the total system heat loss conductance equal to:

$$hA = h_2A_2 + h_2'A_2' \tag{20}$$

The value of h_2A_2 for the chimney was estimated previously. It is estimated that the additional loss conductance for piping, etc., $h_2'A_2'$, is approximately:

$$h_2'A_2' \simeq \tfrac{1}{2}h_2A_2$$

Thus:

$$hA = \tfrac{3}{2} h_2 A_2 \simeq 45 \quad (Btu/hr\ ^oF)$$

The inflow term in Equation (18) is due to the electric heater. The power input to the heater was measured to be:

$$S \simeq 23\ kW$$

or $S = (23)(3413) = 78500 \quad (Btu/hr)$

Since the slope of the water and metal heatup curves (Fig. *14)* are similar, the storage term becomes:

$$(M_w C_w + M_m C_m) \frac{d\theta}{dt} \simeq (M_w C_w + M_m C_m) \frac{\theta_2 - \theta_1}{t_2 - t_1} = \overline{MC} \frac{\Delta\theta}{\Delta t} \qquad (21)$$

where

$M_w C_w$ = heat capacitance of all water in the system (Btu/^oF)

$M_m C_m$ = heat capacitance of all metal in the system "

$\overline{MC}$ = mean value of total system heat capacitance "

Substituting into (18) and solving for $\overline{MC}$ gives:

$$\overline{MC} = \frac{\Delta t(S - hA\theta)}{\Delta\theta} \qquad (22)$$

Reading the slope between 1 and 2 hr on Fig. 14 where the heat losses are small and using previously defined values of S and hA, one obtains from (22):

$$\overline{MC} \simeq 1670 = M_w C_w + M_m C_m$$

The water inventory is known and the water capacitance is estimated to be:

$$M_w C_w \simeq 1100 \ (Btu/^oF)$$

This leads to:

$$M_m C_m = 570 \quad (Btu/^oF)$$

or with $C_m \simeq 0.11 \quad (Btu/lb_m \ ^oF)$:

$$M_m \simeq 5200 \ lb_m$$

This is close to the value estimated in Table 6. However, in order *to* gain confidence in these evaluations more data needs to be evaluated.

Future Experiments

To study production processes from stimulated wellbores or chimneys, the formulation of a mathematical production model has been initiated. The model includes: (1) the water/rock system of essentially infinite permeability contained within the stimulated region or chimney, (2) the wellbore and associated two-phase flow problem, and (3) a simplified model of the recharge of hot fluids from the surrounding geothermal reservoir. With this model the effect of the various parameters on the fluid production and the energy extraction processes can be studied systematically. In particular, the conditions under which the flash front can be made to move into the chimney will be studied in the production modes described in Progress Report No. 1.

The analytical model for fluid production from the chimney will be applied initially to predict the production from the chimney model. Consideration is being given to the heat transfer from the vessel to the water/rock system contained inside. A mathematical model of this heat transfer process has been formilated based on measured temperature/time histories of the metal and chimney heat losses deduced from cool-down transients. Production data from the chimney model will provide some basis for correction and improvement of the analytic model such that the applications of the analytic model to real stimulated wellbores or chimneys can be made with some degree of confidence. Programming efforts on the fluid production model will develop rapidly after the basic data on the system performance are acquired.

The future test program outlined here is subject to revision because the course of the actual testing will be governed by practical considerations such as availability and adequacy of equipment to perform each task. The testing to date has been concerned with: (1) checking and calibration of instrumentation, (2) obtaining heatup transient data, (3) obtaining cool-down transient data, and (4) obtaining fluid production data with water only in the system. These data provide the basis for: (1) the determination of the effective masses of the various system components, and (2) the deduction of chimney model effective heat losses

which eventually will be used in the analytic model for heat transfer from the metal to the water/rock system.

A number of rock types will be tested in the chimney model. These may include, (1) granite, (2) chimney rock (obtained from the Piledriver chimney at the Nevada Test Site), (3) Berea sandstone, and (4) limestone. Also, it is expected that several rock sizes of at least one rock media will be tested.

The first loading of granite of about 1 inch diameter size has been completed as of the writing of this report. Production runs are planned to determine the conditions for maximum extraction of energy. The types of tests to be made and data to be obtained include:

a. Vary production rate and corresponding pressureltemperature histories by flow control valve with no recharge. Observe the following parameters: (1) flashing front location; (2) rock, water and vessel wall temperatures; (3) system pressure, and (4) production flow rate and energy content as functions of time.

b. Control recharge flow and energy content. Vary production rate and corresponding pressure/temperature history by flow control valve. Observations as in (a).

c. With controlled recharge conditions, maintain flashing front at various locations by production flow control. Observations as in (a). Alternatively, maintain a specified flash front movement.

Tests of cyclic production with recharge are intended to simulate the inherent capability of a real fractured geothermal system to recharge itself by mass and energy transfer from the surrounding reservoir.

a. Establish production with zero recharge and continue until some lower pressure/temperature limit has been reached,

b. Stop production and use the injection pump to increase system pressure by injecting water at a specified temperature. When the system is refilled with water, resume production with zero recharge.

Tests are also planned to determine the heat transfer conductances from rock. In these tests, the cyclic method will be applied to the rock/water system to determine the heat transfer Stanton number vs. the flow Reynolds number for various fluid states, rock sizes and rock media. These tests include:

a. Maintain various degrees of subcooling and constant flow rate. Generate a sinusoidal variation of water inlet temperature by control of the heater. Measure corresponding water outlet temperature amplitude and phase change. Use this information to deduce the Stanton number, St, from an analytic solution.

b. Establish saturated conditions in the chimney and repeat the above procedure for various system steam qualities, flow rates, etc. Use this information to deduce the Stanton number, St, from analytic or numerical solution of the same problem.

Since the chimney vessel is made of carbon steel, the experiments involving water quality aspects of the program will be made at a later period. However, during the clean water experiments, problems of water quality must also be considered to avoid extensive corrosion of the system.

At the high temperatures of the production experiments, several chemical elements contained in the various rock types may go into solution in the vessel and precipitate in areas of lower temperature, such as in the discharge line, strainer, flow control valve, condenser, etc., as well as in areas where phase changes take place. Monitoring the chemical composition of the water at various points in the system and observation of deposition of chemicals at such locations will be used to provide information about the water quality aspects of production. Various tracer element tests are also being planned to define these problems. At the conclusion of the production testing, when most of the tests have been completed, brine solution production data will be initiated. txtensive inspection of the system for signs of corrosion attacks in order to safeguard the integrity of the system will be maintained during the life of the program.

An indirect benefit from the test program will be data that can be used for the verification and testing of the analytic fluid production model. A number of the assumptions inherent in the model can be verified directly by using these data.

BENCH-SCALE MODELS

The test objectives and apparatus involved in the bench-scale models was presented in Progress Report No. 1. In brief, these experiments were designed to test fundamental concepts for non-isothermal boiling two-phase flow through porous media. This work is aimed at the entire reservoir, while the chimney model deals most directly with the wellbore and near-well reservoir conditions. The combination should be broadly useful in the new field of geothermal reservoir engineering.

The term "geothermal reservoir engineering" is an adaptation of "petroleum reservoir engineering," the branch of engineering which deals with assessment of and planning of optimum development of petroleum reservoirs. Fortunately, there is much that is useful for geothermal engineering in the literature of oil recovery. Oil recovery by steam injection and underground combustion present some of the important features of non-isothermal two-phase flow which appear pertinent to geothermal reservoirs. But there has been no specific study of the flow of single component (water) two-phase (thus non isothermal) flow in porous media. In particular, there is no information whatever on the important phenomena involved when normally immobile liquid saturations (practical irreducible water saturation) vaporize with pressure reduction. In view of the fact that all heat effects, sensible heat, latent heat of vaporization, etc., are much greater for water than for hydrocarbons, it would be expected that some severe anomalies might be found. The bench-scale models were planned to permit a thorough examination of thermodynamic and fluid mechanic aspects of this special flow regime of such extreme importance to engineering of geothermal systems. It is likely that the results will have broad impact on the entire field of flow through porous media.

The first bench scale model planned is a steady-state flow experiment involving linear flow (in the axial direction) through a cylindrical core.

The Linear Flow Model

The linear flow model was described in Progress Report No. 1. All necessary components have been acquired, and fabrication of the preliminary test model completed. A schematic diagram of the completed apparatus is shown in Fig. 15. A photograph of the apparatus is shown in Fig. 16. Referring to the flow diagram in Fig. 115, cold feed water is pumped through a tubular furnace and into a core contained in a Hassler sleeve type core holder. The core holder is contained within an air bath used to set ambient temperatures as high as 410^{o}F. An accumulator is located immediately downstream of the pump to eliminate flow pulsations, The accumulator is a diaphragm type with nitrogen pressure above the diaphragm. The nitrogen source can also be used to hold pressure on the Viton sleeve in the Hassler core holder.

Flow rate is measured both upstream and downstream of the core. A flowrator is upstream of the coice, while the total mass rate can be determined by timed weighing the condensed water from the outflow of the system, Both regulating and metering valves are used to adjust the back pressure and flow rate. Helicord pressure gages are installed on each side of the core. Porous metal filters (60 micron elements) are located before the tubular furnace and before the back-pressure valve.

The temperature of the flowing fluid is measured after the tubular furnace, at the core inlet and exit, and throughout the entire length of the core via a traversing thermocouple. The traversing thermocouple is a 1/25 inch diameter sheathed thermocouple inside a 1/16 inch O.D. stainless tubing. All temperatures are recorded. In addition to temperature, pressures are measured at the inlet and outlet and at three locations along the core by means of pressure transducers. A detailed description of the major components of the linear flow model are as follows:

Core Holder--A modification cf a Hassler-type core holder designed by the Marathon Oil Company (personal communication, S.C. Jones) was employed. This core holder is shown schematically in Fig. 17. The core

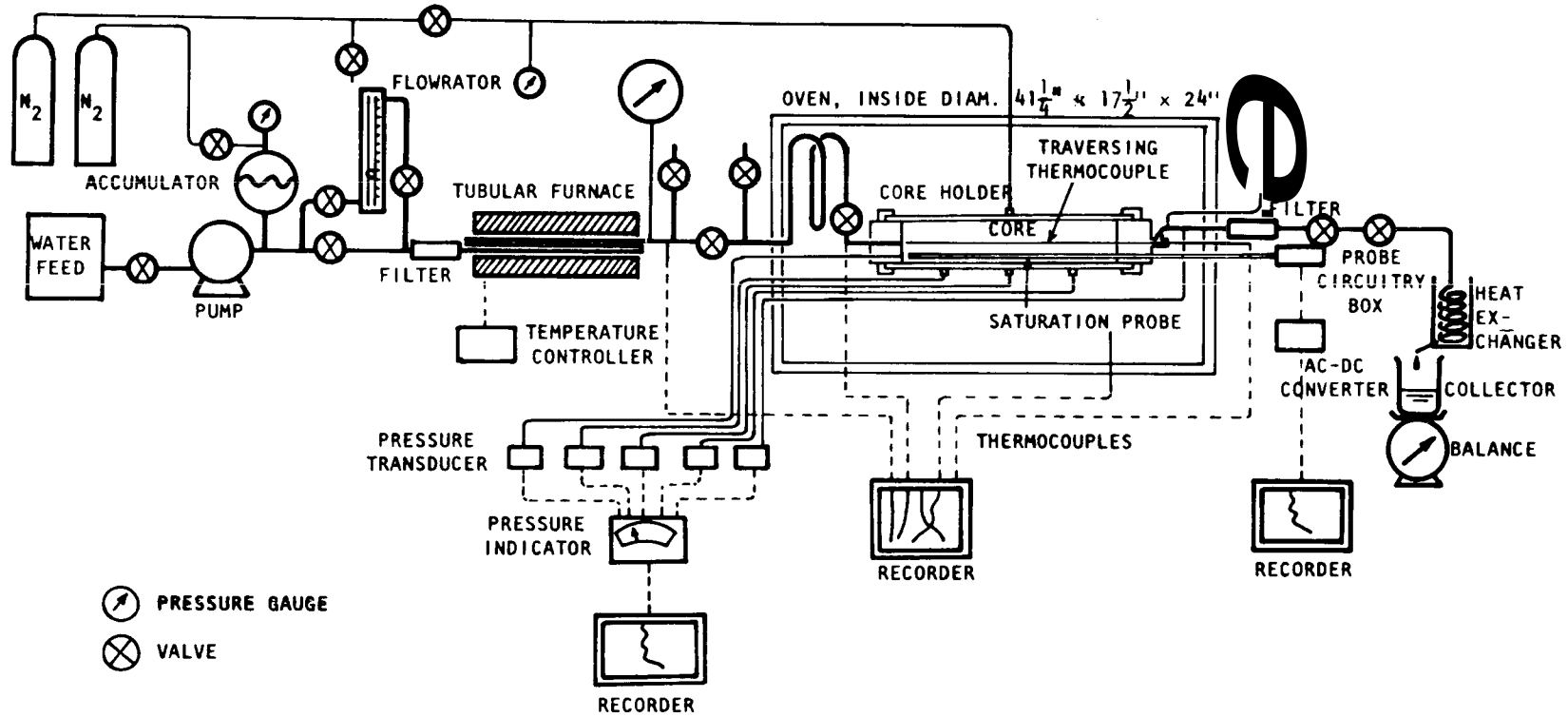

Figure 15. Schematic Diagram of the Linear Flow Model Apparatus.

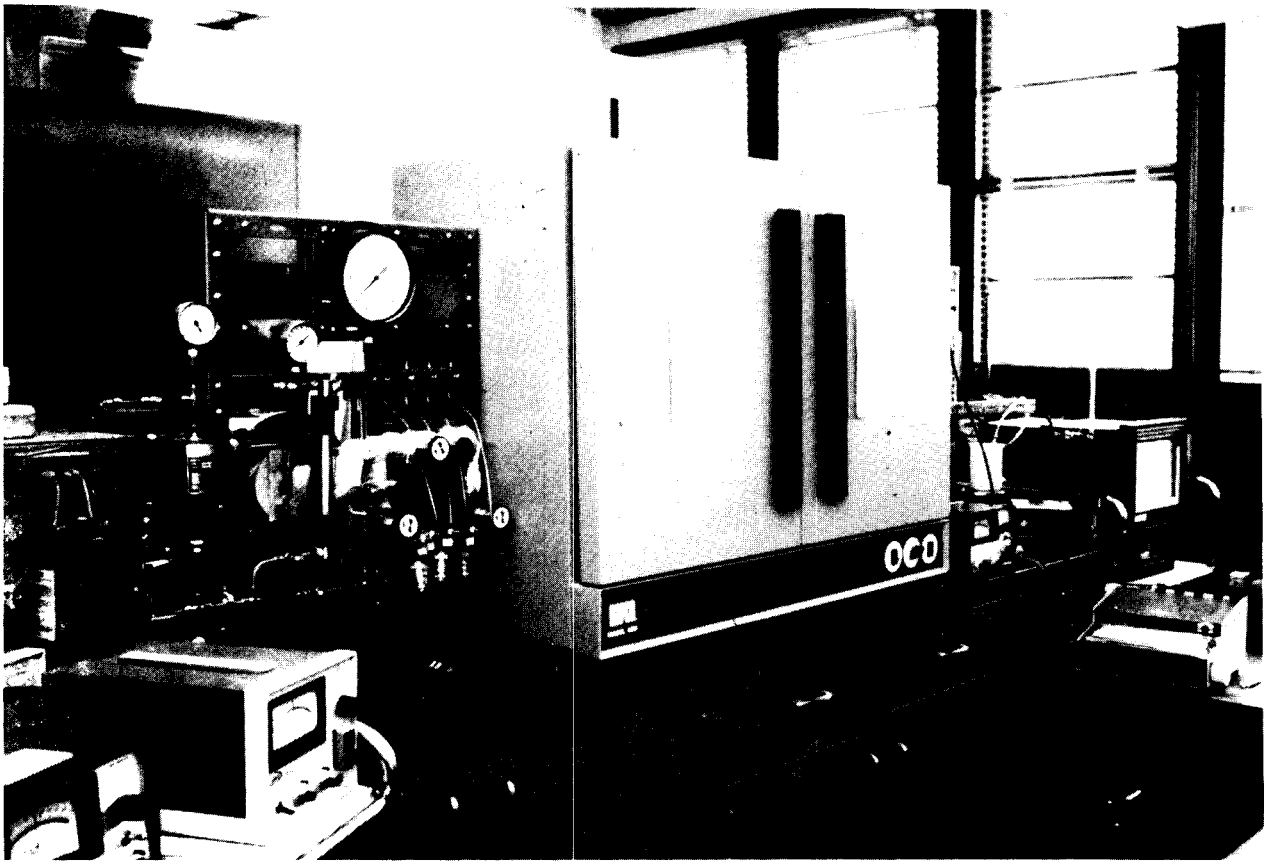

Figure 16. Photograph of the Linear Flow Model Apparatus.

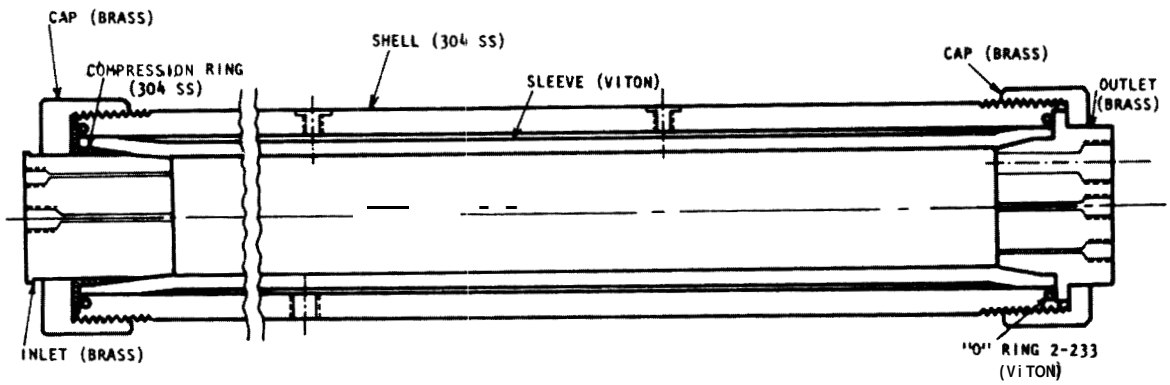

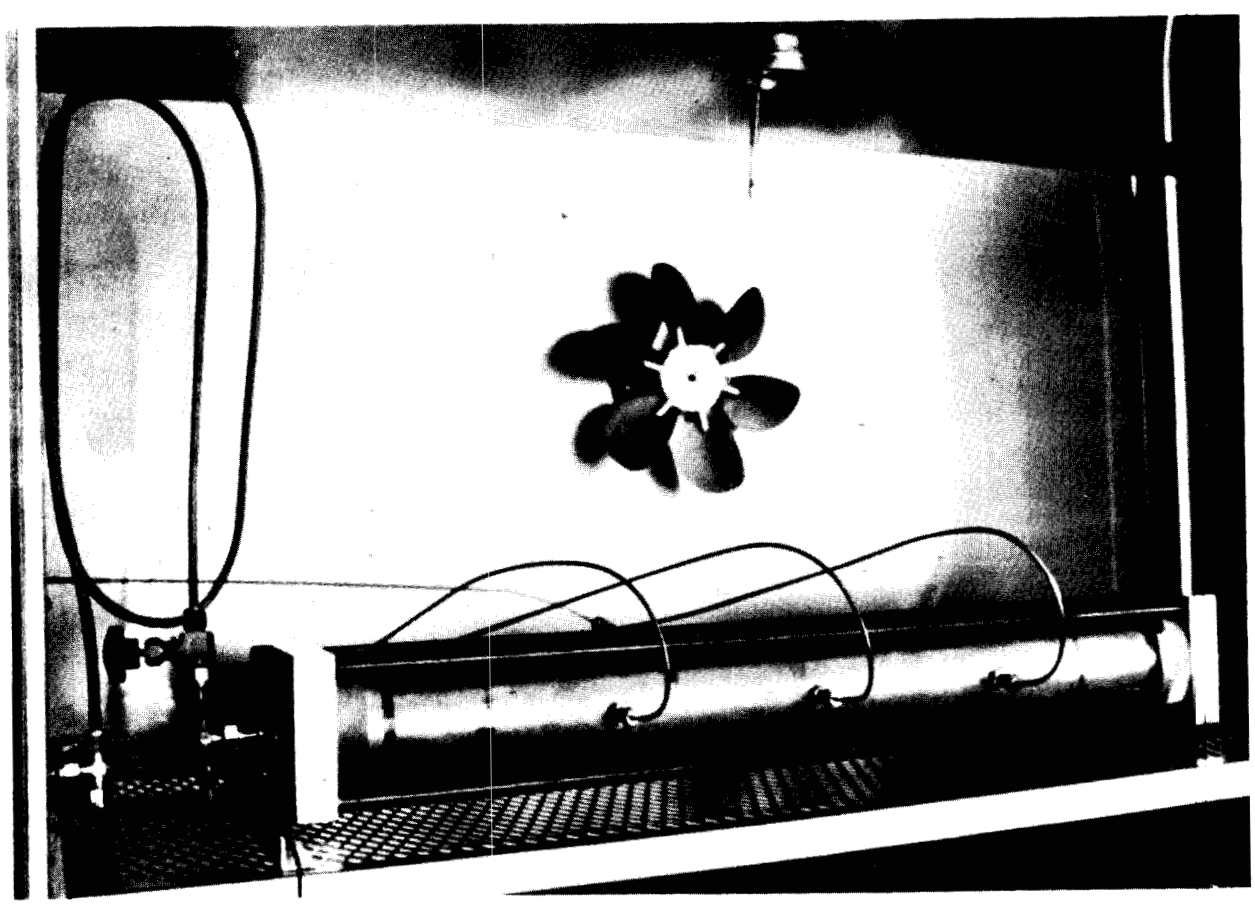

Figure 17. Core Holder.

holder consists of an outer shell, the Viton tubing, and several end pieces. The shell is 26 inches long by 3.5 inches O.D. with a 0.438 inch wall thickness. The shell has four entry ports or taps: one for the overburden pressure, and three for pressure measurements at intervals of 6 inches along the core. The Viton tubing is 26 inches long by 2.5 inches O.D., and 0.25 inches wall thickness, The Viton tubing makes a good seal with the contained core and the pore pressure throughout its length. The inlet plug has taps for inlet flow and pressure measurement. The outlet plug has taps for exit flow, a pressure tap, the inlet fitting for the temperature probe, and a fitting for the liquid saturation probe.

Porous Media--Two types of porous media have been used to date: a Berea sandstone core, and several synthetic consolidated sandstone cores. In the case of the Berea sandstone core, a groove was cut on the side surface and a 1/16 inch O.D. stainless steel tubing with one end plugged by silver solder was cemented in the groove. Fondu calcium aluminate cement, silica sand of about 100 Tyler mesh size, and water were used as the materials to make the synthetic cores. The proportions of sand and cement were 80% sand by weight, and 20% cement by weight. The sand-cement mixture was prepared by thoroughly mixing sand, first with the blending water (0.5% by weight), secondly with cement. The mixture was poured into a mold formed with a plastic tubing in which a glass tubing for the liquid saturation probe and a thermocouple tubing were held in place. While pouring sand, the mold was tapped from time to time in order to compact the sand. Water was injected through a fitting on a disc flange connected to the end of the mold. After the breakthrough of the injected water, the mold was disconnected from the water and allowed to hydrate for one day. After 24 hours, the plastic tubing was peeled off and the core was machined (filed) to a desired size: 2 inches O.D. by 23.5 inches long.

Liquid Saturation Probe--The term "saturation" is used here to mean

the volume fraction of pore space. The liquid saturation probe was originally developed by the Chevron Oil Company (Baker, 1972) in connection with a study of oil recovery by injection of steam. The instrument uses the difference in dielectric constant between the materials present (liquid water and steam) in the pore space. The instrument consists of a probe which moves in a glass guide cast in the synthetic core, electronic circuitry, and a recorder. The probe is a capacitor coupled with an oscillator whose resonant frequency changes with the changing capacitance of the probe. The capacitance of the probe is affected by the liquid content of the porous medium surrounding the glass tube. The probe condenser consists of a 0.238 inch O.D. pyrex tube 36 inches long, silver plated on the outside, with a 1/16 inch brass rod down the inside connected to a 1/4 inch O.D. copper tube at the end. Most of the capacitance is between the brass rod and the silver plate and is fixed. The sensitive and variable portion of the capacity is between the silver plate and the copper tube. For recording, the frequency change is converted to a DC voltage whose magnitude is proportional to the input frequency.

Preliminary Experiments

It was decided to run a series of basic single-phase experiments prior to performing the boiling two-phase, non-isothermal flow experiments. These basic experiments included: (1) measurement of absolute permeability to gas and liquid water at a range of temperatures, (2) injection of hot water into a system containing water at a lower temperature, (3) cold water injection into a system containing hot water initially, and (4) injection of steam into a system containing liquid water at a lower temperature. The results are as follows.

Figure 18 presents absolute permeability to nitrogen vs the reciprocal mean core pressure for a variety of temperatures ranging from 75°F to 342°F. Figure 18 is a standard graph used to determine both the absolute permeability to gas (at zero reciprocal atmospheres) and the Klinkenberg slip factor, b, the slope of the straight line on Fig. 18. As can be seen,

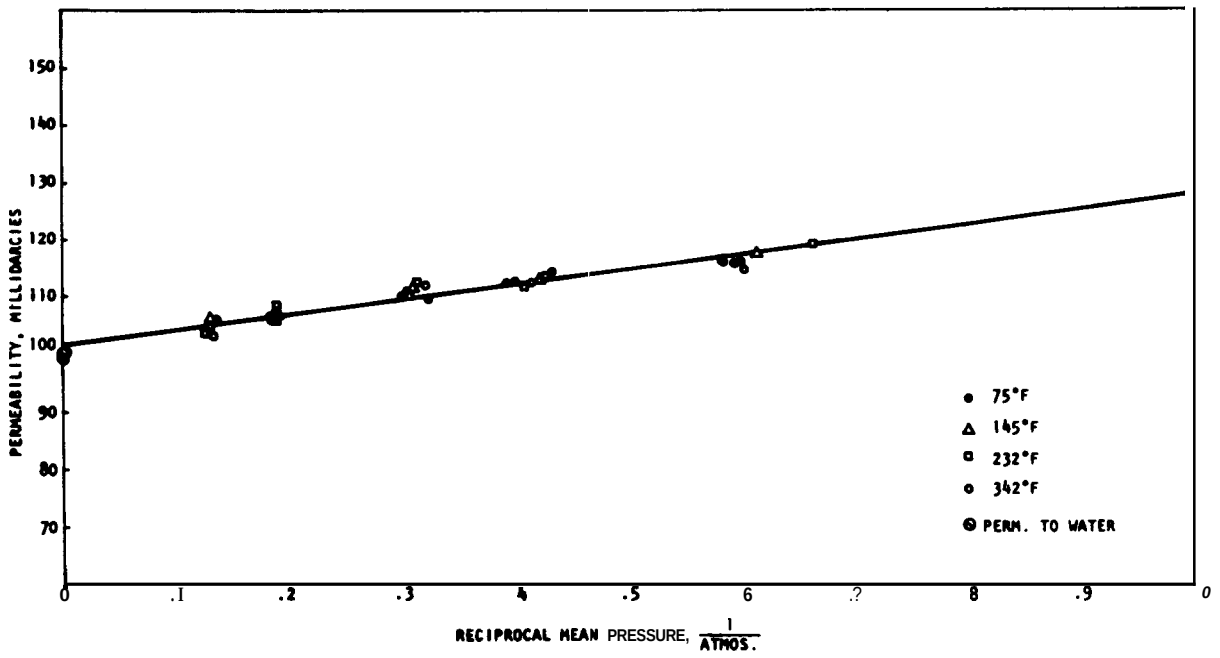

Figure 18. Permeability to Nitrogen vs. Reciprocal Mean Pressure.

all data for the synthetic sandstone core can be represented by a single line, indicating no significant effect of temperature level for the range of temperatures studied. However, the Klinkenberg factor is 3.77 psi, much higher than would be expected from correlations for natural sandstone cores. Also shown on the ordinate of Fig. 18 is the absolute permeability to water for the synthetic core. It is a few percent lower than the absolute permeability to gas: 99 millidarcies vs 102 millidarcies. Although not evident on Fig. 18, the permeability to water was measured for a range of temperatures from 76°F to 340°F. Unlike previous findings by Weinbrandt, Ramey, and Casse for natural sandstones, no effect of temperature was found. One significant difference other than the nature of the core was that the core loading pressure (pressure on the Hassler sleeve) was only 300 psi for our runs as compared to at least several thousand psi for the Weinbrand, et al., study.

Figures 19 and 20 present temperature vs. distance along the core for injection of hot water into a core initially at room temperature. Two different injection rates were used. Figures 21 and 22 show the reverse procedure: injection of relatively cool water into a core initially at about 250°F. Finally, Fig. 23 presents temperature vs distance for injection of steam into a synthetic core initially containing cold water.

Much useful information can be extracted from data such as are shown in Figs. 19-23. Figures 19-22 provide basic information on single-phase non-isothermal flow, effective thermal conductivities in the direction of flow, and heat loss radially from the core. In regard to radial heat loss, two determinations can be of interest: (1) the thermal efficiency of the injection, and (2) the overall heat transfer coefficient for the core within the sleeve to the surroundings. In the former, thermal efficiency has been defined in oil recovery by hot fluid injection as the fraction of the cumulative heat which is still within the injection interval (the remainder being lost to overburden and underburden). In the case of cold water injection, we would be interested in the heat gained from the surroundings. This would be analogous to a cold water

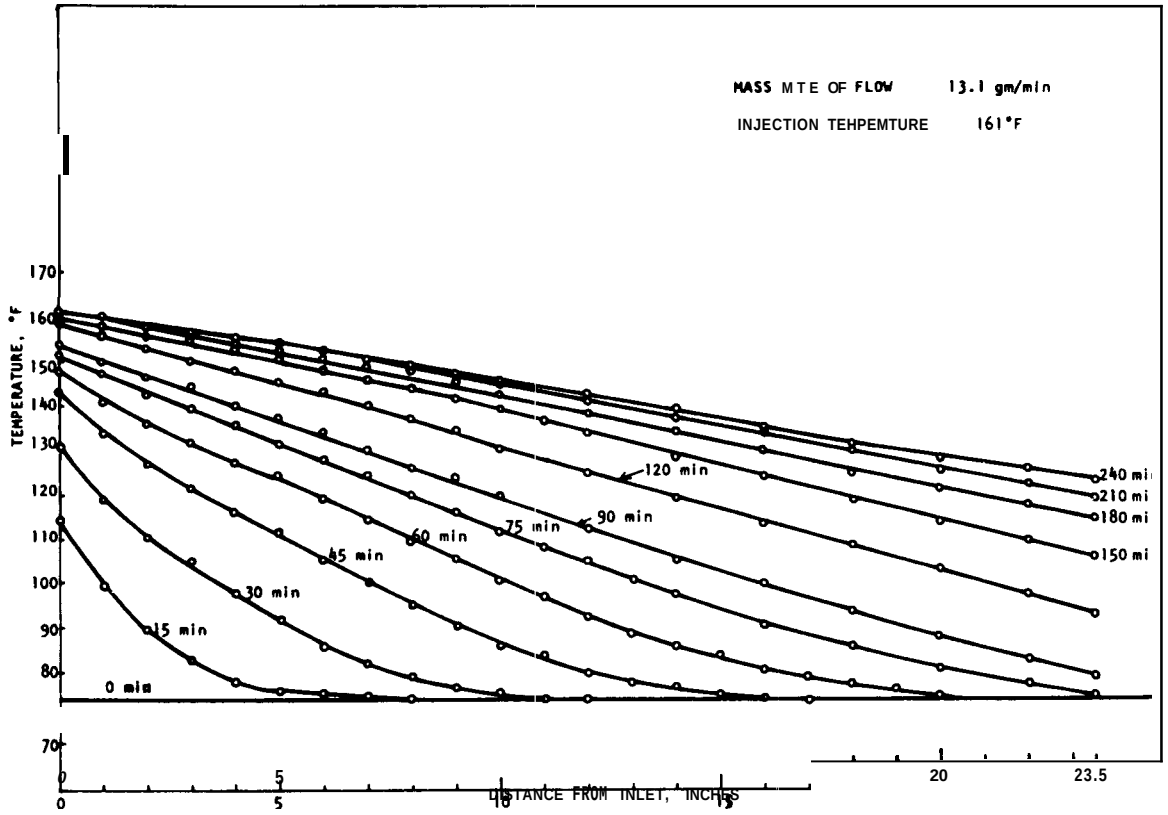

Figure 19. Temperature vs. Distance for Hot Water Injection.

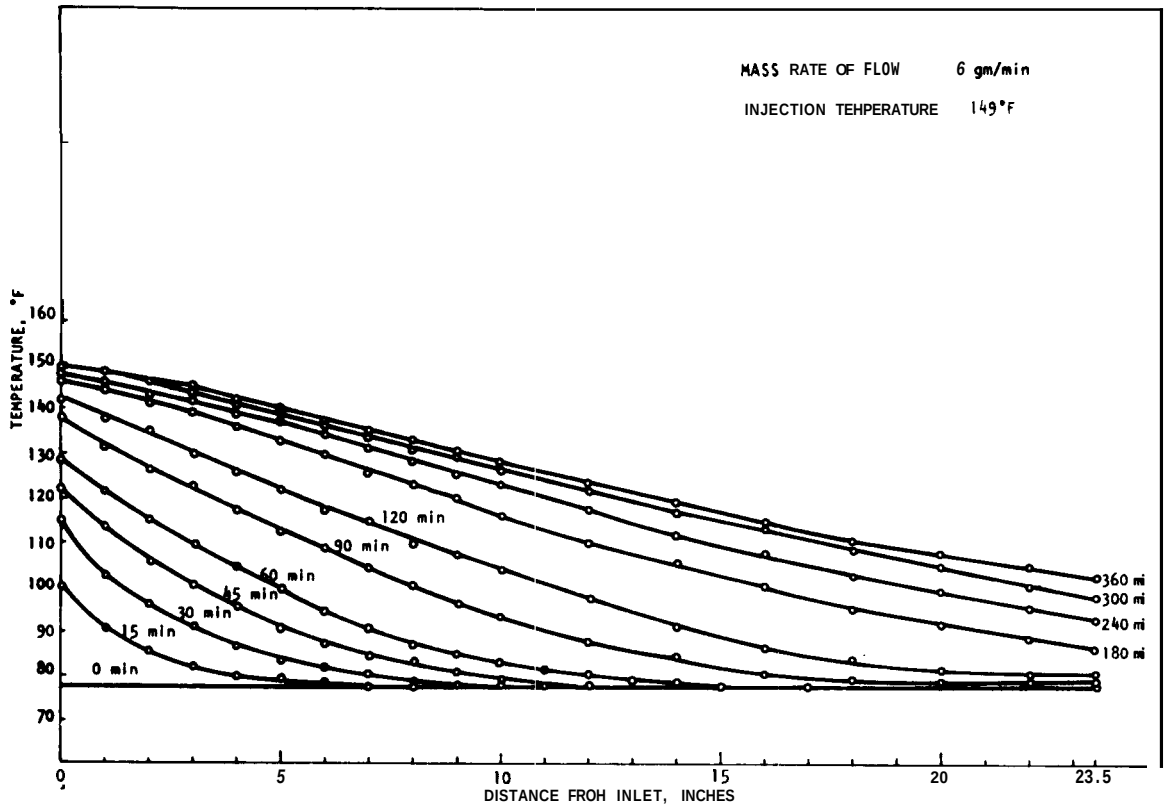

Figure 20. Temperature vs. Distance for Hot Water Injection.

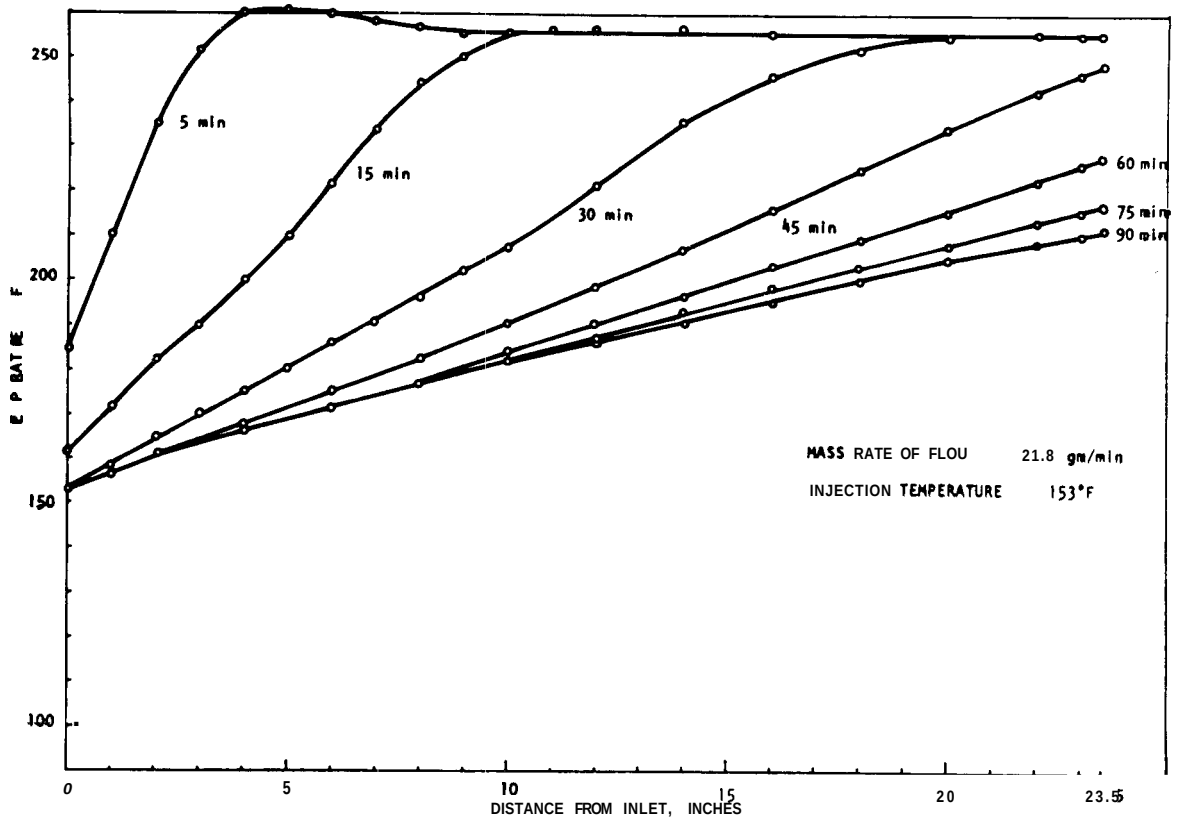

Figure 21. Temperature vs. Distance for Cold Water Tnjection.

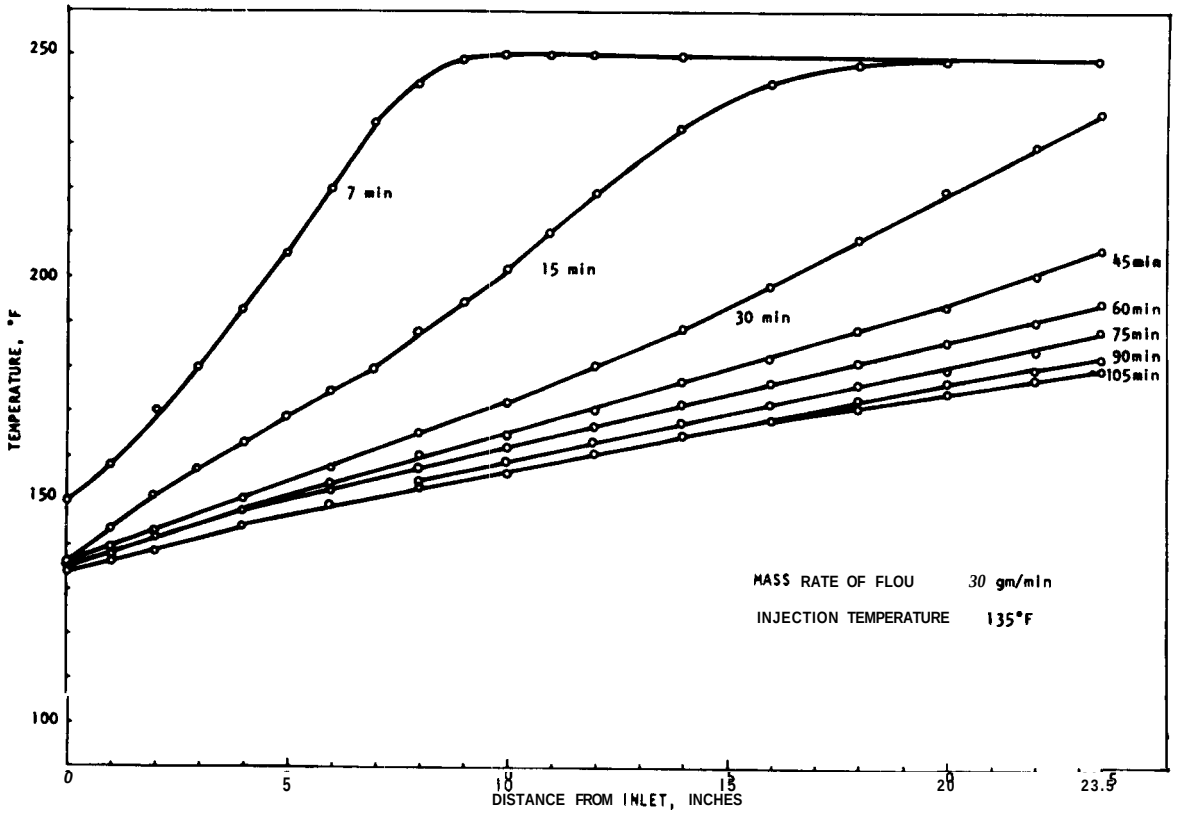

igure 22. emperature vs. Distance for Cold Water Injection.

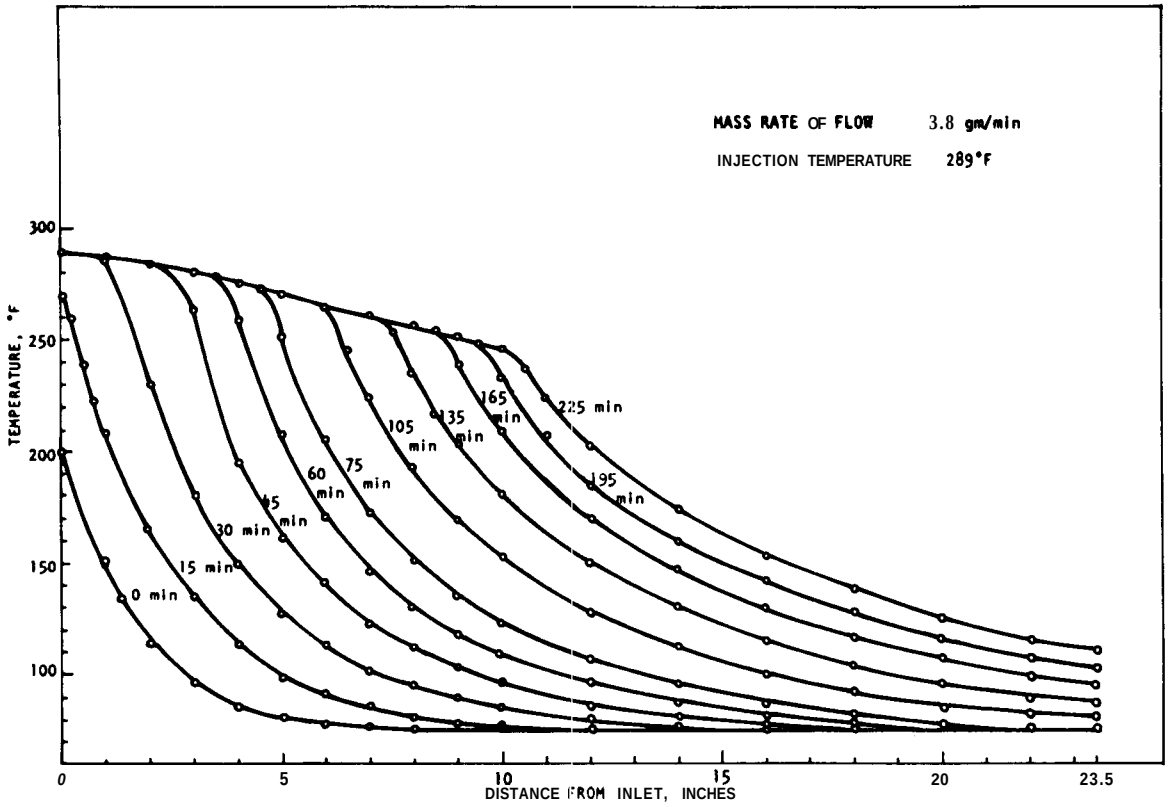

Figure 23. Temperature vs. Distance for Steam Injection.

water injection for heat scavenging in geothermal energy operations. The thermal efficiency can be determined readily by integration of the sensible heat with respect to volume of the core (see Crichlow). In regard to the overall heat transfer coefficient for the core holder, several interesting possibilities can be seen in Figs. 19-23. For the single phase flow experiments, the temperature profiles become linear at long injection times indicating the heat loss per unit length is a constant. Thus the total heat. loss can be averaged and a simple determination of the overall heat transfer coefficient made. Another possibility can be seen in Fig. 23 for the steam injection case. The linear portion of the temperature profiles from the inlet of the core is the condensing steam region. All radial heat loss would have to be supplied by latent heat of condensation. The sharp break downwards indicates that all steam has been condensed. It is thus possible to determine the heat loss from the inlet of the core to the steam front, and thus the overall heat transfer coefficient.

At this stage, our main effort has gone into design, construction, and preliminary operation of the apparatus. Learning to make satisfactory synthetic sandstone cores was a painstaking procedure itself. Although a great deal of experimental information has been obtained, far beyond that illustrated in the preceding figures, it has not been possible to make other than preliminary analyses of the data. These analyses will be made in the near future.

Two-Phase Flow Experiments

It should be clear that the steam injection experiment shown on Fig. 23 actually involves two-phase flow of steam and liquid water in the steam zone from the core inlet to the steam front. More work will be done with this sort of experiment. But the main experiment considered under the category of "Two-Phase Flow Experiments" was steady injection of hot, compressed liquid water into one end of a core at a rate such that a boiling front would form somewhere within the core length leading to a definitive two-phase, declining temperature and pressure flow region.

The experimental procedure is as follows, First, the core is saturated with water and heated to an initial temperature and pressure well within the compressed liquid region for flat-surfce water-steam equilibrium. During the heating procedure, hot water is circulated at a low rate through the core with the outlet conditions maintained in the liquid region. After temperatures along the axis have stabilized, two-phase flow is initiated by opening the outlet valve and increasing the flow rate and thus the pressure drop across the core. A variety of experimental conditions can be ohtained by changing the inlet temperature and the pressure drop across the core,, Pressures at the five transducer taps and temperature in the axial direction are measured. It is possible to achieve very steady temperature and pressure distributions, although it had been anticipated that conditions would never be truly steady state.

Figure *24* presents temperature vs distance along the core for injection of cooler water into a core initially containing hot water. This is an interesting experiment which will he subject to replication and a great deal of analysis in the coming year. Figures 25-28 show temperature and pressure vs distance along the synthetic core for a range of flow rates. These figures show it is experimentally possible to produce significant changes in both temperature and pressure within the two-phase boiling flow region in the synthetic core. Analyses of these runs have not been completed at this time. As described in Progress Report No. 1, calculation of the heat loss via the overall heat transfer coefficient should permit calculation of the flowing relative permeability ratio (effective liquid permeability divided by effective gas permeability) at each point along the core, If liquid saturation (pore volume fraction containing liquid phase) can be determined, it will be possible to produce relative permeabilities to steam and hot water vs liquid content. The preliminary runs described in the preceding figures were made with synthetic cores without the glass tube for the dielectric constant liquid saturation probe. The main purpose had been the checking of the design parameters other than liquid content measurement. At the time of this reporting, a synthetic core with a glass liquid content probe has been made and

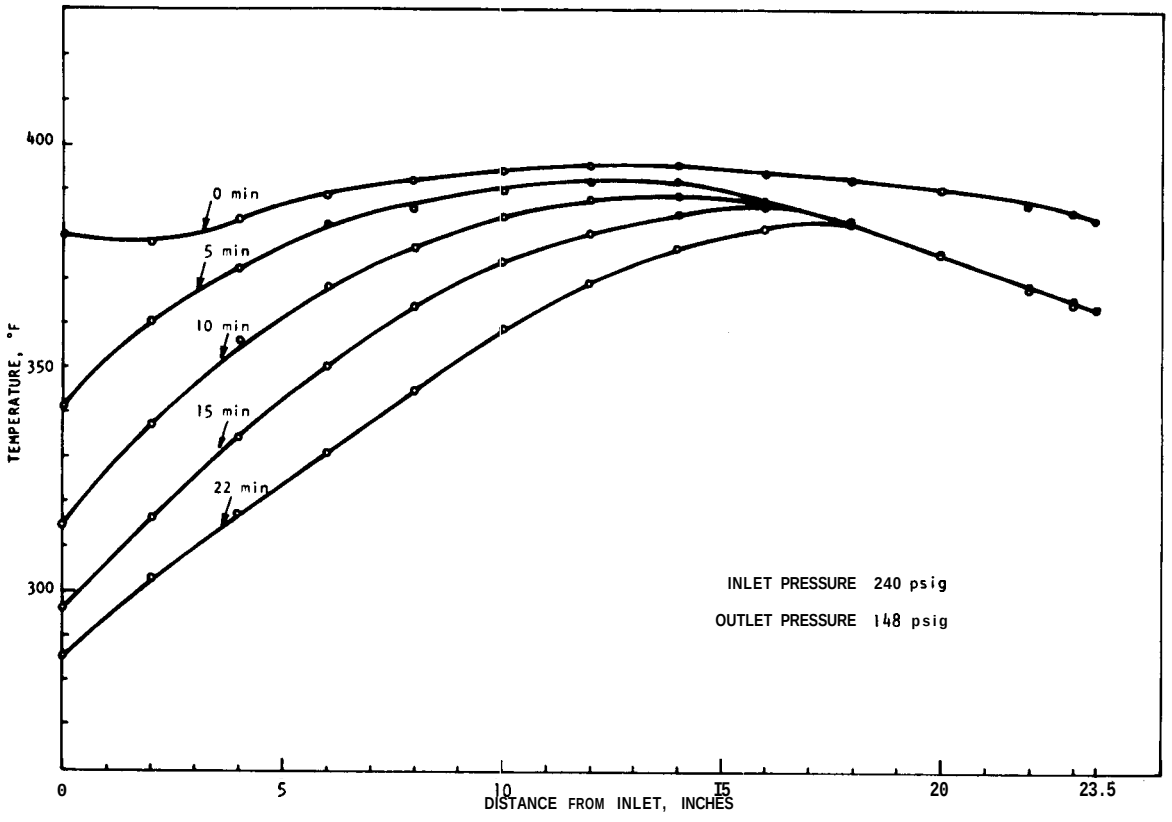

Figure *24.* Temperature vs. Distance for Two-Phase Flow.

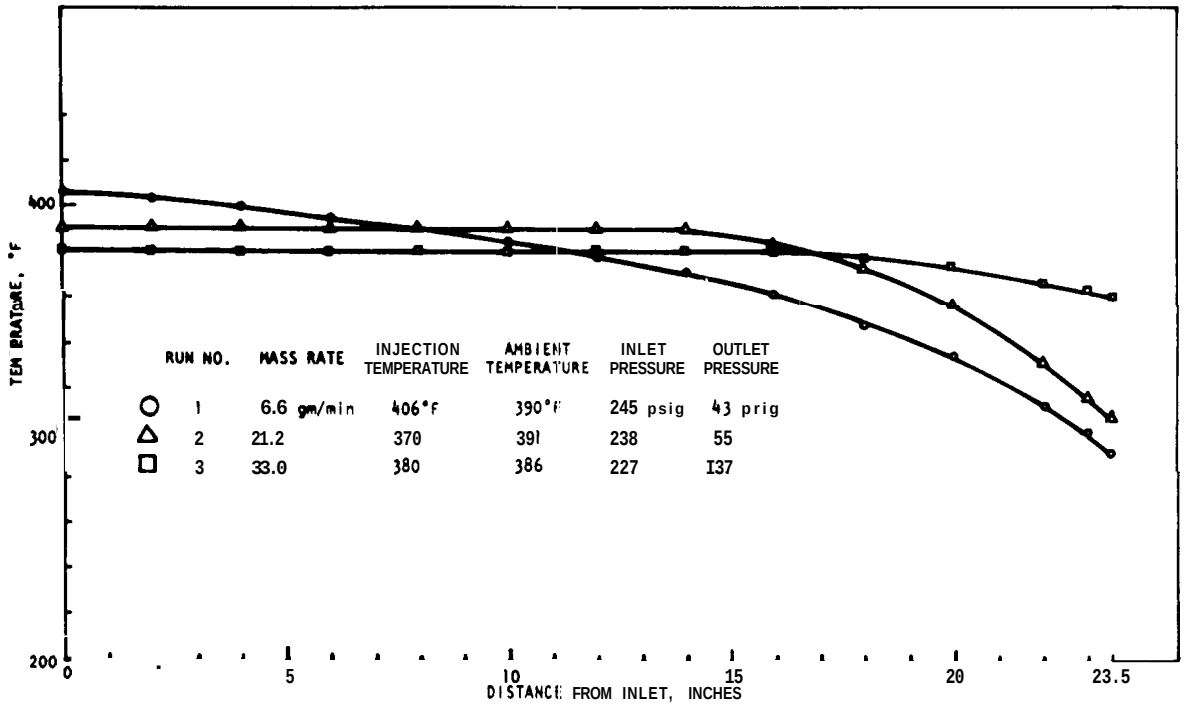

Figure 25. Temperature vs. Distance for Two-Phase Flow.

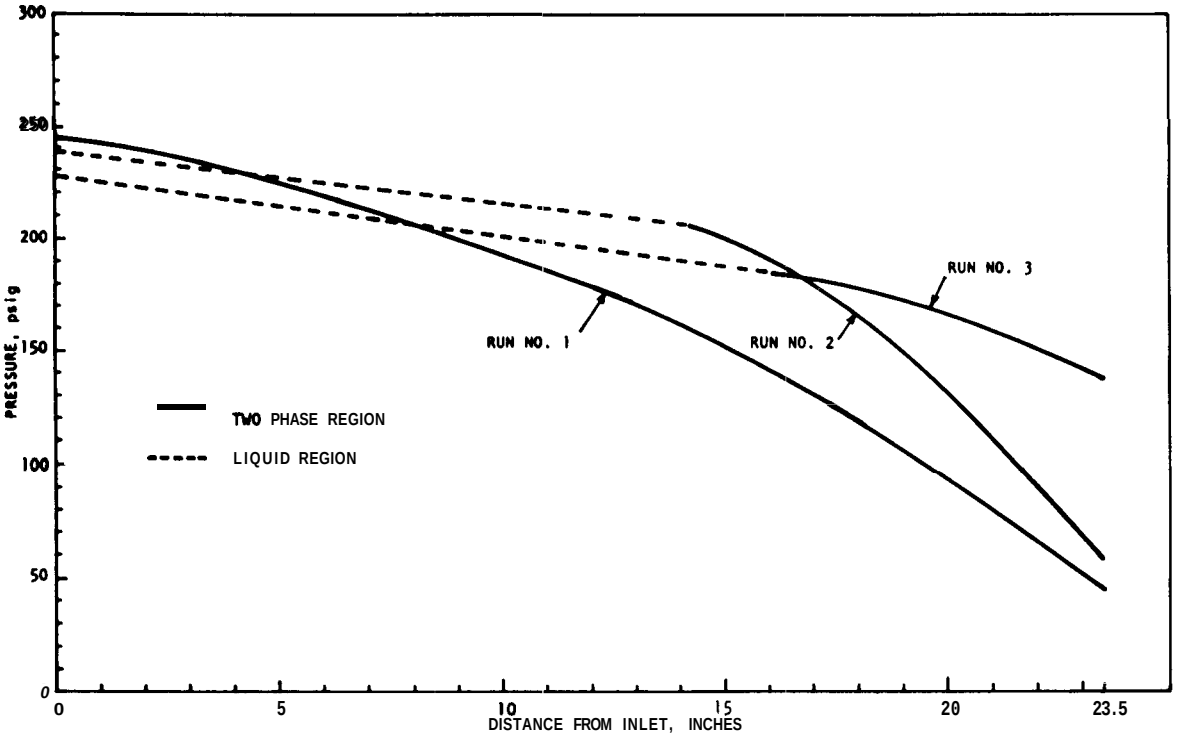

Figure 26. Pressure vs. Distance for Two-Phase Flow.

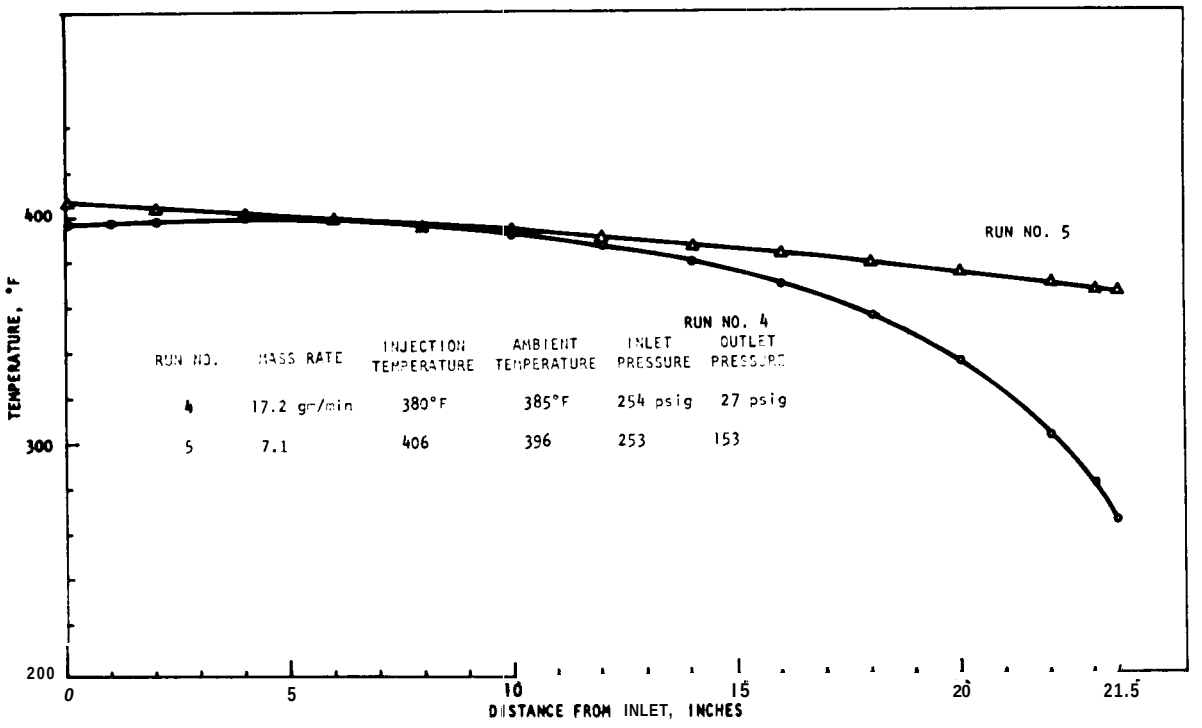

Figure 27. Temperature vs. Distance for Two-Phase Flow.

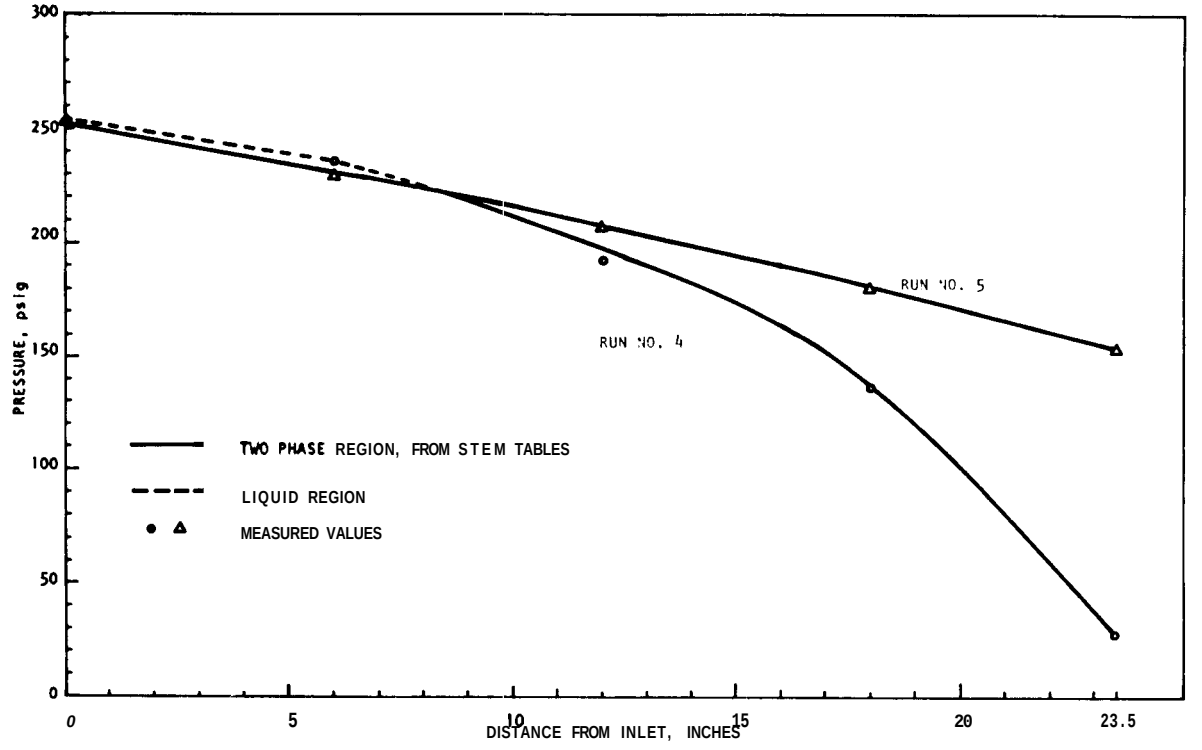

Figure 28. Pressure vs. Distance for iwo-Phase Plow.

tested at room temperature. During heating of the air bath, it appears the pyrex tube failed and we are currently exploring the reason for the failure. It is reassuring that the probe appeared to be functioning well prior to the failure.

As an aid to the planning of liquid content measurement, calculations of potential liquid saturations for runs such as Runs 2 and 4 were made, To do this calculation, it was necessary to assume a relative permeability ratio-liquid saturation relationship. Two cases were assumed: the data of Weinbrandt for consolidated sandstones, and the Muskat, Wykoff and Botset data for unconsolidated sands. Figure 29 presents the computed liquid saturation vs distance along the core, and Fig. 30 presents the calculated steam-water relative permeabilities. It is likely that the Weinbrandt data will be closer to reality for the consolidated cores of this study than the unconsolidated sand data of Muskat, et al.

Future Plans

This project requires slow, painstaking experiments to achieve high quality information. In order to minimize waste of resources, a single apparatus has been used during the last year with minimal instrumentation necessary to achieve typical results. With the exception of the liquid saturation probe, all design systems have been proven as operational. During the coming period, it is intended to duplicate the bench-scale models such that several cores can be run in parallel, rather than in series. This should speed acquisition of data considerably. In addition, functional instrumentation (particularly pressure transducer taps) will be increased to provide more detail. in profile data.

Another major effort will be proving the liquid saturation dielectric constant probe, or selection of some alternate system (radioactive tracers, microwave attenuation, gamma ray, etc.). Because Baker has used the dielectric probe under steam injection in other flow model work, we are hopeful that this method will prove successful. But whether successful or not, it appears wise to prepare a thorough study of the

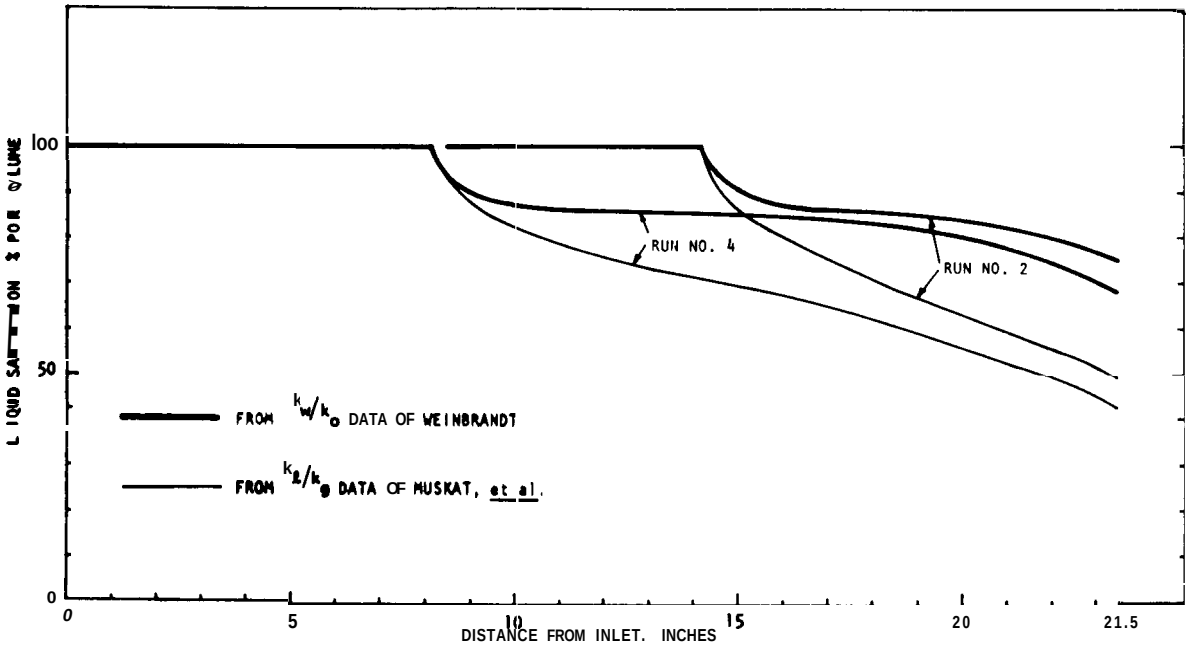

Figure 29. Calculated Liquid Saturation vs. Distance for Two-Phase Flow.

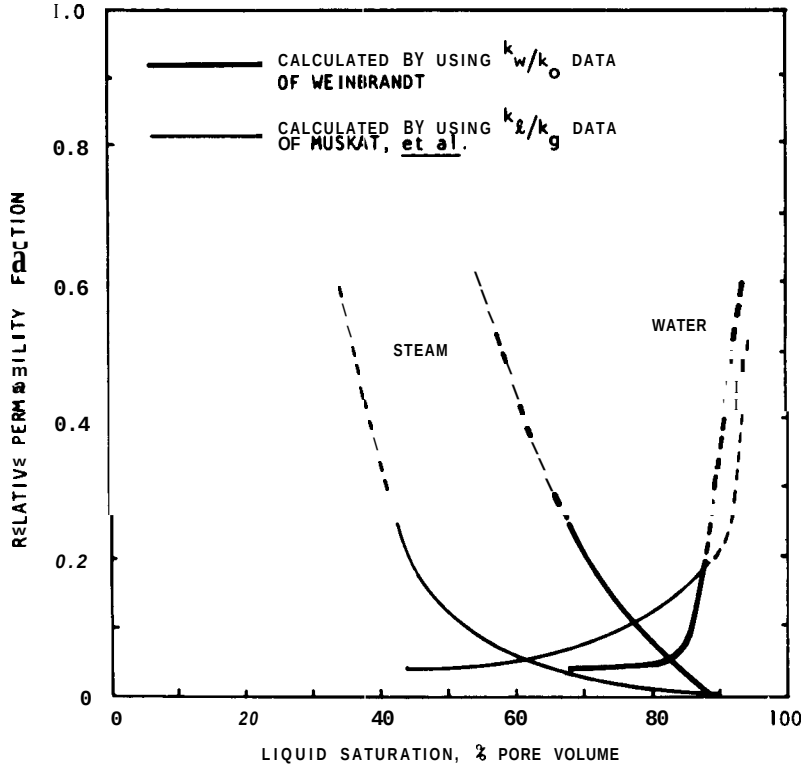

Figure 30. Calculated Water-Steam Relative Permeability.

variety of methods which might be useful for this purpose. In-place phase saturation determination has always been a difficult problem in multiphase flow in porous media.

LABORATORY EXPERIMENTS

During the last year, it has become apparent that several laboratory experiments should be run in parallel rather than in series if the application of research results to practical problems can be made to meet national energy objectives. For this reason, several experiments were moved up in the program time schedule. These included experiments on heat and mass transfer in porous fractured rocks and fractured non-porous rocks, and operation of geothermal reservoir models. A discussion of each follows.

Mass Transfer in Porous and Fractured Media

Fractured porous rocks contain two types of void space; macropores, which are void volumes between rock fragments, and micropores, the pore space inside individual rock fragments, Micropores may be either natural porosity or fractures. Fluid flow through certain geothermal reservoirs is expected to occur primarily through the macropores. However, if mass transfer does exist beteen the water inside the micropores and potentially cooler water in the macropores, heat extraction by circulating fluids may be significant,

Heat may be recovered from fractured rock in a geothermal reservoir by circulation of geothermal fluids through the formation. The heat transfer is accomplished by two mechanisms; forced convective heat transfer and fluid mass transfer. Forced convective heat transfer occurs between the hot rock and the injected fluid flowing through the macropores. The mechanism of fluid mass transfer between hot water inside the micropores and cooler water inside the macropores has not been studied,

The study of mass transfer phenomena inside a highly fractured geothermal reservoir can be simplified by measurement of mass transfer within individual rocks. An effective means of making such studies is by addition of a tracer to the micropore water. A tracer which has proven of immense value in studies requiring chemical and physical properties essentially similar to water is the radioactive isotope of hydrogen,

^{3}H, (tritium, T), available in the form of tritiated water, HTO. The preliminary laboratory experiments involve spherical rocks initially saturated with tritiated water. These rocks are suddenly immersed in a completely-mixed tank of unlabeled water, and measurements of the concentration of the tritiated water in the external water are made as a function of time.

A mathematical model has been designed to represent this physical system. The mass transport is evaluated in terms of an effective diffusivity parameter. The mathematical model then can be used to plan the laboratory experiments to test: the validity of the concept and to estimate the value of the effective diffusivity parameter. If the model is valid, the effective diffusivity determined from the experimental data can be related to rock properties by parameters which have reasonable values.

The Mathematical Model--Figure 31 represents a time sequence of a simple model of diffusion of tritiated water from a single rock into a surrounding fluid. An effective core of porous, permeable rock of radius r_c is used to denote the average spherical region into which the external water front has not yet diffused, so that the initial concentration of tritiated water within the core, C_c, is constant. Figure 31a shows the concentration profile in a rock initially saturated with N_i molecules of HTO in a surrounding fluid of external water with zero molecules of HTO. Figure 31-b represents the HTO concentration in the rock at time t. Figure 31-C exhibits the HTO concentration after an infinite time.

With the assumption of a pseudo-steady state system in which, after an initially rapid transient period, the rate of change of concentration is slow, the transfer rate of the tritiated water is constant throughout the diffusion zone and is given by:

$$\frac{dN}{dt} = -4\pi r^2 Q = 4\pi R^2 Q_S = 4\pi r_c^2 Q_c = \text{constant} \qquad (23)$$

where:

N = number of molecules of tritiated water

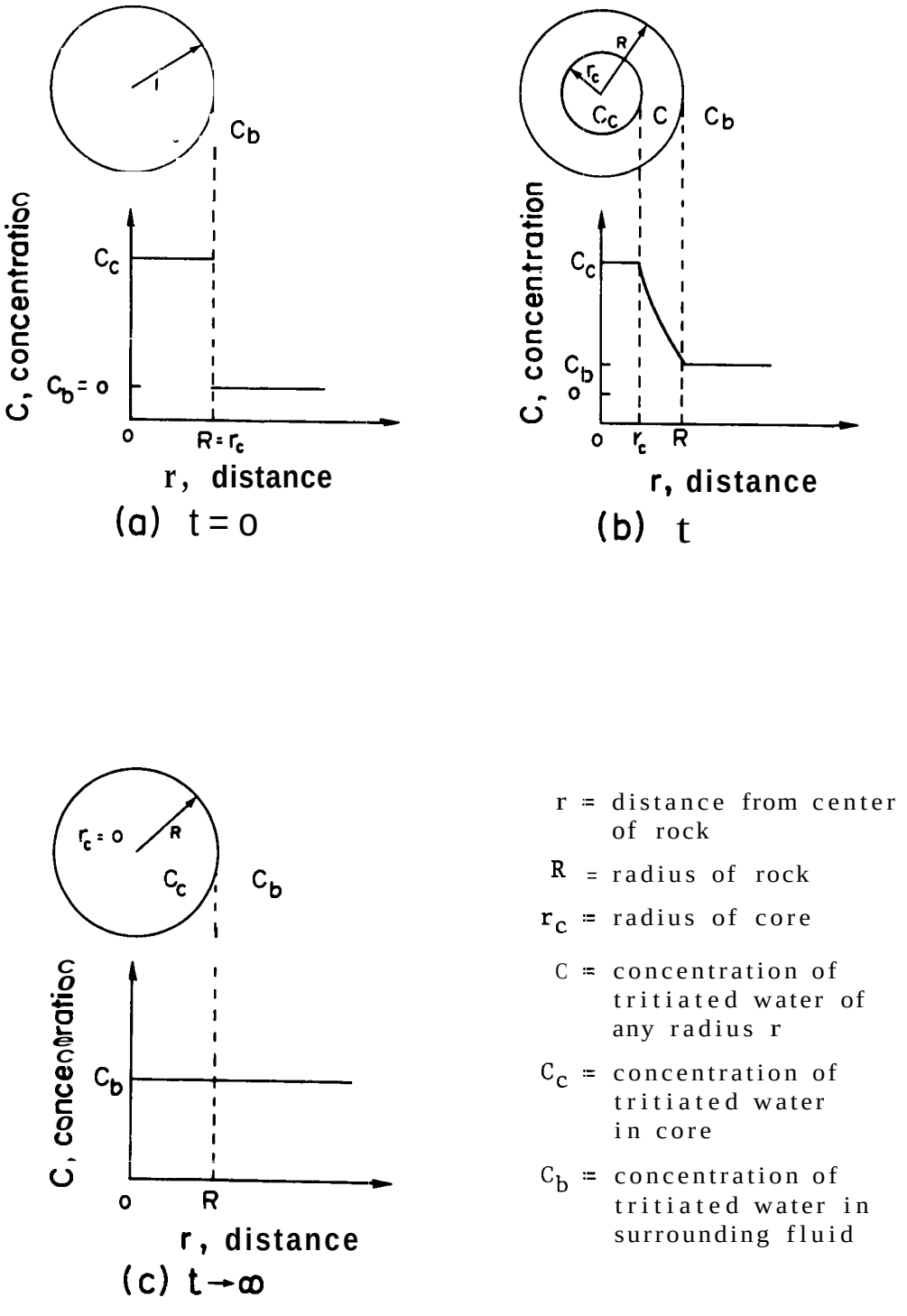

Figure 31. Representation of Diffusion into a Spherical Rock as a Function of Time.

Q = flux of tritiated water through a surface at radius r

Q_S = flux of tritiated water through the rock surface

Q_C = flux of tritiated water through the core surface.

The flux of tritiated water through the surface at radius r may be expressed by Fick's law for diffusion as:

$$Q = D_e \frac{dC}{dr} \tag{24}$$

where D_e is the effective diffusion coefficient of water in the rock. The value of D_e should be a function of the porosity and permeability of the porous media, and of the orientation, density and connection of fractures.

From (23) and (24), we can obtain the transfer rate through a surface of radius r as:

$$\frac{dN}{dt} = 4\pi r^2 D_e \frac{dC}{dr} = \text{constant} \tag{25}$$

The transfer rate in the partially diffused rock can be related to the core radius by integrating (25) from R to r_c.

$$\frac{dN}{dt}\int_R^{r_c} \frac{dr}{r^2} = 4\pi D_e \int_{C_b}^{C_c} dC \tag{26}$$

with the solution:

$$\frac{dN}{dt} = 4\pi D_e (C_c - C_b)\frac{Rr_c}{(r_c - R)} \tag{27}$$

However, the size of the core does change slowly with time, and as the core shrinks, the transfer rate will also decrease, The decrease of tritiated water in the core, dN, is related to dr_c by:

$$dN = \phi\frac{4}{3}\pi C_c \, d(r_c^3) = \phi 4\pi C_c r_c^2 dr_c \tag{28}$$

where ϕ is porosity of the rock.

Replacing dN in (27) by (28), we obtain:

$$\phi C_c r_c^2 \left(\frac{1}{R} - \frac{1}{r_c}\right)\frac{dr_c}{dt} = D_c (C_c - C_b) \tag{29}$$

or:

$$\phi C_c \left(\frac{1}{R} - \frac{1}{r_c}\right) r_c^2 dr_c = D_c (C_c - C_b) dt \tag{30}$$

Integrating from the end of the rapid transient period,

$$\phi C_c \int_r^{r_c} \left(\frac{1}{R} - \frac{1}{r_c}\right) r_c^2 dr_c = D_e \int_0^t (C_c - C_b)^{dt} \tag{31}$$

The effective diffusivity, D_e, is:

$$D_e = \frac{C_c R^2 [1 - 3(\frac{r_c}{R})^2 + 2(\frac{r_c}{R})^3]}{6\phi \int_0^t (C_c - C_b) dt} \tag{32}$$

The effective core radius, r_c, can be related to measurable quantities through a material balance for the tritiated water. The tritiated water exists in three phases: core, the surrounding fluid, and the layer between the core and the surrounding fluid.

Because the core concentration, C_c, is constant, and the external fluid concentration, C_b, can be measured, only the distribution of tritiated water in the intermediate layer needs to be determined. The pseudo-steady state material balance of tritiated water in the intermediate layer at time t results from the following equation:

$$\frac{d^2C}{dr^2} - \frac{2}{r}\frac{dC}{dr} = 0 \tag{33}$$

with the boundary conditions: $C = C_b$ at $r = R$ and $C = C_c$ at $r = r_c$. The solution of (33) is:

$$C = \frac{C_c - C_b}{\frac{1}{r_c} - \frac{1}{R}} \frac{1}{r} - \frac{RC_b - r_c C_c}{R - r_c} \tag{34}$$

The initial amount of tritiated water in the rock is given by:

$$N_i = \frac{4}{3}\pi R^3 \phi C_c \tag{35}$$

At time t, the inventory of tritiated water is distributed in the core, the surrounding fluid, and the intermediate layer:. The amount inside the core is:

$$N_c = \frac{4}{3}\pi r_c^3 \phi C_c \tag{36}$$

The amount in the surround fluid is:

$$N_b = C_b V, \tag{37}$$

where V is the volume of the external fluid. The amount in the intermediate layer can be obtained from:

$$N_\ell = \int_{r_c}^{R} \phi C 4\pi r^2 dr \tag{38}$$

Substituting *(34)* into *(38)* results in

$$N_\ell = \int_{r_c}^{R} \phi\pi\ 4\ r^2 \left(\frac{C_c - C_b}{\frac{1}{r_c} - \frac{1}{R}} \frac{1}{r} + \frac{RC_b - r_c C_c}{R - r_c} \right) dr$$

$$= \frac{2\pi\phi(C_c - C_b)}{\frac{1}{r_c} - \frac{1}{R}}(R^2 - r_c^2) + \frac{4\pi\phi(RC_b - r_c C_c)}{3(R - r_c)}(R^3 - r_c^3) \tag{39}$$

Therefore the material balance for tritiated water in the total system can be written as:

$$\frac{4}{3}\pi R^3 \phi C_c = \frac{4}{3}\pi r_c^3 \phi C_c + C_b V + \frac{2\pi\phi(C_c - C_b)}{\frac{1}{r_c} - \frac{1}{R}}(R^2 - r^2)$$

$$+ \frac{4\pi\phi(RC_b - r_c C_c)}{3(R - r_c)}(R^3 - r_c^3) \tag{40}$$

and simplified to:

$$\left[\frac{2}{3}\pi R\phi(C_c - C_b)\right] r_c^2 + \left[\frac{2}{3}\pi R^2 \phi(C_c - C_b)\right] r_c + \left[C_b V - \frac{4}{3}\pi R^3 \phi(C_c - C_b)\right] = 0 \tag{41}$$

Equation *(41)* relates the measurable quantities, C_c, C_b, R, ϕ and V, to the effective core radius r_c for a pseudo-steady-state model, The effective diffusivity, D_e, can be calculated from (32) and *(41)* from the known values of R, ϕ, V, C_c, and the measured values of C_b as a function of time.

Proposed Experiment--A sphere of sandstone saturated with tritiated water of known concentration is suddenly placed in a completely-mixed tank of water. The concentration of tritiated water in the tank is measured at several times with a liquid scintillation counter. From these data, a curve of the concentration as a function of time can be obtained. A schematic of the experiment is given in Figure 32.

The effective diffusivity, D_e, can be determined from (32) and *(41)* by graphical integration of $\int_o^t (C_c - C_b)dt$. One test of the validity of the model is the constancy of D_e over a reasonable period of time.

The effective diffusivity, D_e, is independent of the size of the rock sample. Another way to verify the validity of this model is to check whether D_e is reasonably constant for a range of rock sizes.

The effective diffusivity, D_e, should be sensitive to several properties of porous media, such as grain size and degree of cementation. Natural sandstone as well as artificial sandstone with different grain size and different degree of cementation will be employed in the experiments.

Fractures may be another important factor influencing D_e. Artificial fractures will be made in some rock specimens. Direction and connection of fractures may make D_e anisotropic. The effect of fractures on mass transfer will be further studied after experience has been gained with ideal porous media.

Heat Transfer in Fractured Rock

An important property of fractured rock in a geothermal reservoir is its thermal conductivity. The importance of artificial fracturing methods to stimulate the productivity of geothermal reservoirs will depend partly on the change in the thermal conductivity of the rock caused by

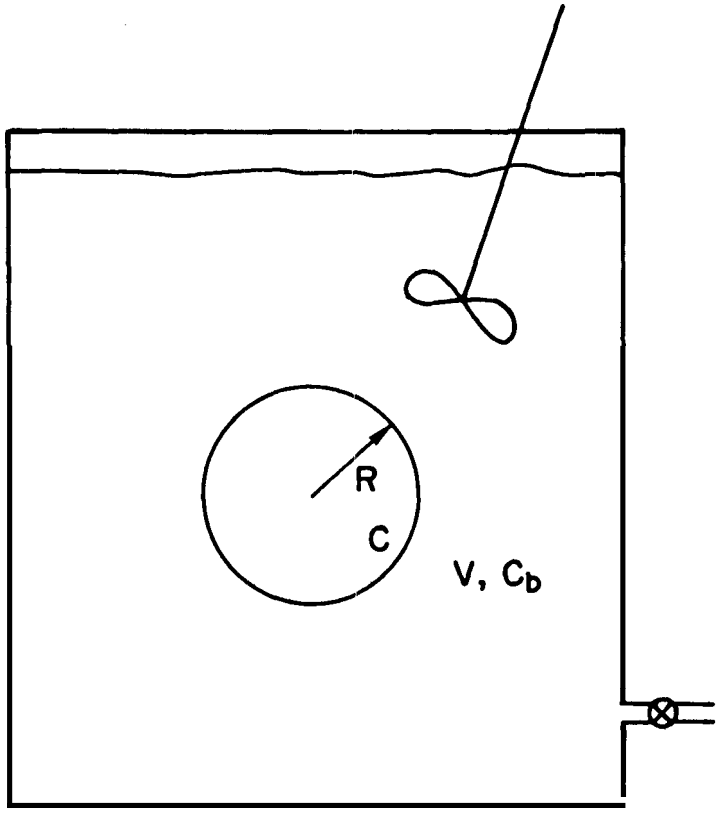

Figure 32. Schematic of Proposed Mass Transfer Experiment

fracturing. To our knowledge, there is no information on the effect of crack porosity on the thermal conductivity of rock samples. Appendix A lists five general approaches to the evaluation of effective thermal conductivity of a porous medium. The series parallel, and combination series-parallel models are derived from potential flow analogies. The geometric mean approach uses porosity to evaluate the effect of the pore conductivity on the effective conductivity of the media. The electric analog is developed from the similarity of electric conductivity through a solid containing inclusions to thermal conductivity through a solid containing pores (which act as heat flow barriers). Studies have been reported on the thermal conductivity of rock fragments in water (Sass and Lachenbruch, 1971). This study will examine the thermal conductivity of saturated consolidated rock with varying degrees of cracking. Figure 33 shows the hypothetical thermal conductivity vs porosity for a solid containing fractures. A lower conductivity results when heat flow is normal to existing cracks.

In an idealized geothermal reservoir, the void space may be filled with liquid water and/or steam. The pressure and temperature history of the reservoir and the mass produced and its enthalpy should determine the relative abundance of each phase. The effective heat conductivity of the rock-water system will depend depend at least on the fluid phases present. As the pressure is reduced, the liquid may flash to steam, and the thermal conductivity of the fluid could be reduced by a factor of 15 to 20, depending on the temperature of the fluid and other factors.

The heat extracted from the reservoir could be a function of the heat content of the geothermal fluids and the heat transfer from the ock to the produced fluid. The thermal conductivity of the rock would then affect the time response of the heat transfer from a hotter rock to a colder circulating fluid. This is generally expressed in terms of the Biot number, Bi, defined as the ratio of convective heat transfer, from the solid to the fluid, to the conductive heat transfer of the solid; and the Fourier modulus, Fo, defined as the ratio of the solid conductivity to the solid heat capacity. An energy balance on the rock-fluid system for a differential time can be expressed as:

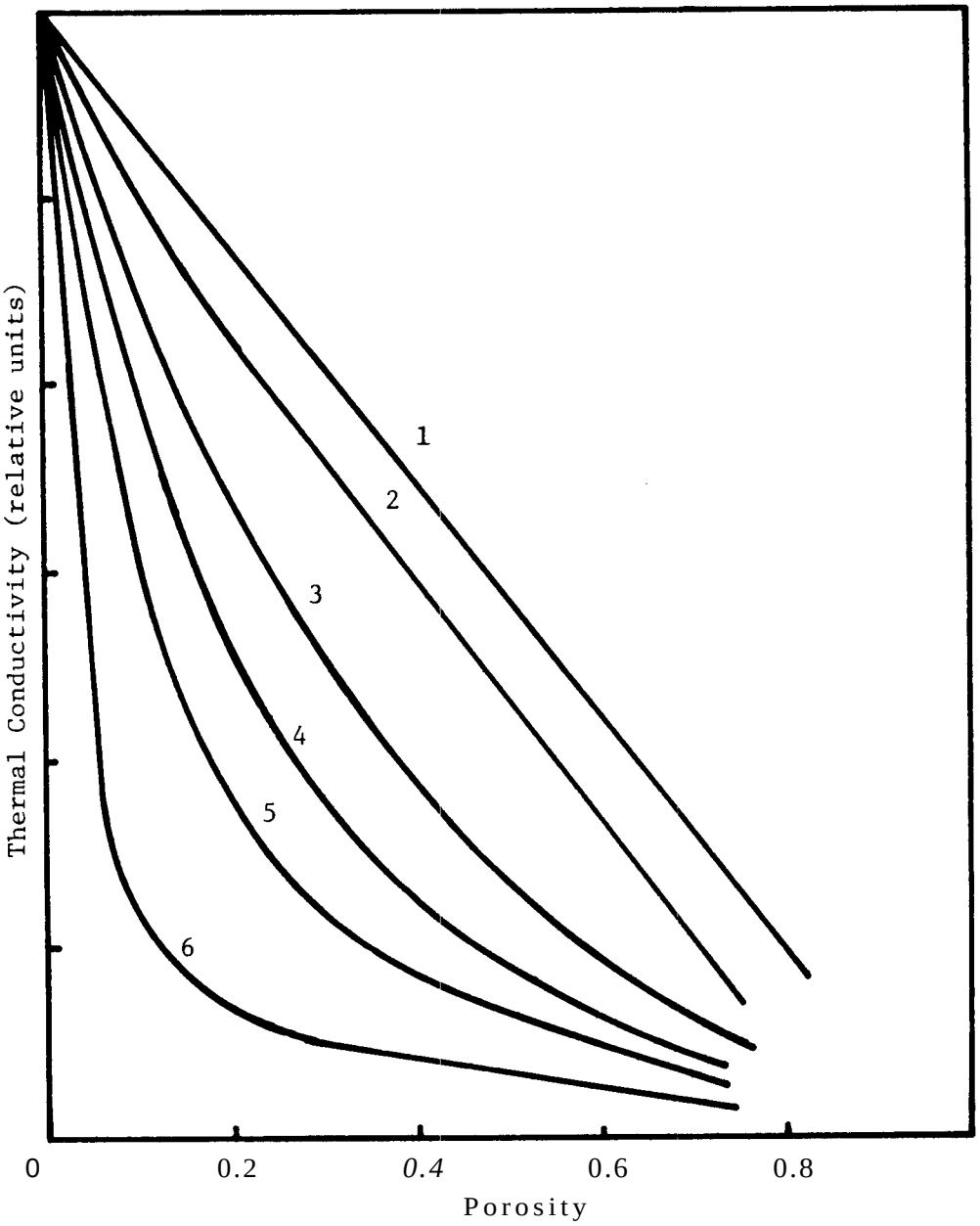

1. heat flow parallel to fractures
2. isolated spherical pores
3. isolated cubic: pores
4. mean curve of the cubic type
5. bimineral rocks (reduced to grain contacts)
6. heat flow across fractures

Figure 33. Relative Effect of Porosity on Thermal Conductivity.

$$\frac{dT}{(T - T_\infty)} = \frac{d(T - T_\infty)}{(T - T_\infty)} = \frac{hA_s}{c\rho V}\, dt \qquad (42)$$

where:

T = temperature (^oF)

T_∞ = temperature of circulating fluid (^oF)

A = surface area (ft^2)

c = heat capacity ($Btu/lb_m\,^oF$)

h = convective heat transfer coefficient ($Btu/hr\text{-}ft^2\text{-}^oF$)

t = time (hr)

ρ = density (lb_m/ft^3)

V = volume (ft^3)

Bi = Biot number (hL/k_s) (dimensionless)

Fo = Fourier modulus ($k_s t/cL^2$) (dimensionless)

ϕ = porosity (dimensionless)

L = characteristic length = V/A (ft)

Integration with respect to tine yields

$$\frac{T - T_m}{T_o - T_\infty} = e^{-(Bi)(Fo)} \qquad (43)$$

where T_o is the initial temperature of the rock (^oF).

Expressing *(42)* in terms of heat flow and integrating with respect *to* time yields:

$$\frac{Q}{hA\,(T_\infty - T_o)} = [1 - e^{-(Bi)(Fo)}]\left[\frac{c\rho L}{h_s}\right] \qquad (44)$$

where Q is the total heat flow (Btu/hr). Equation *(44)* is valid for Biot numbers less than 0.1 (Kreith, 1969). For these low Biot numbers, the internal resistance of the solid is small, and the internal energy needed *to* be removed to decrease the surface temperature a unit amount can be treated as a lumped parameter expressed by $c\rho V$. For larger values of Hi, i.e., small thermal conductivity or large L, the internal resistance must be taken into account. Solutions for this case which involves the ratio of the heat capacity of the rock to the heat capacity of the fluid

may be found in Carslaw and Jaeger (1959).

Temperature gradients arising in the rock could initiate a heat pipe effect, increasing the heat conduction. Pressure gradients associated with temperature gradients will cause evaporation in warmer parts and condensation in cooler parts of the system. The latent heat of evaporation accounts for the higher conduction of heat due to the heat pipe effect. An energy balance constructed about an elemental section yields an additional heat conduction term which is a function of the latent heat of vaporization, mass flow, temperature gradient, and saturation. The resulting thermal conductivity, $k_{h.p.}$, due to the heat pipe effect is:

$$k_{h.p.} = \frac{2\bar{m}h_{fg}l^2}{3\Delta T(1 - \phi S_v)} \tag{45}$$

where:

$k_{h.p.}$ = thermal conductivity of solid due to heat pipe effect (Btu/hr-ft-^oF)

$\bar{m}$ = average mass flow rate ($lb_m/hr\text{-}ft^3$)

h_{fg} = latent heat of vaporization (Btu/lb_m)

S_v = saturation (dimensionless)

l = length of specimen (ft)

Changes in effective pressure (overburden pressure minus pore pressure) also causes changes in the open crack spaces, The critical pressure necessary to close an ellipsoidal crack is given (Walsh, 1965) by:

$$P_c = \frac{\alpha\pi E}{4(1 - \nu^2)} \tag{46}$$

where:

P_c = critical pressure necessary to close a crack (lb_f/ft^2)

α = aspect ratio of the crack (ratio of length to width)

E = Young's Modulus (lb_f/ft^2)

ν = Poisson's Ratio

As the pore pressure is reduced the effective pressure increases, which

results in further closing of cracks with large aspect ratios. The increase in heat conduction with the pore pressure decline is due to a reduction in the number of low conductivity barriers to heat flow through the system.

The experimental objective of this study is the evaluation of the thermal conductivity of cracked, saturated granite. Uniaxial loading will produce long narrow slits which can be preferentially aligned normal to the applied heat flow. Samples cracked in this manner should exhibit the greatest change in thermal conductivity. Because the degree of cracking is related to the applied stress, specimens of varying degrees of cracking can be produced. Thermal conductivity measurements will be made before and after stressing of dry saturated samples (Messmer, 1964; Woodside and Messmer, 1961). The pressure effects (vaporization of pore fluid and crack closure) will be examined by measuring the thermal conductivity of samples saturated at elevated temperature with varying confining pressures. The heat pipe effects will be examined by producing a temperature gradient along the core axis. The use of fluids to saturate the rock with different latent heats of vaporization should show the extent of an increase in heat conduction due to the heat pipe effect in cracked rock specimens. The apparatus to be used to evaluate the mentioned parameters in terms of their effect on the thermal conductivity of fractured rocks is shown in Fig. 34. The apparatus is not drawn to scale. Rock specimens are right circular cylinders 1.5 inches in diameter and 3.0 inches long.

Geothermal Reservoir Physical Models

Whiting and Ramey originally postulated the application of energy and material balances to geothermal reservoirs. Although applied to a field case with at least limited success, later applications indicated a real need for modification within the bounds described by Whiting and Ramey (see Cady, 1969; Cady, Bilhartz, and Ramey, 1972; and Strobel, 1973). The cited works included both limited laboratory study and a single geothermal field case history. The need for actual data to test

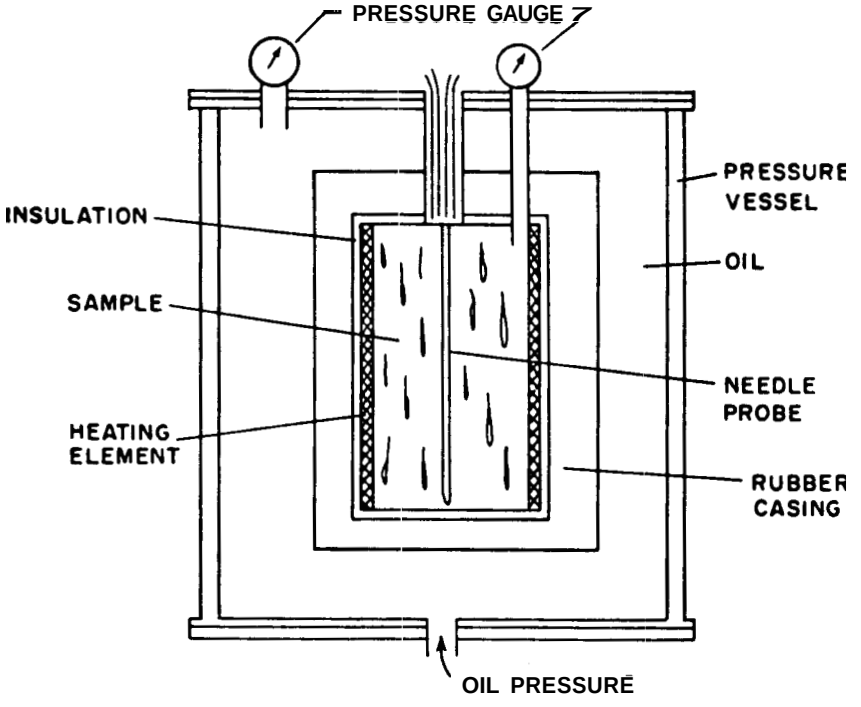

(a) Schematic

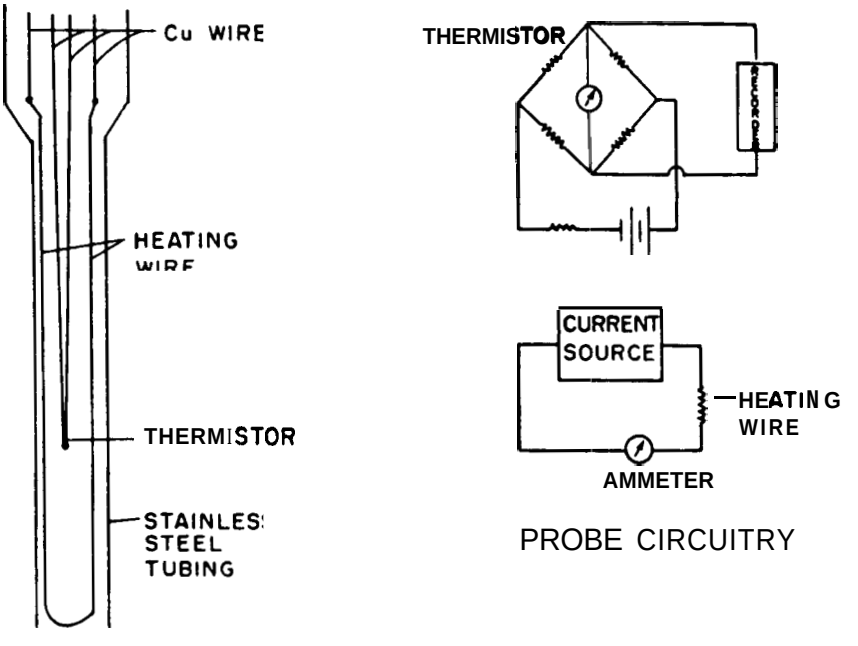

(b) Probe Design

Figure *34.* Thermal Conductivity Measurement Apparatus.

conceptual models has been apparent for some time (White, Muffler, Truesdell, and Donaldson). Previous works by Cady and Bilhartz concerned unconsolidated sand geothermal models. A previous study by Strobel did concern a consolidated sand, but there were not sufficient runs to establish reproducibility. For this reason, it was decided important to extend this experimental work of Strobel. A complete report on all previous studies was presented at the May 24, 1974 project meeting at Stanford University.

Strobel's study concerned cyclic production and reheating of a consolidated sandstone geothermal reservoir model. The sandstone was a natural core. This work will be repeated with both natural and synthetic sandstone cores with more complete instrumentation. Liquid saturations will be measured for the synthetic: cores during the runs. Strobel and previous workers were only able to keep material balances over the entire core. Techniques for manufacture of synthetic cores developed during the project to date should make this step straightforward. The core will be positioned vertically and produced from the top. These experiments will provide additional data for checking numerical modelling results.

RADON IN GEOTHERMAL RESERVOIRS

The study of radon occurrence and transport in geothermal resources has been undertaken as an initial evaluation of the use of radon as a diagnostic tool for studying performance of geothermal reservoirs, especially under conditions of stimulation. Another purpose was the initial evaluation of environmental implications of radon release. The objectives of this study included three major tasks: (1) selection and implementation of a method for measuring radon, (2) evaluation of possible field sampling techniques, and (3) survey of actual radon occurrence in geothermal resource areas, both vapor- and liquid-dominated.

Stimulation of geothermal energy extraction by explosive, hydraulic-fracturing, or thermal-stressing should result in increased specific surface area, effective porosity, and heat transfer rates.

Radon gas may serve as a useful natural tracer for evaluating such stimulation processes. Radon, with a half-life of 3.8 days, is a noble-gas product of its precursor 1602 year ^{226}Ra, present in rocks at a mean concentration of about 1 pg/g, generally in equilibrium with the natural uranium decay series. The buildup of radon activity from its radium parent to equilibrium concentration is shown in Fig. 35.

Radon emanation has been studied with respect to groundwater flow, natural gas production, and uranium prospecting (e.g., Tanner, 1964; Tokarev and Shcherbakov, 1960; Bunce and Sattler, 1966). The extent of radon release to convective geofluids is dependent on several factors including the distribution of radium through the rock matrix and the surface area available for escape of recoiling radon atoms into the fluid. For homogeneous rock, the release of radon is related to particle size, d, as $1/d^n$ where $0.5 \leq n \leq 1.0$ depending on the dominant mechanism of release (Andrews and Wood, 1972). In heterogeneous material other factors may obscure particle size dependence.

The concentration of radon in geofluids produced from a well in a fractured or porous medium depends on geometry and flowing characteristics as well as the emanation from rock to fluid. A simple linear model for flowing liquid in a homogeneous porous medium illustrates some of the

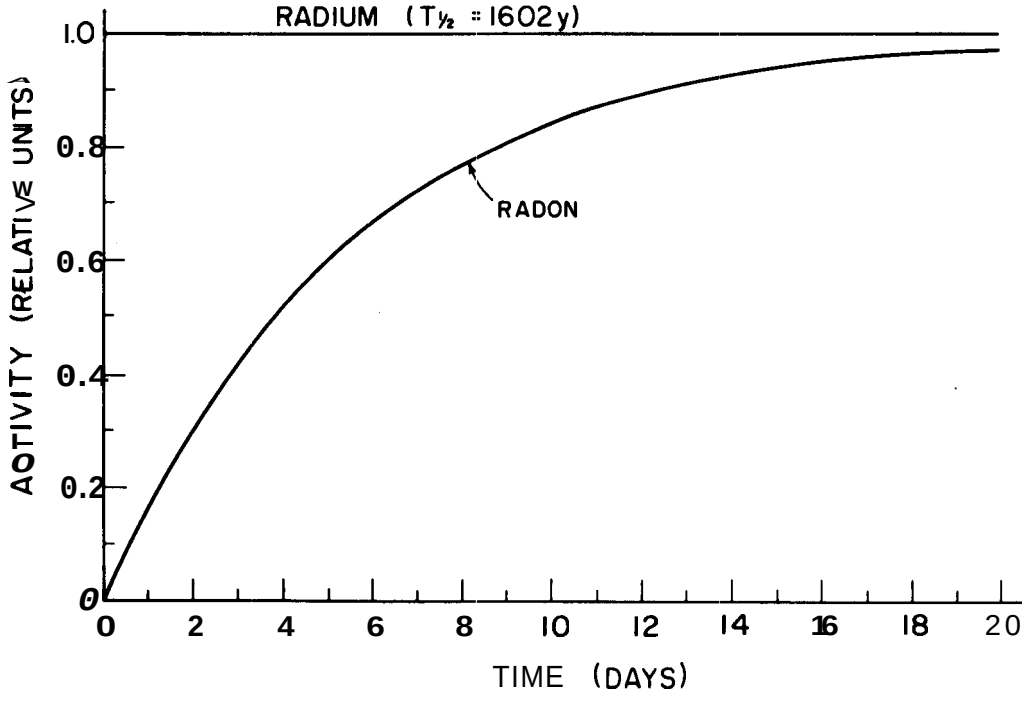

Figure 35. Radon Buildup, Radium Parent

possibilities. The system can be visualized by the following diagram

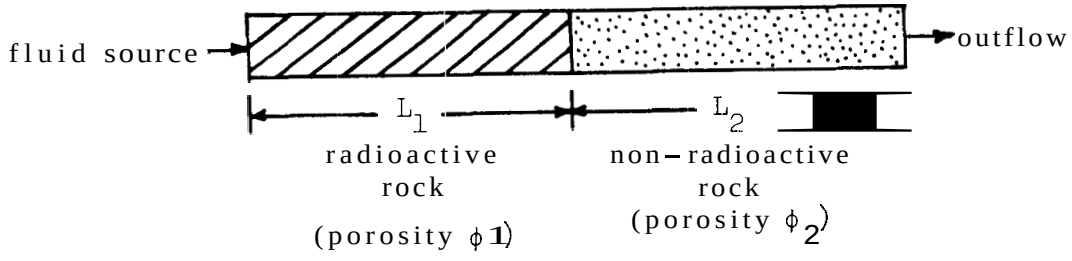

The concentration of radon (C) in the outflow will be given by:

$$C = \frac{E}{\phi_1 \lambda} \left[1 - \exp\left(-\frac{\phi_1 L_1}{Q}\lambda\right)\right] \exp\left(-\frac{\phi_2 L_2}{Q}\lambda\right) \qquad (47)$$

where:

Q = flow velocity (m/sec)

E = volumetric emanation of radon in radioactive rock (pCi/m^3 sec)

λ = decay constant for radon (sec^{-1})

For this geometry it is espacially easy to see that the flowrate will determine the residence time in the radioactive rock where radon concentration in the fluid will increase and approach the limiting value of secular equilibrium with the emanating power of the rock. Flow rate will also determine the residence time in the nonradioactive rock where radon could increase, decrease, or remain constant with flowrate, depending on the relation between the rock parameters and Q. One case of interest would be that of uniform emanation power in a large formation, that is, L_1 is very large and L_2 very small. In this case the concentration of radon in the outflow would be essentially independent of flowrate and be determined primarily by emanating power of the rock and the formation porosity.

A qualitatively similar result is obtained for steady-state radial flow of a fluid in homogeneous material. That is, in the case of uniform emanating power and a Large reservoir, the radon concentration in the outflow is expected to be essentially independent of flowrate. A mathematical model of compressible gas flow transport of radon (Sakakura, Lindberg, and Faul, 1959) also indicates that. radon concentration in natural gas is only slightly dependent on flowrate in the case of a

large reservoir of rock of uniform emanating power.

Thus, it would be expected that radon in geothermal fluids will be strongly influenced by the emanating power of the rock and the effective porosity of the medium. Both of these parameters may be expected to be changed by stimulation techniques. Both can be expected to be strongly related to the geological setting and history of a resource area. For example, Wollenberg (1974) indicates that radium and radon activity is much higher in $CaCO_3$ dominated systems as compared to silica dominated systems. Accordingly, our field sampling program was established to include different geologic situations.

The question of radon as a possible environmental contaminant has been raised by Scott (1972) largely on the basis of data obtained in New Zealand resource areas (Belin, 1959). Large radon concentrations were observed in fumaroles and pools in the Rotorua-Taupo region. Therefore, our sampling program was also conducted with a view to estimating the magnitude of any potential environmental problem. Some of the tasks already accomplished include:

1. Radon Measuring System

The radon measuring system was selected on the basis of three principal criteria: reliability, wide range of response, and low background. A secondary criterion was compatibility with existing counting equipment in order to minimize unnecessary expense. The technique, chosen after consultation with other workers, is based on adsorption of radon on activated charcoal and measurement by scintillation counting. The approach has been utilized extensively in health physics applications (Lucas, 1957, 1964).

The apparatus was constructed in two parts. The vacuum line system, shown in Fig. 36, includes traps for removing water vapor and CO_2 prior to adsorption of radon on cooled charcoal. A heater on the charcoal trap permits subsequent desorption of the collected radon. A peristalic pump is used to transfer the radon in helium carrier gas into small scintillation flasks which have a coating of activated zinc sulphide. The second part of the apparatus, shown in Fig. 37, is the detection system. A standard 2-inch photomultiplier tube fitted in a specially constructed light baffle is connected to a conventional power supply

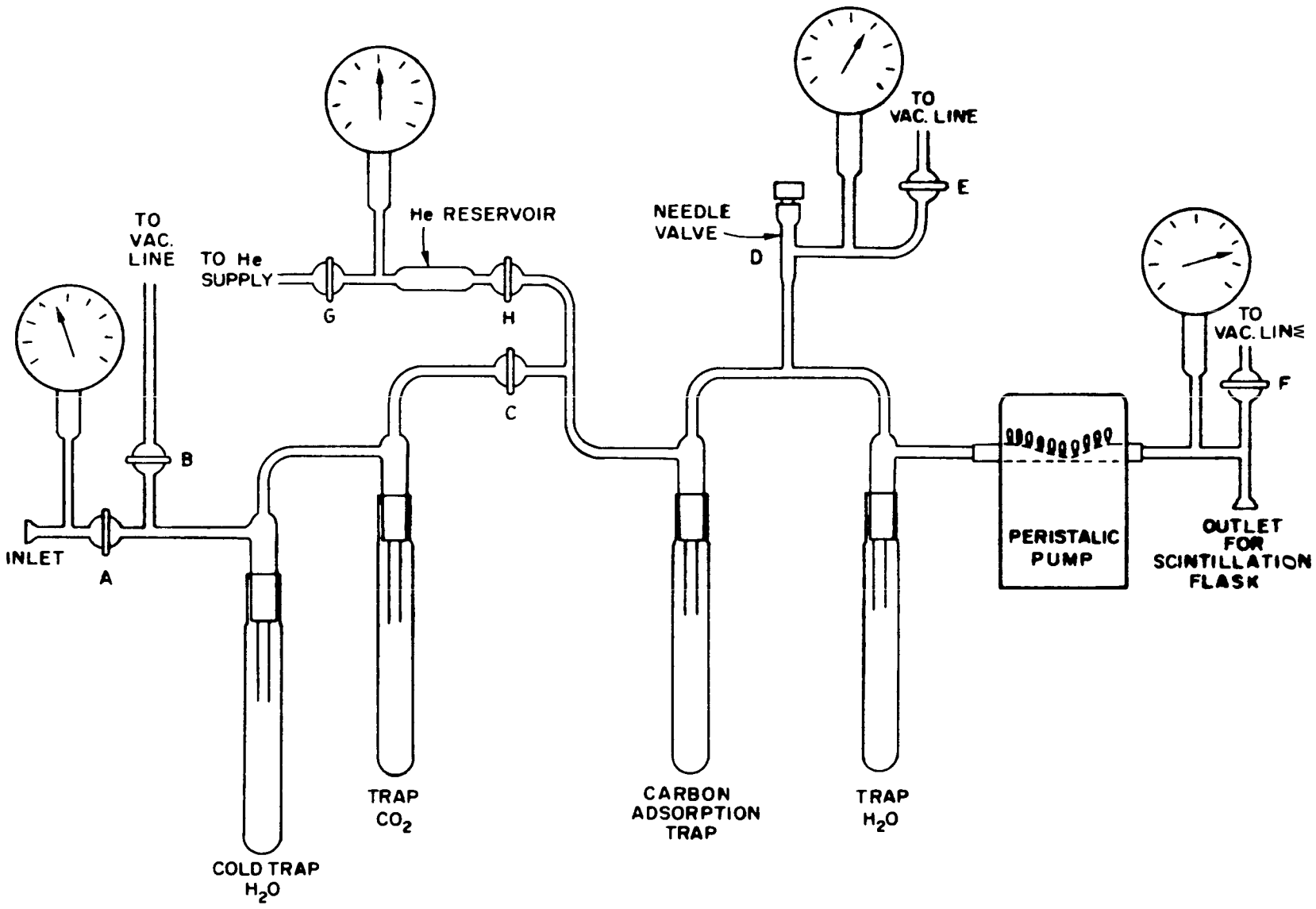

Figure 36 Radon Extraction System

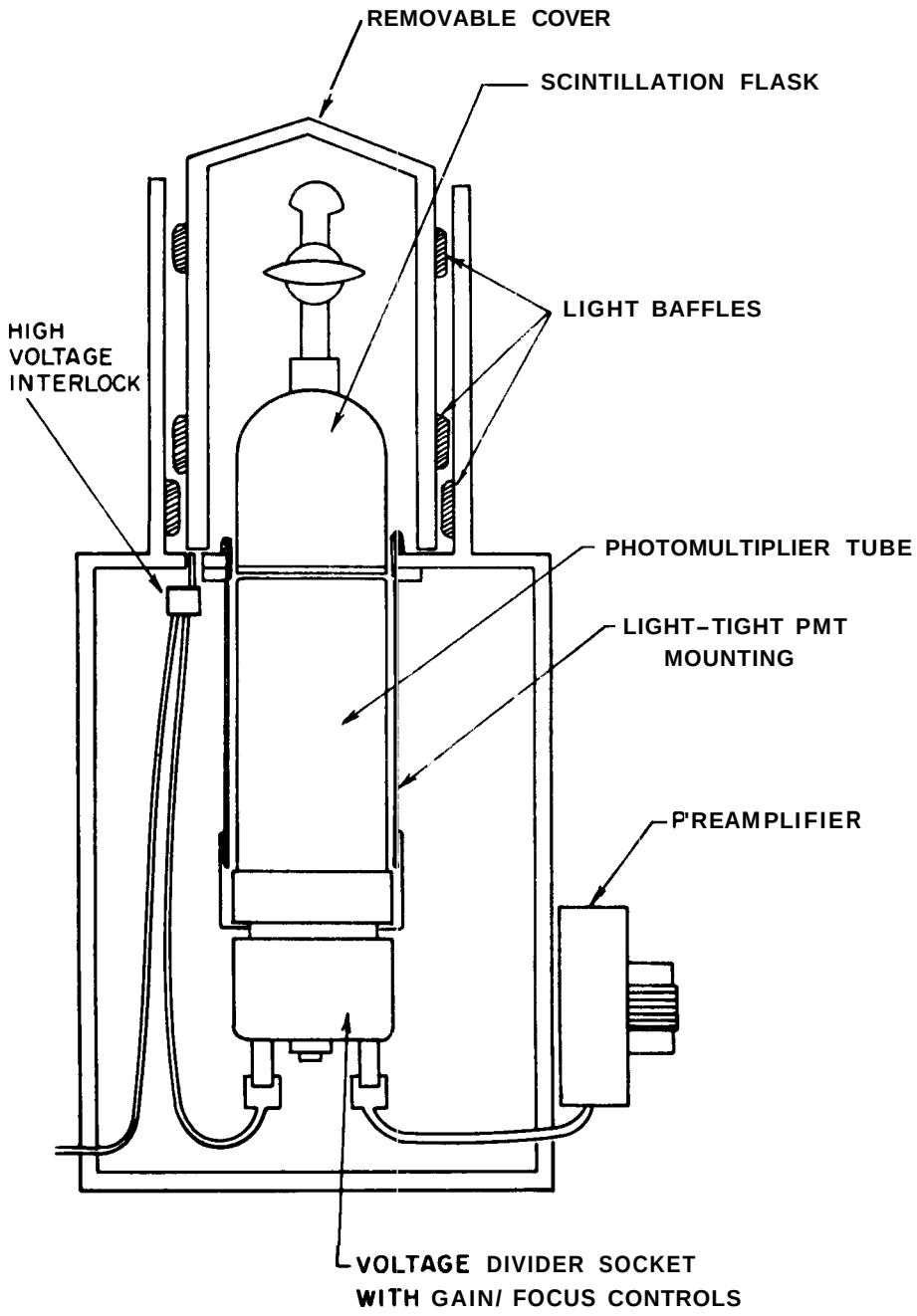

Figure 37. Radon Detection System, **Cutaway** View

and scaler-timer to count the scintillation pulses.

The charcoal-adsorption collection system permits accumulation of radon from various types of samples with recovery on the order of 95 per cent. The detection system gives an overall background on the order of 0.1 cpm. The overall efficiency of the system has been calibrated using a Radium-Radon standard obtained from the National Bureau of Standards. Reproducibility of measurements based on the standard are on the order of 2 per cent. The overall sensitivity of the system permits detection of as little as 10^{-13} Ci of total radon activity. This is equivalent to a concentration detection limit on the order of 10^{-4} Ci/ℓ for samples in the range of *3* to *30* liters of either liquid or gas.

2. Sampling Technique

The sampling technique used for geothermal wells was developed with several criteria in mind: ease of field operation, consistency, and simplicity of equipment for reliability. Review of accepted methods (e.g., Finlayson, 1970; Ellis, Mahon and Ritchie, 1968) and consultation with other works provided a basis for the method. Steel cylinders of approximately *4* to 30 liter capacity were used in several configurations in field trials. The two basic approaches consisted of flow-through and evacuated-tank sampling. The adopted standard technique, shown in Fig. *38*, consists of using an evacuated cylinder connected to the well-head with a T-line so that all air can be blown out of the connecting lines prior to opening the sample tank. The tank is opened for a standard length of time to permit pressure equilibration and only a limited amount of condensation in the case of steam samples.

Sampling of ambient air is accomplished by drawing the sample into an evacuated 30-liter cylinder at the desired location. Soil gas flux is measured by using a large inverted cylindrical tank of approximately 100-liter capacity which functions as an accumulator for the radon issuing from the covered area. A series of *3* or *4* samples is extracted over a period of several hours to determine the increased radon concentration in the confined volume, from which flux may be computed.

In addition to radon analysis, each well sample has been analyzed

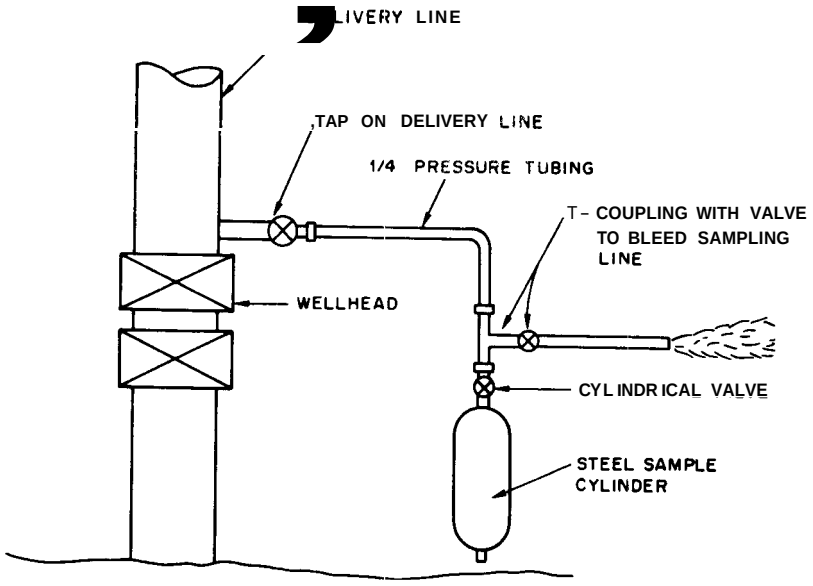

Figure **38.** Well Sampling Configuration.

for major non-condensable gases including O_2, N_2, CO_2, CH_4, and H_2. A small fraction of the gas was extracted from the sample cylinder into a syringe for injection into a gas partitioner. The liquid, or condensate, volume was measured, and in some cases, the liquid was analyzed for dissolved constitutents.

3. Survey Program

Sampling has been accomplished at several geothermal wells in both the vapor-dominated Geysers area and the liquid-dominated Imperial Valley. Cooperation from private industry and the Bureau of Reclamation made possible sampling under several conditions of well flow and testing. Because of the proprietary nature of some of the information associated with the testing program, quantitative results are not given in this summary. It is anticipated that the complete report will be published after approvals for release of information are complete.

Some qualitative results can be reported on the basis of preliminary examination of the radon concentration in the geothermal fluids. The overall radon levels are strongly related to geologic formations. In general, the levels observed in the Geysers area are substantially higher than those of the Imperial Valley. Different wells within either area show substantially different levels. A given well seems to exhibit a nearly constant level over a period of time under steady-state flow. For a given steam well, the radon concentration reaches essentially constant steady-state levels at: different flow rates as determined during pressure drawdown tests starting from shut-in conditions and running for relatively short periods of about 8 hours. This result is somewhat complicated by the problem of non-condensable gas buildup in the wellbore of steam wells during shut-in or low rate bleeding.

Evaluation of the radon concentration in the non-condensable gases, especially CO_2, is underway. Preliminary results for radon concentration in the non-condensable gas content are less definitive. Non-condensable gas analysis has presented several problems. Early problems of leakage of air into some samples were corrected by better seals and improved care in handling. Some analyses were plaged by instrumental difficulties. A continuing problem is accurate measurement of the total volume of non-condensables in a sample when the amount of gas is quite small. Mano-

metric measurement of total pressure in the sample cylinder and subtraction of water vapor pressure for the appropriate temperature often yields results with high uncertainties.

preliminary evaluation of the environmental measurements indicate that radon release from geothermal resources production will not be significant on a basinwide basis. The total radon release from a hypothetical power plant at The Geysers field would be of the same order as the natural release of radon from a relatively small area of soil containing normal radium content. Measurements in and near some steam plumes indicate that dilution is rapid and the additional radon is virtually undetectable at relatively small distances. Ambient air measurements show very low levels of radon as would be expected due to the influx of Pacific Ocean air. The only situations in which radon might be expected to be a problem from these preliminary results is in a confined area with poor ventilation.

These initial results of the field sampling of geofluids indicate general agreement with the expectation that radon concentrations will be independent of flow rate for production of fluid from a large reservoir. Confirmation of this will be important to establish primary dependence on emanation power and porosity. In this case the potential of radon for indicating changes in these parameters under stimulation will be enhanced. One type of confirming test that is being planned is a long term test involving at least two flow rates. A well flowing at a constant rate will be sampled regularly over a two- to three-week period. Then the flow rate should be changed, preferably to a higher rate, and the sampling continued for another two- to three-week period. The length of time is necessary to insure that radioactive equilibrium is closely achieved. Two weeks is sufficient to attain about *94* per cent of secular equilibrium. This type of test would not suffer from the possible non-equilibrium problems of the short time tests conducted *so* far. In the short time tests it is conceivable that variations with flow rate were not observed only because of the relatively large size of the reservoir compared to the relatively small distances traversed by flowing fluid in the time periods observed.

Continuous improvement is being sought for reliability and accuracy

of the non-condensable gas analyses to ascertain more clearly whether the radon is more closely associated with the water or with the gases. This may require substantial revision of sampling and analysis techniques.

Several laboratory scale tests on the emanating power of various rock types are being contemplated, perhaps some including measurement of rock subjected to reservoir conditions in the geothermal chimney model. Other tests would include a more detailed study of the effects of various methods of fracturing on the emanating power of different rocks.

The survey of radon content in different geological settings is being continued. Further data of this type serves at least two purposes: (1) additional characterization of the radon emanation of different geological conditions may yield correlations useful for reservoir analysis or prospecting, (2) the survey would provide the complete data base needed for thorough evaluation of any natural changes in formation properties or in environmental implications. For environmental purposes, the preliminary indications of the magnitude of the emissions should be confirmed by further measurements under various meteorological conditions and by tracing the transport and fate of radon through the entire power generation cycle.

MATHEMATICAL MODEL

Advances have been made in the modeling of geothermal fluids production in three main directions. The first direction is a general view of the many physical processes occurring in a geothermal system. A general geothermal fluids reservoir model includes complex thermal, fluid dynamics, and other physical processes. It would indeed be exceedingly difficult to model such a general system in three dimensions. For this reason a continuing attempt is being made to ascertain what are thought to be characteristics of geothermal reservoirs which have the greatest need of being studied. These attempts have been theoretical as well as practical, and have included discussions with scientists and engineers familiar with numerous geothermal reservoirs around the world (e.g., The Geysers, Larderello, Cerro Prieto, Wairakei).

The second direction is the formulation of a mathematical description of a much simplified system with an attempt to obtain a solution describing the behavior of this system. The particular system presently being modeled is the same one as is being simulated with bench-scale experiments. The mathematical solution of this system formulation has proceeded slowly, while at the same time much has been learned about the numerical characteristics; and requirements of such a solution. However, it has been possible to compare numerical results with experimental results.

The third direction is research with the bench-scale experimental equipment to physically simulate the boiling flow of steam and water at elevated temperatures. An attempt has been made to use both artificially consolidated and natural porous media. The synthetic core allows for temperature and volumetric liquid saturation probes to be cast in place and results in more accurate measurement of the pertinent variables.

General Characteristics of Reservoir Modeling

During the last year studies have been directed to the undisturbed reservoir away from the wellbore. It was felt that the need for a better

understanding of basic hydrothermal reservoir fluid mechanics was great enough to warrant this focus. In addition, consideration has been given primarily to a study of porous media, and in particular to the laminar flow regime where Darcy's Law for multiphase flow is pertinent. Although the fluid flow modeling considers a porous medium in particular, this should not restrict the results of such work to only those geothermal reservoirs whose fluid content is contained in a homogeneous porous medium such as sandstone. Transient pressure analysis of' gas flow based upon the model of a porous medium have been successfully applied to fields known to be highly fractured (Ramey, personal communication; Elkins and Skov, 1967).

Modeling efforts during the past year have been directed primarily at two-phase boiling flow of steam and water, and ultimately at the formation of a dry steam zone in the flow system. The formation of a dry steam zone vertically above a boiling zone is of great practical interest, because this case has been proposed as a model for vapor-dominated systems such as The Geysers field in California. The reason for this emphasis is that compressed-liquid and dry-steam flow tends to be isothermal. These isothermal single-phase flow regimes have been extensively studied within the fields of hydrology and petroleum reservoir engineering. The simultaneous flow of steam and water has not been studied from a fundamental flow viewpoint. Miller studied the single-component boiling two-phase flow of propane. However, the thermal effects of propane flow (latent heat of vaporization $\simeq$ 150 Btu/lb at 70^{o}F) are much smaller than those of saturated steam/water flow ($h_{fg} \simeq$ 1000 Btu/lb at 212^{o}F). In addition, within petroleum technology there has been a significant amount of work done on the simulation of thermal recovery processes for oil which involve hot water and steam injection (most recent is work of Crichlow, 1972; Shutler, 1969; arid Coats, et al., 1973). These studies have been aimed at understanding the particular oil recovery process rather than at understanding the basic mechanisms involved in nonisothermal two-phase boiling flow.

The injection of cold recycled water into a hot reservoir system

will also be of great interest in geothermal systems. The case where a reservoir containing compressed liquid undergoes injection of a cooler compressed liquid has received a fair amount of attention within the petroleum literature (see, e.g., Marx and Langenheim, 1959; Lauwerier, 1955; and Crichlow, 1972). Mercer has also recently studied the nonisothermal, single-phase flow of a compressed liquid, and has applied the analysis to the Wairakei geothermal field in New Zealand. The case where cold water is injected into a hot dry system seems to have received very little attention. This case should be important for heat scavenging in depleted vapor-dominated systems as well as the impervious hot dry rock case.

In the production of oil and gas reservoirs, the occurrence of vertical segregation of fluid phases has been found to affect field performance significnatly (see, e.g., Shutler, 1969; and Coats, et al., 1973). This will undoubtedly also be the case for geothermal reservoirs. For example, consider the case of a single well producing steam and water from a homogeneous (possibly anisotropic) aquifer of constant thickness, h, shown in Fig. 39. Tn the first case, Fig. 39-a, wherein there is no vertical segregation, the value of liquid saturation, $S_L(r,t)$, is constant over the interval, h. The flow of steam to the wellbore is restricted by the presence of liquid in the flow channels. However, this is not the case in Fig. 39-b, where $S_L(r,h,t)$ may be equal to or close to zero at the top of the producing formation. Under these conditions, the flow of steam in the upper portion of the interval is much less restricted. Hence there will be a tendency for liquid to boil in the lower part of the reservoir, and supply steam to the upper part of the reservoir, where it can then flow to the wellbore much more easily. Case 39-a would occur if there were little vertical permeability within the reservoir. In case 39-b, vertical communication is good. The mathematical formulation of this flow problem would be in terms of two space dimensions. Its mathematncal solution is more complex than the one-dimensional case. The solution of this two-dimensional problem has not yet been undertaken, but it is one of the ultimate goals of the

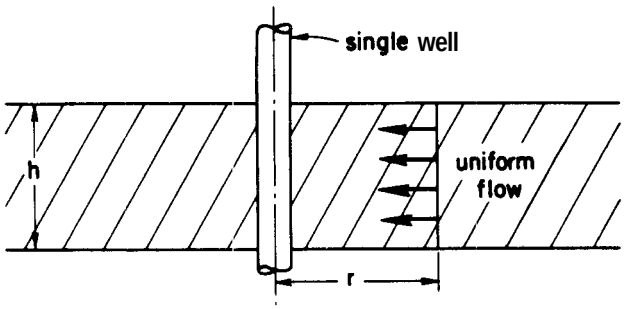

(a) No Vertical Segregation.

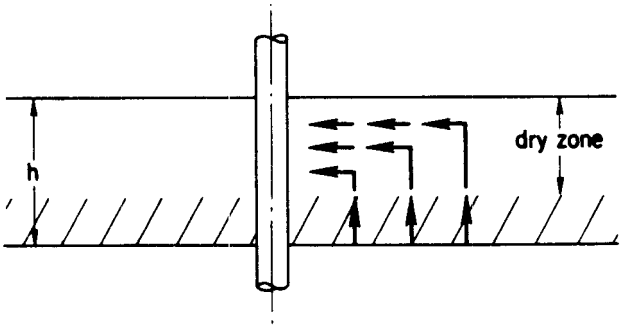

(b) Complete Vertical Segregation.

Figure 39. Schematic of Potential Effect of Vertical Segregation on Geothermal Reservoir Behavior.

present work.

The simplest system that can be considered is linear horizontal flow with no vertical segregation. Such a system has initially been the focus of both the mathematical modeling and bench-scale experimental work done to date. For a system such as has been constructed in the laboratory, it is not expected that vertical segregation will occur, as the ratio of buoyant to viscous forces is small. Thus, using numerical results, the transient behavior of a boiling flow system can be studied and verified against the bench-scale experimental results. A study of linear flow for vertical systems is being planned. In this case the ratio of buoyant to viscous forces is larger than for the horizontal flow case, and vertical segregation will be more likely to occur.

Many aquifers, and in particular those found in hot geothermal areas, contain significant dissolved solids. If the hot aquifer is produced in the two-phase boiling flow regime,, it would be expected that much of the dissolved solids will precipitate, and may block flow channels. This can be considered mathematically by hypothesizing that the precipitation of solids from the flowing channel will in some fashion reduce the absolute permeability. It would not be difficult to compute the precipitation from a simple system of dissolved salts by using solubility data. Theoretical considerations could be used to construct a simple model of permeability reduction by precipitation. The test for such a model would of course be verification of numerical results by physical experimentation. Boiling flow experiments using brine are planned.

Early mathematical formulations of the boiling flow problem were given in Progress Report. No. 1. For a porous medium of small grain size, the transient response of heat flux from the solid particles is rapid compared to the rate at which the temperature of the fluid changes. This is basically a result of the fact that the areal contact between the rock and fluid is very large on a surface area per unit bulk volume of rock basis, and this causes the time constant for the transient response to be small. Thus the total heat flow from the rocks over a time

step can be taken as:

(specific heat of rock particles) x (mass of rock)

x (temperature change over time) = $C_p M_r \Delta T$ (48)

In the case where matrix particle sizes are large, the transient response will not be as rapid. Hence it would be necessary to consider the lag in heat flow from the rocks to the fluids.

Mathematical Formulation of the Physical Problem

A discussion of the mathematical formulation of the particular linear flow problem discussed in the previous section is presented in the following. Specifically, we wish to look at the linear boiling flow of steam and water through a dipping porous medium. Due to the large thermal effects in such flow, it is necessary to consider energy as well as mass flux through the system. A consideration of mass and energy conservation applied to an elemental volume of core, along with rate equations and other assumptions leads to the following nonlinear coupled partial differential equations (derived in Appendix B):

$$\frac{\partial}{\partial x}\left[\left(K_\ell(p,S_L)\alpha_1(p) + K_g(p,S_L)\alpha_2(p)\right)\frac{\partial p}{\partial x} + \left(K_\ell(p,S_L)\alpha_3(p) + K_g(p,S_L)\alpha_4(p)\right)\frac{g}{g_c}\sin\theta\right] = \phi\frac{\partial}{\partial t}\left(\alpha_5(p) + S_L\alpha_6(p)\right) \quad (49)$$

and:

$$\frac{\partial}{\partial x}\left[\left(K_\ell(p,S_L)\beta_1(p) + K_g(p,S_L)\beta_2(p) + \kappa\beta_7(p)\right)\frac{\partial p}{\partial x} + \left(K_\ell(p,S_L)\beta_3(p) + K_g(p,S_L)\beta_4(p)\right)\frac{g}{g_c}\sin\theta\right] = \frac{\partial}{\partial t}\left[(1-\phi)C_{pr}\rho_r\left(T(p)-T_o\right) + \phi\left(\beta_5(p) + S_L\beta_6(p)\right)\right] + \dot{q}'''_{loss}(x,t) \quad (50)$$

where:

parentheses "()" indicate specified functional dependence on one or both of the dependent variables:

pressure, p, or volumetric liquid saturation, S_L;

x and t are independent variables for distance and time,

K_ℓ = effective permeability to the liquid

K_g = effective permeability to the gas

α_i, i = 1,6 and β_i, i = 1,7 } specified standard physical and thermodynamic properties of saturated steam and water; defined in Appendix C

$\frac{g}{g_c}$ -- conversion factor from mass base to a force base

θ = angle of dip as measured from horizontal

ϕ = fractional porosity of the porous medium

κ = effective thermal conductivity of the medium in the direction of flow

$(C_{pr}\rho_r)$ = specific heat of matrix rock on a volume basis

T_o = datum temperature

$\dot{q}'''_{loss}$ = heat loss rate from system on a unit surface area exposed per unit length basis

These two equations are similar to Eqns. 10 and 11 presented in Progress Report No. 1 (1973). Basic differences are that in the equations presented above, the effect of dipping flow has been included, and the physical and thermodynamic properties of water are expressed in a more general form. The formulation presented here can also be specified for the single-phase flow regime (isothermal or nonisothermal). This is discussed in Progress Report No. 1 (1973).

Physical Considerations--It should be noted that temperature does not appear as a dependent variable in (49) and (50). This is because an appropriate vapor pressure relationship fixes temperature, T, as a function of pressure, p, for boiling flow. Hence temperature is implicitly described in (49) and (50). As volumetric liquid saturations become very small, and a dry steam zone begins to form, there is a physical basis for expecting a vapor pressure lowering effect. This would be due to

surface effects between the gas, liquid, and solid. Such behavior has been studied by Ramey and co-workers (Cady, 1969; Cady et al., 1972; Chicoine, 1974; Strobel, 1973) but has not yet been clearly observed. However, investigations of this phenomena will be continued in the Stanford program during the coming year. If it is determined that vapor pressure lowering does indeed affect the development of a dry steam zone, a modified vapor pressure curve will have to be specified for low saturations and for the particular porous medium. Figure 40 illustrates such a relationship.

When the volumetric liquid saturation, S_L, falls below the residual liquid saturation, S_{Lr}, nonisothermal single-phase gas flow should occur. That is, the liquid phase would become immobile below the commonly referred to "irreducible" liquid saturation, although it could still boil. So long as there is still liquid water remaining in the pore space (S_L greater than zero), the equations describing such flow are (49) and (50). If vapor pressure lowering effects become important, then the gas will appear to be superheated (from the point of view of flat surface vapor pressure data) even though it may be in equilibrium with the liquid phase. It may be necessary to specify modified properties for the gas to account for this. When S_L becomes zero, Eqns. (49) and (50) are still valid although somewhat simplified. Volumetric liquid saturation, is constant (zero), and the two dependent variables are pressure, $p(x,t)$, and temperature, $T(x,t)$. In this case the physical properties for the superheated steam would have to be specified as functions of both pressure and temperature.

The determination and verification of effective permeability to each of the fluid phases as functions of pressure, temperature, and volumetric liquid saturation, is one of the main goals of the present research effort. In spite of the fact that various workers have concluded that the temperature dependence of effective permeability to a particular phase needs to be considered (see, e.g., Coats et al., 1973), such dependence has not been the subject of much study. Ramey and co-workers (Poston, et al., 1970; Weinbrandt, 1972; Weinbrandt et al., 1973)

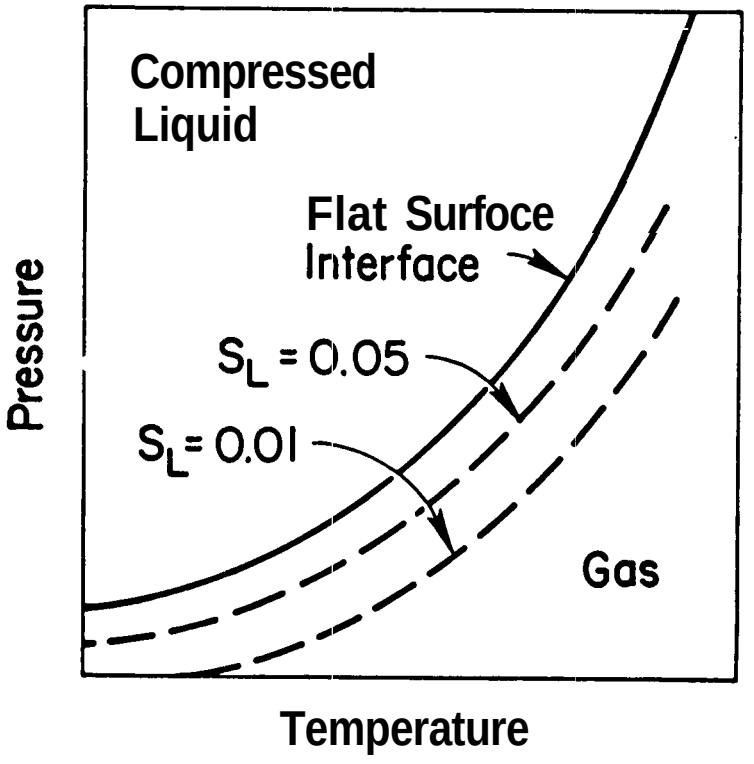

Figure *40*. Diagram of an Effective Vapor Pressure Curve Including Capillary Pressure Effects at Low Volumetric Liquid Saturations, S_L.

have investigated the nonisothermal multiphase flow of fluids through porous media, and a continuation of such work is underway.

The parameter θ in *(49)* and (50) is the angle of dip from the horizontal. We will be principally interested in only two values of θ; zero for horizontal flow, and 90^{o} for vertical flow.

The volumetric thermal energy capacity of the rock matrix will depend upon the rock type, and also possibly on temperature. Because much of the thermal energy for vaporizing liquid comes from the rock matrix, it may be desirable to include the effect of temperature on $(C_{pr}\rho_{r})$. Initially this will not be done, as it will not greatly affect the overall solution of the flow problem. In a similar fashion, the porosity, ϕ, may well be a function of both pressure and temperature. But for the same reason just mentioned, this functional dependence will not be included in the present problem formulation.

The effective thermal conductivity in the direction of flow should also be a function of flowing conditions. However, it is shown in Appendix C that the contribution of conductivity to the energy flow term is small, except under somewhat adverse physical conditions. Thus, even if the contribution of conductivity to enesgy flow is to be included in the problem formulation, an accounting for limited variation in effective conductivity would not be necessary.

The nonlinear coefficients, $\alpha_{i}(p)$ and $\beta_{i}(p)$ contain specified standard thermodynamic properties of water, and are defined in Appendix C. This appendix presents a discussion of dimensional considerations of the coefficients within the flow equations. It also shows the variation of the nonlinear coefficients over a range of pressure, and discusses an evaluation of conditions under which some coefficients dominate the nonlinear terms in the flow equations.

Mathematical Considerations--The flow equations *(49)* and (50) can be expressed in a more compact form:

$$\frac{\partial}{\partial x}\left(\gamma_{1}(p,S_{L})\frac{\partial p}{\partial x} + \gamma_{2}(p,S_{L})\right) = \frac{\partial \gamma_{3}}{\partial t}(p,S_{L}) \qquad (51)$$

$$\frac{\partial}{\partial x}\left[\gamma_4(p,S_L)\frac{\partial p}{\partial x} + \gamma_s(p,S_L)\right] = \frac{\partial \gamma_6}{\partial t}(p,S_L) + \dot{q}'''_{loss} \tag{52}$$

where the coefficients γ_i are defined in Appendix B. These are two highly coupled nonlinear partial differential equations in the dependent variables, pressure, $p(x,t)$, and volumetric liquid saturation, $S_L(x,t)$.

In order to solve these equations, it is necessary to specify both pressure, $p(x,0)$, and liquid saturation, $S_L(x,0)$, as initial conditions. For boundary conditions, we could specify pressure or flux as realistic examples. The first kind of boundary condition is a Dirichlet type of condition and is of the form: $p(0,t) = f(t)$, where $f(t)$ is a specified function of time. A specification of liquid saturation at the boundary does not seem to be necessary. The second condition is comparable to the Neumann condition for linear equations, except that it becomes more complex in the nonlinear case. A specification of total mass flux rate, for example, leads to a nonlinear condition because flux is a function of liquid saturation and pressure: $\dot{m}'' = g(t)$, where $\dot{m}''$ is the specified flux on a unit cross sectional area to flow basis; $g(t)$ is a specified function of time:

$$\dot{m}'' = \sum_{i=1}^{2} \frac{\dot{q}_i \rho_i}{A}$$

$$= -\frac{\partial p}{\partial x}\left[\frac{\rho_\ell(p)K_\ell(p,S_L)}{\mu_\ell(p)} + \frac{\rho_g(p)K_g(p,S_L)}{\mu_g(p)}\right]$$

$$-\frac{g}{g_c}\frac{dz}{dx}\left[\frac{\rho^2(p)K(p,S_L)}{\mu_\ell(p)} + \frac{\rho_g^2(p)K_g(p,S_L)}{\mu_g(p)}\right]$$

$$= -\gamma_1(p,S_L)\frac{\partial p}{\partial x} - \gamma_2(p,S_L) \tag{53}$$

In the case of horizontal flow, a zero flux boundary condition

reduces to:

$$\left.\frac{dp}{dx}\right|_{boundary} = 0 \tag{54}$$

Specified pressure and zero flux boundary conditions are being used in the present modeling efforts for horizontal flow.

Nondimensional Considerations--Because of the nonlinear nature of the flow equations it is not possible to place them in useful dimensionless form. However, by defining modified space and time variables:

$$x_D \triangleq \frac{X}{L} \tag{55}$$

$$t^* \triangleq \frac{t}{L^2} \tag{56}$$

the flow equations become:

$$\frac{\partial}{\partial x_D}\left(\gamma_1 \frac{\partial p}{\partial x_D} + L\,\gamma_2\right) = \frac{\partial \gamma_3}{\partial t^*} \tag{57}$$

$$\frac{\partial}{\partial x_D}\left(\gamma_4 \frac{\partial p}{\partial x_D} + L\,\gamma_5\right) = \frac{\partial \gamma_6}{\partial t^*} + L^2 \dot{q}'''_{loss} \tag{58}$$

For horizontal flow ($\gamma_2 = \gamma_5 = 0$), and with no heat losses, the equations reduce to a form which does not require the specification of a characteristic length:

$$\frac{\partial}{\partial x_D}\left(\gamma_1 \frac{\partial p}{\partial x_D}\right) = \frac{\partial \gamma_3}{\partial t^*} \tag{59}$$

$$\frac{\partial}{\partial x_D}\left(\gamma_4 \frac{\partial p}{\partial x_D}\right) = \frac{\partial \gamma_6}{\partial t^*} \tag{60}$$

Thus, flow with heat losses and/or dipping character requires specification of a characteristic length, as well as all of the other pertinent physical characteristics.

Purpose and Direction of Mathematical Modeling Efforts--One of the main purposes of mathematical modeling in physical sciences and engineering is to gain a better insight into the physical processes which are occurring. This improved understanding can then be used for analysis and evaluation of the same physical process, but under altered conditions. However, it is extremely important that the mathematical model be verified against an actual physical system.

Steady-State Systems--The steady-state, two-phase flow of boiling steam (a single component) through a linear core could be studied. Muskat, et al. (1937) presented the first steady-state analysis of the solution gas drive flow problem in an oil reservoir. In this case both the oil and gas are flowing, arid gas is initially dissolved in the oil phase. Muskat, et al. did not have to specify energy conservation explicitly for their system in order to obtain the solution. Miller (1951) studied the single-component two-phase flow of propane through porous media, and by applying the principles of mass and energy conservation, he was able to derive an analytic solution for the steady-state case similar to that of Muskat, et al. This solution was used for the boiling steam flow problem during early stages of the present work.

The steady-state two-phase single-component boiling flow of water through a porous medium has a number of characteristics which make it unattractive for physical and mathematical simulation purposes, in spite of the existence of an analytic solution to this problem. In order for the steady-state condition to be reached, the mass flow rate into a core must equal that out of it, and in addition, flow within the core must be strictly isenthalpic (see Miller, 1951). Miller was able to approach these conditions in his experimental work with propane at temperatures between 70 and 110^{o}F. However, water has a much higher latent heat of vaporization than propane (1000 Btu/lb_m vs 70 Btu/lb_m); hence the thermal effects of boiling steam/water flow would be greater than those encountered by Miller. In addition, such experimental work for water should be carried out at temperatures of 212^{o}F or higher, and this requirement compounds the experimental task of ensuring isenthalpic flow (i.e., no heat losses).

The limiting characteristic of the steady-state flow condition is that it cannot develop a dry steam zone. This is a consequence of the fact that the thermodynamic path of flow is isenthalpic. It is a severe limitation because we are ultimately interested in the development of a dry steam zone in the core.

Although steady-state flow will be simulated both physically and mathematically, it will not be the main direction of this work.

Transient Systems--It would seem more appropriate to study transient flow behavior. Such behavior requires less strict control of experimental conditions, and would have application in two practical directions. The first is that conditions required for the development of a dry steam zone might be reached and hence studied. The second application is that it would be necessary to develop techniques for solving the flow equations which could then be extended to the more realistic and field-oriented case of radial flow to a well.

The mathematical modeling efforts have a number of immediate applications. The immediate goal is to simulate transient boiling flow of steam and water under a broad range of physical conditions. These results may then be matched to observed experimental behavior in order to attempt to verify the hypothesized nonisothermal relative permeability characteristics of the particular porous medium. In addition, the sensitivity of calculated flow behavior to numerous physical parameters could be evaluated (e.g., residual gas and liquid saturation, assumed vapor pressure lowering effects, heat losses from the core, etc.). Of great interest with relation to geothermal reservoir development is the amount of energy produced from the system over time, and how this compares to values from the model of Whiting and Ramey (1969).

Numerical Solution of the Flow Equations

The solution of the coupled nonlinear system of Eqs. *(49)* and (50) by analytic means does not seem possible. Of the numerical methods available for obtaining solutions to these equations, the method of finite differences holds

the most promise. In this method the continuous domains of solution $p(x,t)$, and $S_L(x,t)$ are represented by discreet points only. For example, at the point (x_i, t_n) pressure is represented as P_i^n, and volumetric liquid saturation as S_{Li}^n. Values at a small increment of time, dt, later are represented as being at the discreet time level, n+1. Similarly, values in space at x ± dx are represented at discreet nodes i ± 1.

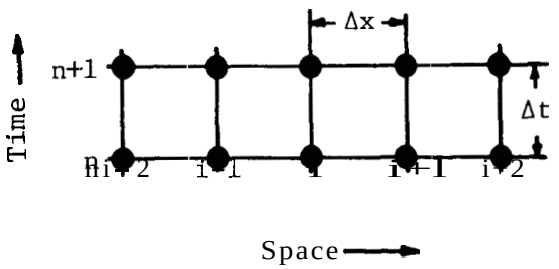

The differential operators in Eqs. (49) and (50) can then be represented in terms of the predefined discreet points. There are numerous methods and schemes for representing partial differential equations in terms of discreet points. Many books are available which discuss these methods as applied primarily to linear problems (see Smith, Mitchell, Ames 1969). Ames (1969) and Richtmeyer and Morton also discuss the application of these methods to nonlinear problems such as those which arise in engineering and the physical sciences.

Culham, et al. have successfully used the Crank - Nicolson differencing scheme to solve two-phase flow problems involving interphase mass transfer. Applying this differencing scheme to Eq. (57) for the case of horizontal flow, and writing it about the ith node at the $n+\frac{1}{2}$ time level:

$$\frac{\Delta[\gamma_1^n \Delta P_i^n] + \Delta[\gamma_1^{n+1} \Delta P_i^{n+1}]}{2} = \delta\gamma_{3,i}^n \qquad (61)$$

where the expression is in terms of finite difference operators (see Ames 1969, Mitchell):

Δ is the central difference operator

$$\Delta U_i = \frac{U_{i+1/2} - U_{i-1/2}}{\Delta x}$$

the self-adjoint difference expression

$$\Delta[a\Delta U_i] = \frac{a_{i+1/2}[U_{i+1}-U_i] - a_{i-1/2}[U_i-U_{i-1}]}{\Delta x^2}$$

δ is a forward difference operator, $\delta U = \frac{U^{n+1} - U^n}{\Delta t}$

and γ^n is evaluated at the nth time level, γ^{n+1} at the n+1th.

It is sometimes convenient to express the time derivative on the right hand side of Eq. (61) explicitly in terms of pressure, and saturation. This is done as follows:

$$\frac{\partial \gamma_3}{\partial t} = \phi\left(\frac{\partial \alpha_5}{\partial t} + S_L\frac{\partial \alpha_6}{\partial t} + \alpha_6\frac{\partial S_L}{\partial t}\right) = \left[\left(\frac{\partial \alpha_5}{\partial p} + S_L\frac{\partial \alpha_6}{\partial p}\right)\frac{\partial p}{\partial t} + \alpha_6\frac{\partial S_L}{\partial t}\right]$$

where α_5, α_6 are known functions of pressure, and ϕ is constant. Thus, the right-hand side of (61) could also be expressed as:

$$\psi_1(P_i^{n+\frac{1}{2}}, S_{Li}^{n+\frac{1}{2}})\delta P_i^n + \psi_2(P_i^{n+\frac{1}{2}})\delta S_{Li}^n \qquad (62)$$

where ψ_1 and ψ_2 are known functions of p and S_L.

In the method of finite differences the problem solution marches forward in time, commonly using only the most recent time level, t_n, of solution in order to calculate the new solution at the next time level, $t^{n+1} = t + dt$. For the first time step from t = 0 to t = dt, the most recent or old level of solution is, of course, the specified initial condition for the problem.

In the finite difference solution of linear partial differential equations, it is possible to express unknowns at the new level of solution in terms of only the dependent variables (p and S_L for this

problem). When the finite difference equations are written about each node within the discreet domain, a set of linear algebraic equations results. It is of the form:

$$A\,\underline{x} = \underline{b} \tag{63}$$

where A = an m x m coefficient matrix
$\underline{x}$ = the solution vector $(x_1, x_2, \ldots x_m)^t$ of dependent variables at the new time level
$\underline{b}$ = a known coefficient vector $(b_1, b_2, \ldots b_m)^t$

From a theoretical point of view, the solution of such a system of equations is easily accomplished, although for large systems this solution can become quite tedious (see e.g., Forsythe and Moler).

The flow equations being discussed here are nonlinear, and hence, the difference expression written about the point i becomes a nonlinear equation of the form:

$$F_{2i-1}(p_{i-1}^{n+1}, p_i^{n+1}, p_{i+1}^{n+1}, S_{L,i}^{n+1}, \gamma_1^{n+1}, \gamma_3^{n+1}) = 0$$

where γ_1^{n+1}, γ_3^{n+1} are evaluated in terms of pressure and saturation values at the (unknown) new time level. This equation can be expressed more concisely:

$$F_{2i-1}(\underline{PS}) = 0 \tag{64}$$

where $\underline{PS}$ is the solution vector $(p_1^{n+1}, S_{L,1}^{n+1}, p_2^{n+1}, S_{L,2}^{n+1}, \ldots p_m^{n+1}, S_{L,m}^{n+1})^t$ at the new time level far a system with m discreet points. This equation is not algebraic. It can, however, be expressed in convenient nonlinear algebraic form by replacing the right hand side of (61) by (62) to give:

$$G_{2i-1}(\underline{PS}) = 0 \tag{65}$$

Applying the Crank - Nicolson difference equation (see Mitchell, Smith) to the energy flow equation (58) for the case of horizontal flow:

$$\frac{\Delta[\gamma_4^n \Delta P_i^n] + \Delta[\gamma_4^{n+1} \Delta P_i^{n+1}]}{2} = \delta\gamma_{6,i}^n + \dot{q}_{loss}^{\prime\prime\prime\,n+1/2} \tag{66}$$

where $\dot{q}'''^{n+\frac{1}{2}}$ is the heat loss from the system per unit length per unit area over the time step dt from t_n to t_{n+1}. This equation can also be expressed more concisely in the nonalgebraic form similar to (61):

$$F_{2i}(\underline{PS}) = 0 \tag{64a}$$

or using an expression similar to (62), in nonlinear algebraic form:

$$G_{2i}(\underline{PS}) = 0 \tag{64b}$$

Writing the two difference equations about m discreet points we will have 2m nonlinear equations in the 2m unknowns: p_i^{n+1}, i = 1,m; S_{Li}^{n+1}, i = 1,m:

$$F_1(\underline{PS}) = 0$$

$$F_2(\underline{PS}) = 0$$

$$F_{2i-1}(\underline{PS}) = 0$$

$$F_{2i}(PS) = 0$$

$$F_{2m-1}(\underline{PS}) = 0$$

$$F_{2m}(\underline{PS}) = 0$$

for the nonalgebraic formulation. In vector notation this is

$$\underline{F}(\underline{PS}) = \underline{0} \tag{64c}$$

where $F = (F_1, F_2, F_3, \ldots F_{2m})^t$, and F_i are nonlinear nonalgebraic functions of $\underline{PS}$. The nonlinear algebraic combination of (65) and (64a):

$$\underline{G}(\underline{PS}) = \underline{0} \tag{64d}$$

is of the form:

$$A(\underline{x}) \cdot x = \underline{b} \tag{67}$$

where A is a coefficient matrix whose coefficients depend on the solution $\underline{x}$.

Compared to the solution of linear algebraic systems of equations of the form (63), the solution of nonlinear systems of equations of the form

(64c), and (67) is not highly developed (see e.g. Isaacson and Keller). Such solution techniques are iterative in nature, and the final solution obtained often depends on the initial vector guess. It can be shown by analysis (Isaacson and Keller) that most of the solution methods will converge to the required answer if certain smoothness conditions are met by the system of equations, and also if the initial guess is "close" enough to the answer. However, "close" can only be used qualitatively in the sense that one method will converge to a solution vector close to it in some normative sense; whereas another method, using the same initial guess, will converge to an answer in a different part of the vector space.

There are a number of methods available for solving systems of nonlinear equations of the form (64c) or (64d). Culham, et al. used the method of successive approximation [also called Picard iteration (Isaacson and Keller)] to solve a nonlinear algebraic formulation of the form (64d), and hence this was the approach initially tested in this work. This approach generated physically unrealistic answers in which both the pressure and :Liquid saturation at the end of the core began to increase instead of decline as they should have. As a consequence, a number of other solution techniques were formulated and tried, but these also generated unrealistic answers. It was then realized that the specified pressure boundary condition that was being used was physically unrealistic:. The pressure at the outlet end was suddenly dropped from an initial condition of 500 psia to a constant value of 3000 psia. A more gradual drop of 10 to 40 psi per time step to the desired boundary pressure was then tried, and found to yield satisfactory results.

At the present time the program being used to solve the flow equations for horizontal flow is formulated in terms of the Crank-Nicholson differencing scheme. Newton-Raphson iteration is used to solve the resulting fully implicit nonalgebraic nonlinear system of equations. The computer program is written in Fortran IV, and executes in double precision. The residuals of the finite difference equations

are used as the criterion for convergence. It has been found that a residual criterion of 10^{-3} is small enough to yield satisfactory results, The answers obtained for this value of the residual criterion do not differ to five significant figures when compared to the results generated for a value of 10^{-10}. The more relaxed criterion requires fewer internal iterations per time step, and hence less computer time for execution.

A material and energy balance evaluation of the numerical solution is also being carried out as an additional check of the validity of the answers. In the present. program the material balance usually falls rapidly to 0.98, and then remains constant at this value for the rest of the run. The energy balance rises slowly with time, and commonly ranges from 1.05 to 1.15 for longer times. This results is not satisfactory, and attempts are being made to improve upon it.

In order to increase the execution speed for an individual simulation, the program has been written so that it will automatically double the time step when a certain criterion has been met. The need for such a requirement is that the early transients of the system are quite rapid, and it is necessary to take small time steps to simulate them accurately. At longer times, the transients are slower, and hence it is possible to increase the size of the time steps. The criterion used to determine whether or not to increase the time step should be indicative of the magnitude of the transients in the system, and of the flux through a given node point. One such criterion which is commonly used in fluid coning simulators, in the oil industry is that the maximum change in saturation over the system for a given time step must be less than some value (W.E. Brigham, personal communication). Satisfactory values for such a criterion have been found to range from 0.002 to 0.008.

The functions $\alpha_i(P)$ and $\beta_i(P)$, containing the physical and thermodynamic properties of water (as defined in Appendix C) are represented as piecewise continuous interpolating cubic splines. The original data points over the range 15 - 3000 psia were taken from the ASME Steam Tables (Meyer, et al).

Initially the equations of Corey et al. were used to represent

relative permeability as a function of liquid saturation. These are analytic expressions which can be derived from an idealized physical flow model:

$$K_L = K_{rL} K_{abs}; \; K_g = K_{rg} K_{abs};$$

$$S_L^* = (S_L - S_{Lr} - S_{gr})/(1 - S_{Lr} - S_{gr});$$

and

$$K_{rL} = (S_L^*)^4$$

$$K_{rg} = (1 - S_L^{*2})(1 - S_L^*)^2$$

The variable S_L^* is volumetric liquid saturation normalized with respect to the mobile liquid saturation in the pore space. Figure 41 presents a graph of the gas and liquid relative permeabilities, K_{rg} and K_{rL}, as a function of S_L^*, which result from the Corey equations. For $S_L < S_{Lr}$, $K_{rL} = 0$ and $K_{rg} = 1$; and for $S_L > (1 - S_{gr})$, $K_{rL} = 1$ and $K_{rg} = 0$. Other representations of relative permeability curves can and will be used. This form was programmed initially because it was convenient, and could be modified easily to include the effects of temperature on the flow characteristics of the porous medium.

The current program has given some indications of instability at long run times, There are a number of possible explanations for this behavior. The first is that although the Crank-Nicolson scheme is stable for all values of $R \triangleq dt/(dx)^2$ for linear systems, it is only marginally so, particularly when applied to nonlinear equations (R, C. Earlougher, Jr., personal communication). Thus it would seem warranted to use a form of the generalized weighting scheme (see e.g. Smith, p. 23, and Ames, 1969, p. 50) in which $\theta = 0$ is the explicit scheme, $\theta = 1/2$ is the Crank - Nicolson scheme, and $\theta = 1$ is the backward-difference, fully-implicit scheme. The use of a value of θ slightly larger than 1/2 (0.6, for example) would allow the inherent accuracy of the Crank-Nicholson scheme to be maintained, while hopefully making it more stable.

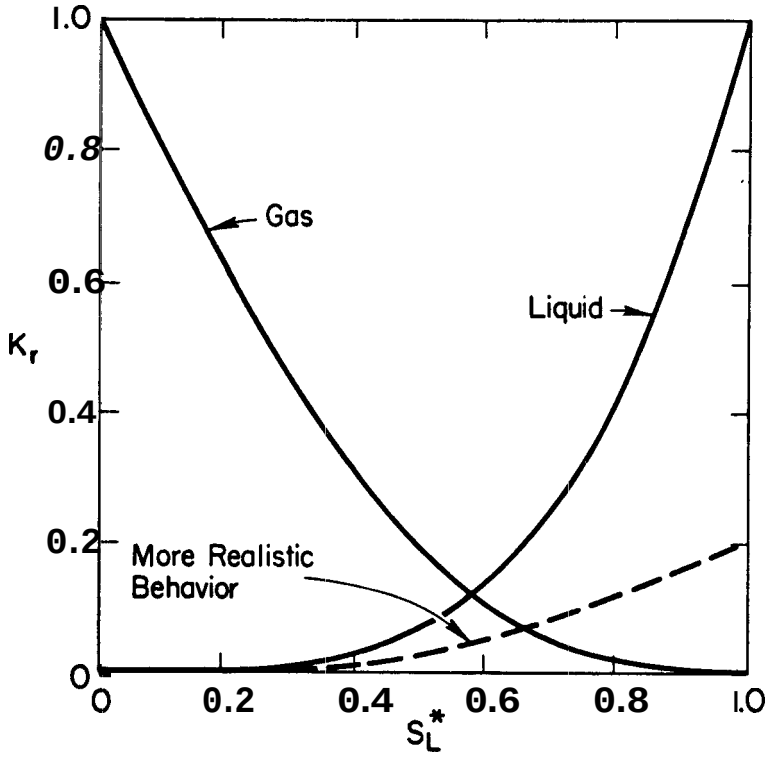

Figure 41. Corey Equations for Relative Permeability, K, as a Function of Normalized Volumetric Liquid Saturation, S_L^*.

A further source of the tendency towards unstable behavior at long run times may be the evaluation of the term $\gamma_{1,i+\frac{1}{2}}$ in (61) and $\gamma_{4,i+\frac{1}{2}}$ in (66) as the average of the two nodes i and i+1. Within oil reservoir simulation technology, it is common practice to evaluate the transmissivity type of coefficients containing the permeability term at an upstream value of pressure. For example, if the evaluation of $\gamma_{1,i+\frac{1}{2}}$ is required, and fluid is flowing from the ith node to the i+1'th node, then γ_1 is evaluated at the pressure upstream, or ith node. Coats, et al. (1973) use this upstream weighting in their numerical simulation of steamflooding in an oil reservoir. There appears to be empirical as well as physical basis to expect that such upstream evaluation will reduce the tendency of a numerical solution to become unstable.

The current program requires approximately 0.1 sec of IBM 360/67 computer time per time step-node. This compares favorably with 0.2 sec/time step-node for a one-dinensional steamflood model reported by Shutler (1969). However, it is slower than the more recent model of Coats, et al., which requires 0.04 equivalent IBM 360167 sec/time step-node, and in addition, solves a more general and more complex system of equations than the one described in this report. The primary reason for the relative slowness of the current model as compared to that of Coats, et al. is that. all coefficients in the flow equations are evaluated fully implicitly for each internal iteration of the simultaneous solution, and in addition, these coefficients are represented by cubic polynomials. Coats, et al. do not evaluate all of their coefficients implicitly, which means that they probably have less coefficient evaluation per time step-node than the model described in this report. In addition to making fewer function evaluations on a normalized basis, Coats, et al. also tended to represent functions with linear expressions instead of with cubic polynomials. This would also result in more rapid execution times.

Comparison of Some Physical and Numerical Results

An experiment was run with the bench-scale equipment with the idea of attempting to simulate the observed results using the computer program. The core was initially closed at both ends with an approximately constant temperature of *370-380*^{o}F and an initial pressure of *267* psia. This corresponded to the liquid being in the compressed liquid state. Keeping the left-hand end of the core closed, the right-hand end was slowly opened to the atmosphere, and the producing pressure was recorded as a function of time as shown in Fig. *43*. The pressure and temperature distributions along the axis of the core were recorded at various times as shown in Figs. *44* and *45*. One striking feature of the observed transient behavior is that it did not die out over the period of observation. Hed the flow been in the single-phase gas or compressed liquid regime, the transients would have dropped more rapidly.

The numerical model is not able to simulate the transition from compressed liquid to saturated two-phase flow. Hence it was necessary to assume for numerical simulation purposes that the initial pressure was the saturation pressure corresponding to the approximate initial temperature of the system. An initial pressure of *174* psia was specified, corresponding to an approximate initial temperature of *370*^{o}F. The purpose of these simulations was simply to determine a qualitative comparison between the physical and numerical results.

The actual core used was an artificially-consolidated sandstone with a thermocouple well cast along the axis. The porous medium had a measured porosity of 36 per cent and a single-phase absolute permeability of approximately 0.1 Darcy, which appeared to be constant over a range of temperatures. Finally, the core was *23.5* inches long, and 2 inches in diameter. In addition to the above information, further data were required by the computer program. Initially it was assumed that there were no heat losses from the core, and that the porous medium had residual volumetric liquid and gas saturations of' $S_{Lt} = 0.30$ and

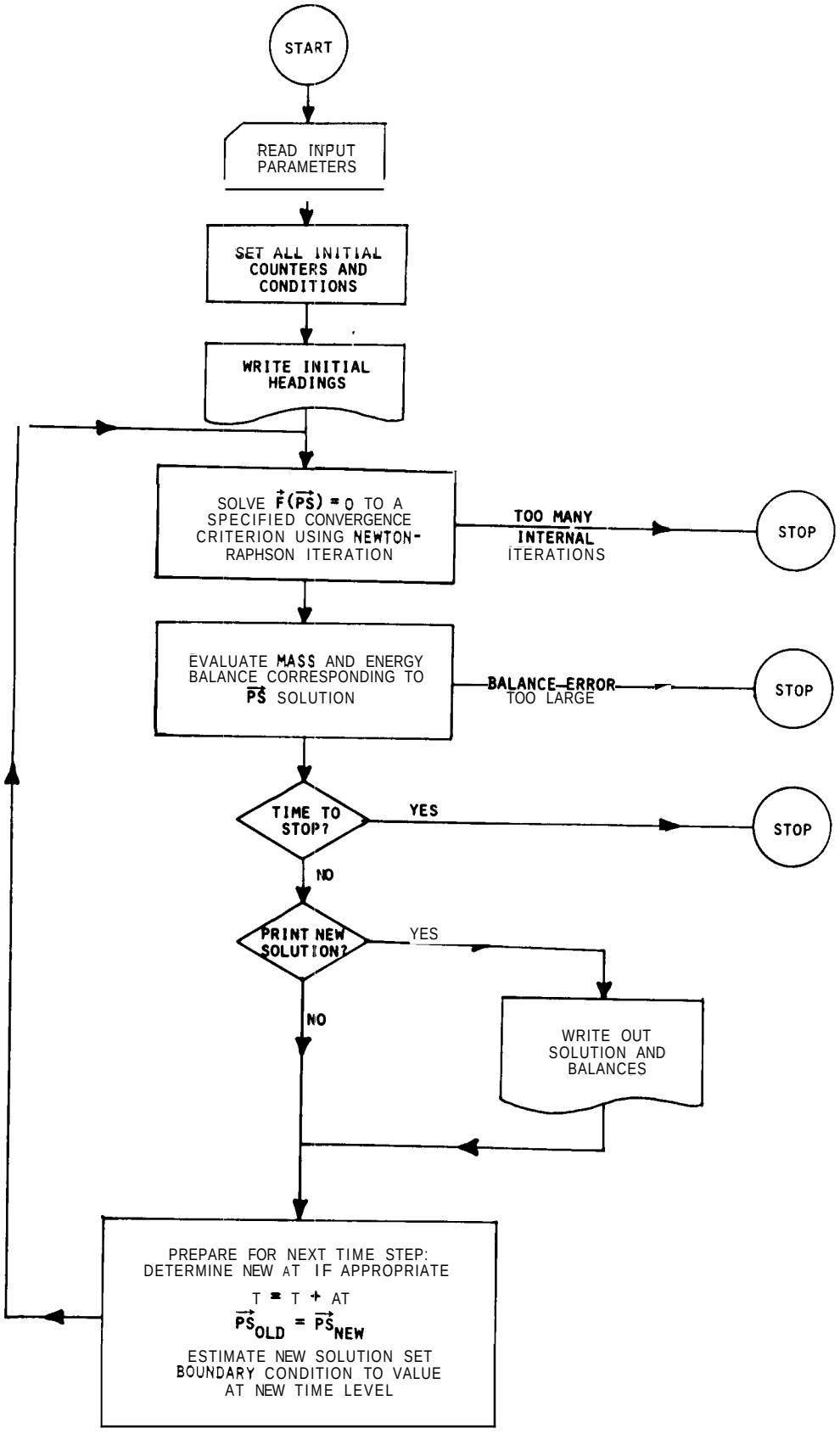

Figure 42. Flow Diagram of Computer Program,

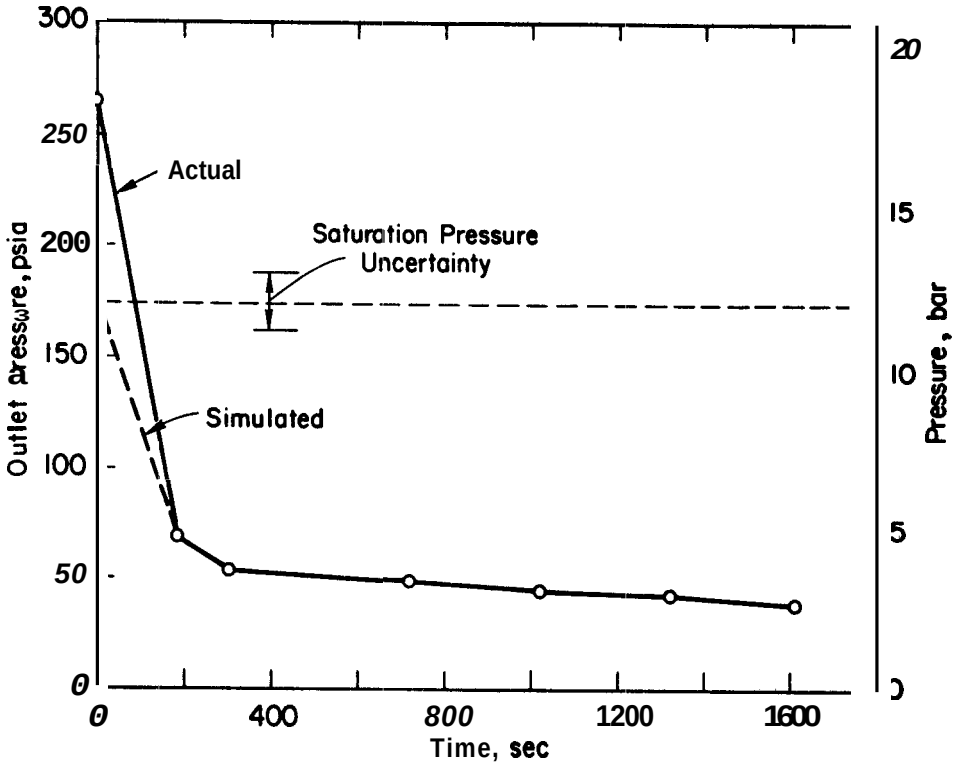

Figure 43. Pressure-Time History at Outlet End of Core.

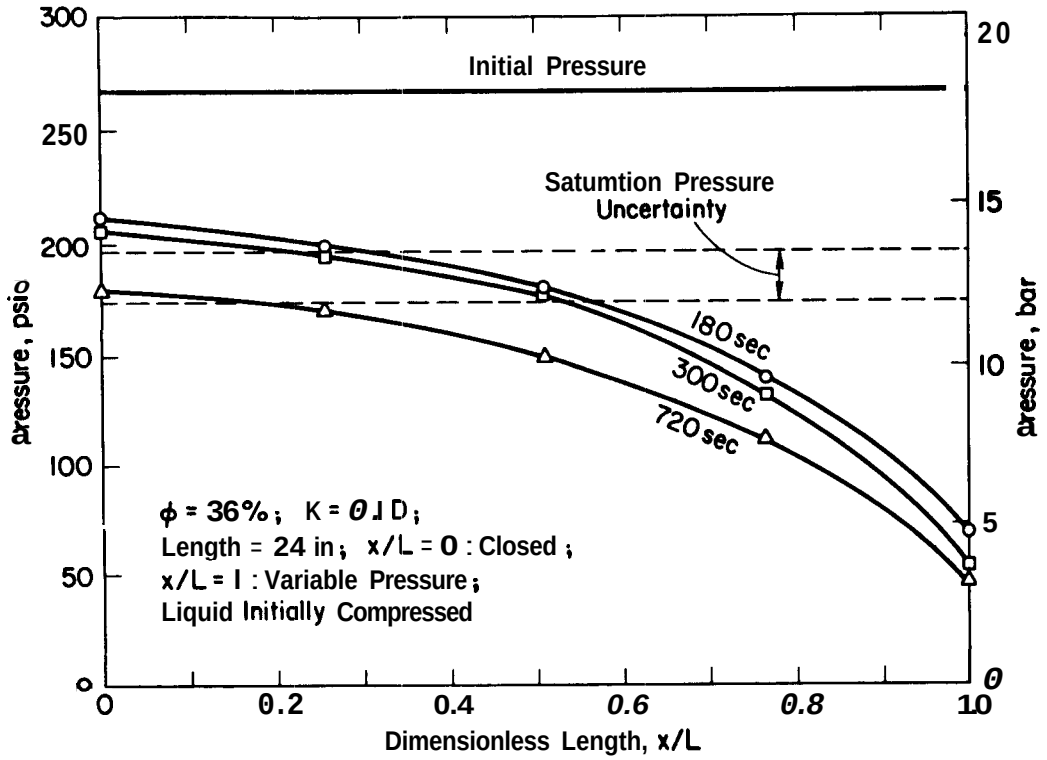

Figure 44. Measured Pressure History for Artificially Consolidated Core.

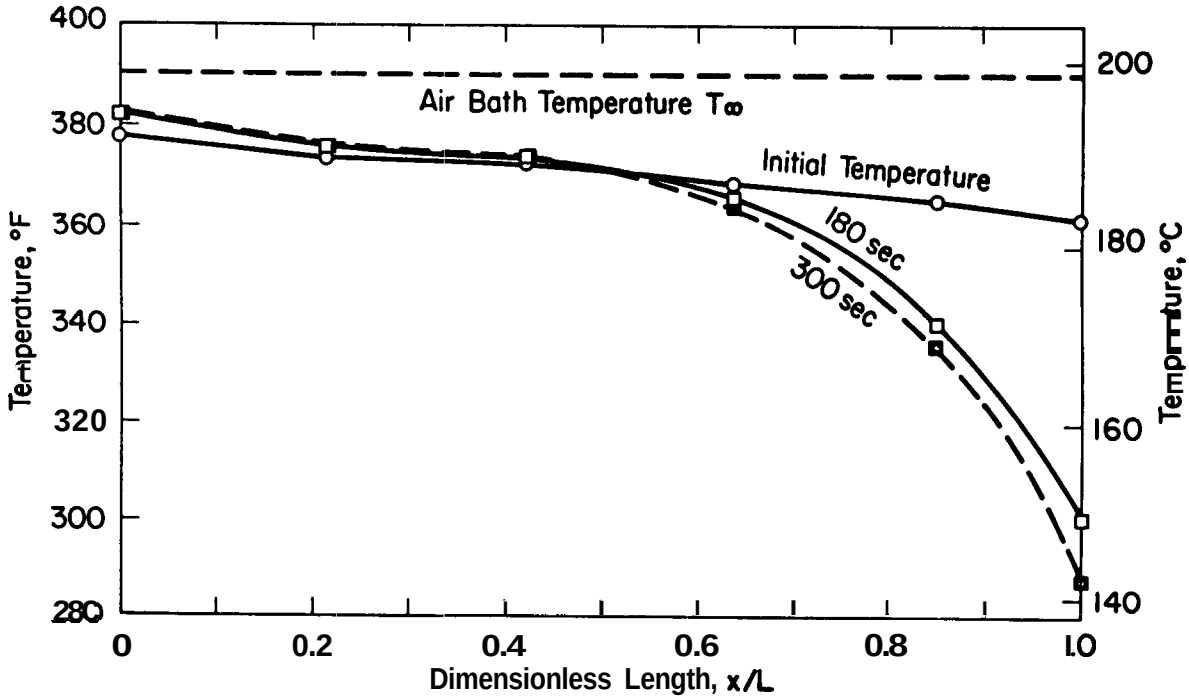

Figure 45. Temperature History in the Artificially Consolidated Core During the Flow Experiment.

S_{gr} = 0.05 respectively. These values were fairly arbitrary, and were simply used as a base case (Simulation No. 1).

Figure *46* presents calculated pressure distributions along the core at various times for Simulation No. 1. Although the shapes of the simulated and actual pressure distributions (see Fig. *44)* are similar at early times (up to 180 sec), the calculated pressures drop more rapidly than actual pressures at longer times. The simulator also predicts transients which are substantially slower than would be observed for single-phase flow. Figure *47* presents calculated liquid saturation profiles along the core. At the present time this variable has been measured within the core only for lower temperatures. Examination of the liquid saturation profiles presented in Fig,. *47* reveals some interesting behavior. The liquid saturation at the outlet end of the core falls rapidly until it reaches the point where relative permeabilities to both phases are approximately equal (compare Fig. *47* with Fig. *41).* This saturation level then moves back through the system until a state of approximately uniform liquid saturation throughout the core has been reached at a time of around 180 sec. Then the profile remains essentially uniform and drops slowly as liquid is boiled off. As a result of the analysis presented in Appendix C, it can be seen that this state of uniform liquid saturation (towards which the system initially tends) is one where the energy transfer due to mass flow is approximately equal in both fluid phases. However at this saturation level, most of the mass transfer is still in the liquid phase. As the liquid saturation approaches the residual liquid saturation, more mass will be transferred in the gas phase, until finally when the residual iiquid saturation has been reached, all of the mass transfer will be in the gas phase. When this stage has been reached, the horizontal flow system will probably have very small pressure gradients, with residual liquid boiling throughout the core. Although the numerical simulations have not yet been run for a time this long, the longest run of *600* sec does suggest that this phenomena will indeed occur. It should be clear that a calculated temperature distribution could also be presented for comparison with measured temperatures.

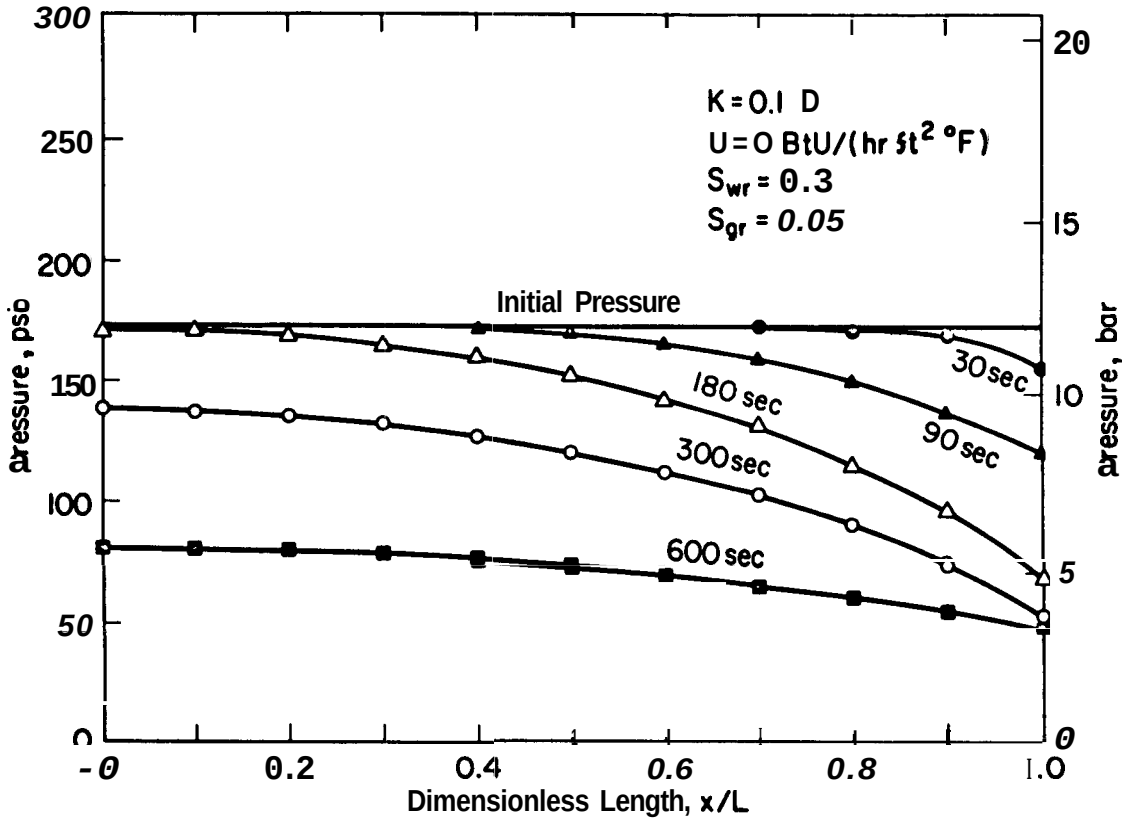

Figure 46. Simulation No. 1 of Pressure History.

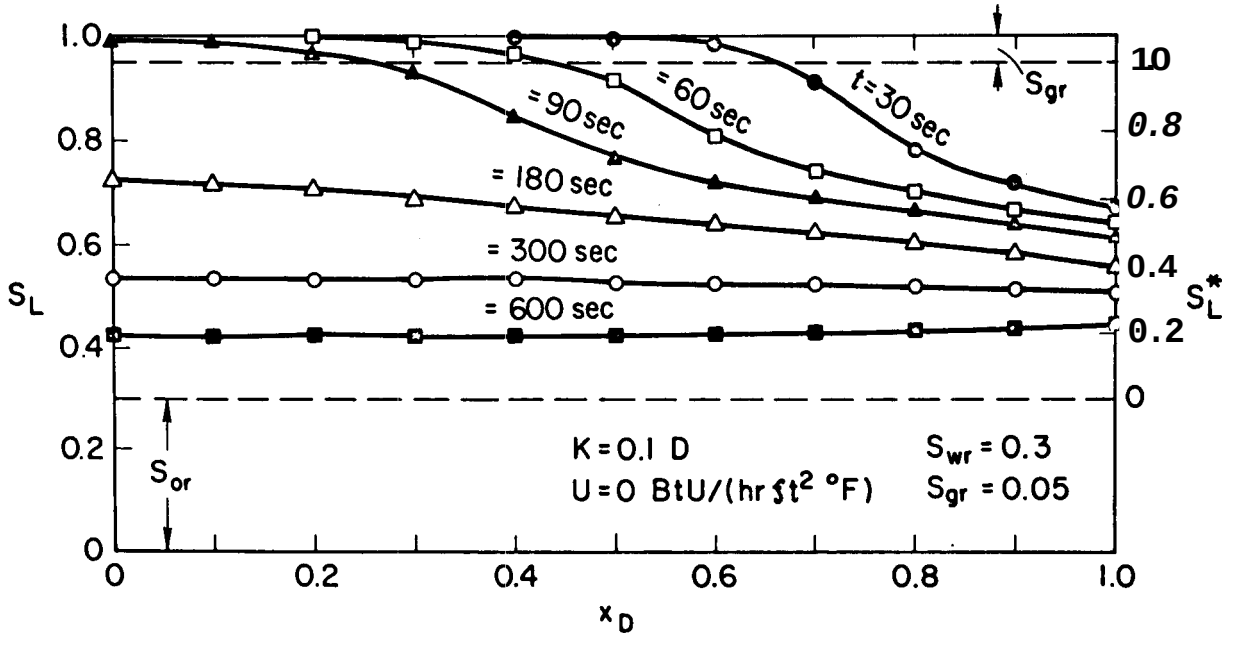

Figure 47. Simulation No. 1 of Saturation History.

Such a graph is presented as Fig. 48.

In order to test the sensitivity of the calculated results to various initial assumptions about physical parameters, three additional simulation runs were made. Simulation No. 2 used the same base conditions as No. 1, except that the effect of heat transfer from the air bath to the core was included. It was assumed that the air temperature was 390^{o}F as compared to an initial temperature in the core of 370^{o}F. The overall convective heat transfer coefficient, U, between the core and environment was assumed to be 4 Btu/hr-ft^{2} ^{0}F, probably a somewhat high value. Figures 49 and 50 present the calculated pressure and saturation profiles for Simulation No. 2. The effect of adding heat due to conduction to the flow system is predictable: higher pressures and lower liquid saturations throughout the core. However, as can be seen from the figures, this effect was small (only a few psia and saturation per cent values) and did not influence the overall behavior of the system greatly.

During Simulation No. 1, an arbitrary assumption about residual gas and liquid saturations was made which affected the two-phase permeability characteristics of the system. Two further simulation runs were made to test the sensitivity of calculated results to this assumption. Simulation No. 3 used all of the basic input from No. 1, with the one exception that. a residual gas saturation of only 0.01 was specified (compared to 0.05 in No. 1). The pressure and saturation profiles calculated for this run are presented in Figs. 51 and 52. Simulation No. 4 similarly used a different residual gas saturation of 0.1. This run was calculated to a total time of 50 sec. Two saturation profiles for the run are presented in Fig. 53. No pressure profiles are presented for the early times of this run as they are essentially similar to those for Simulations No. 1 and No. 3. A comparison of calculated behavior for Runs No. 3 and No. 4 to that of Run No. 1 shows that varying residual gas saturations from 1 per cent to 10 per cent does not affect the two-phase transient flow behavior of the core significantly. In particular, the behavior of Runs No. 1, 3, and 4 with regard to the normalized liquid

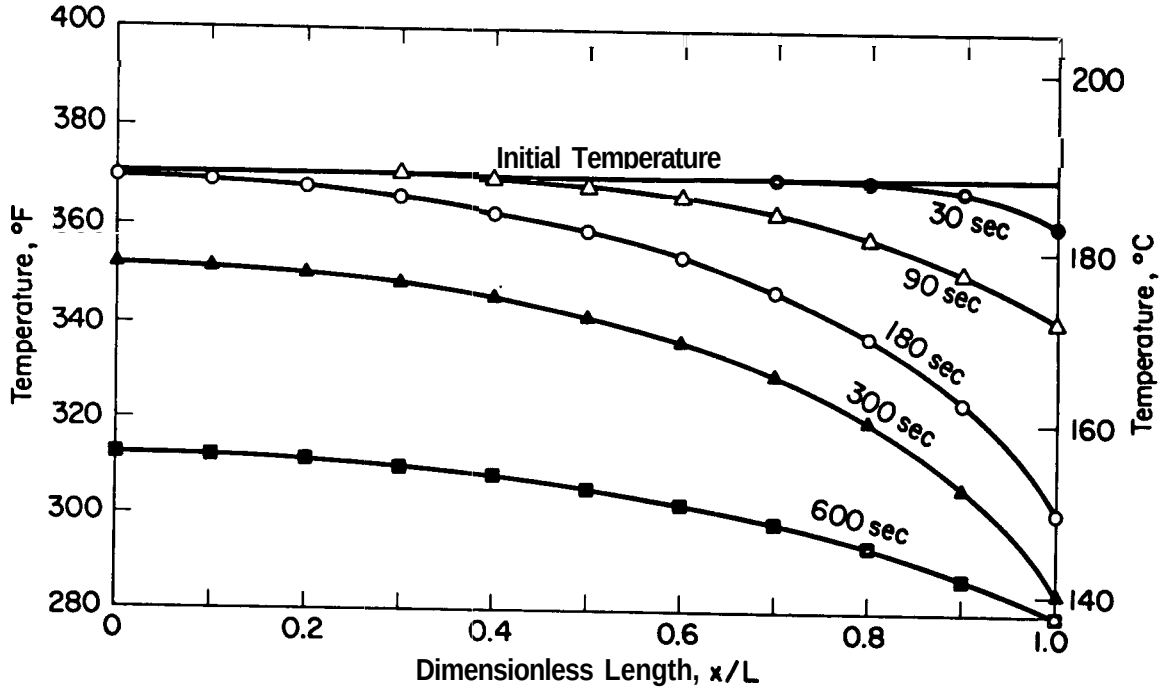

Figure 48. Simulation No. 1 of Temperature History.

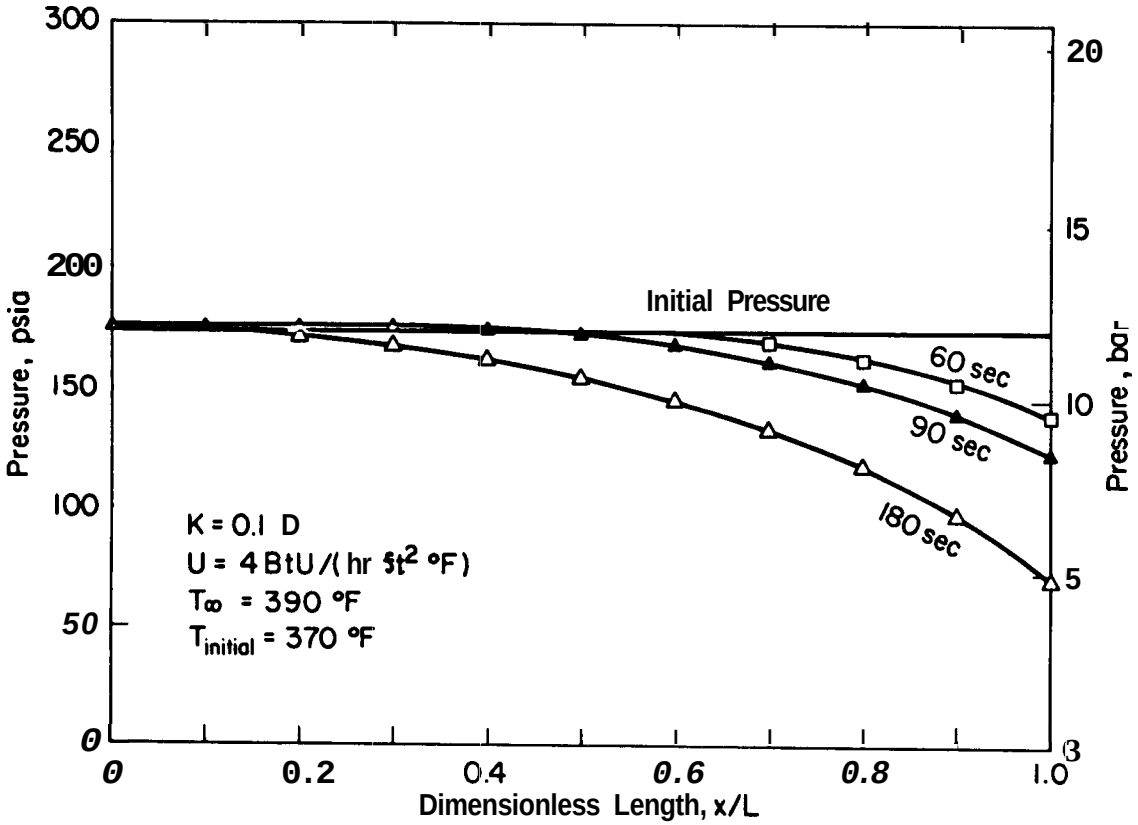

Figure 49. Simulation No. 2 of Pressure History.

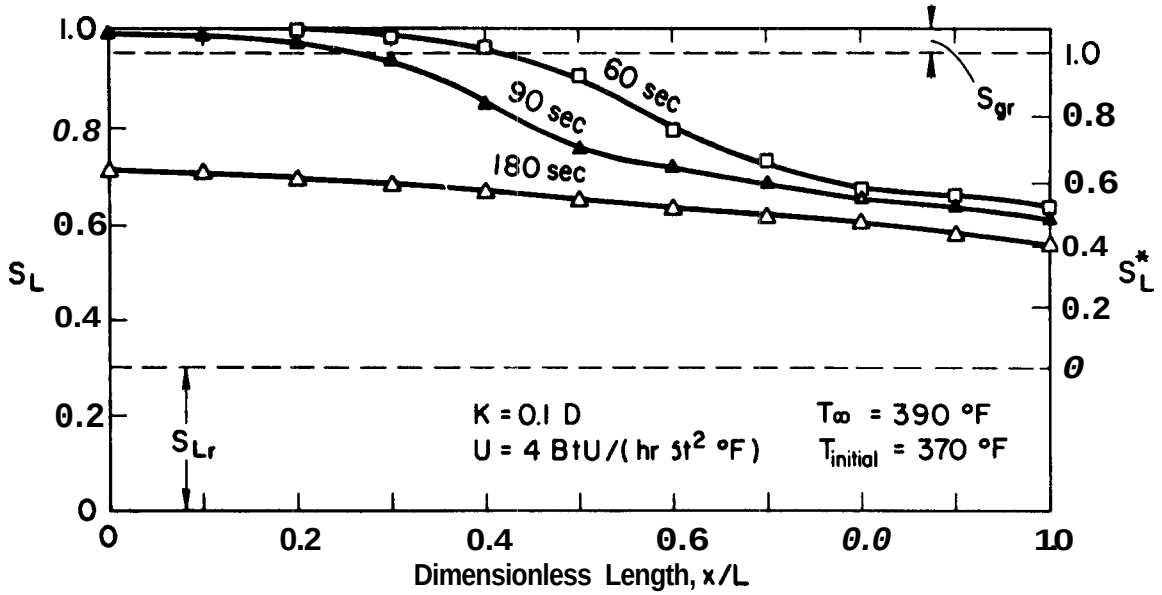

Figure 50. Simulation No. 2 of Saturation History.

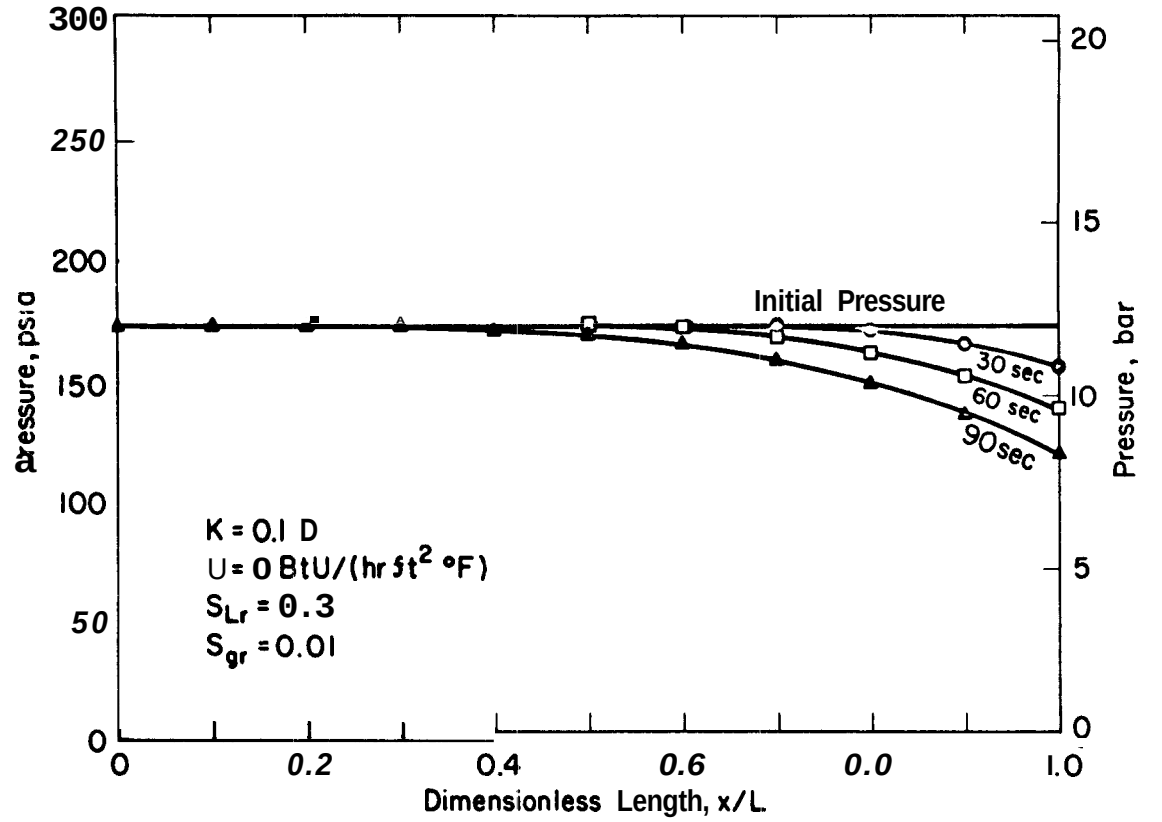

Figure 51. Simulation No. 3 of Pressure History.

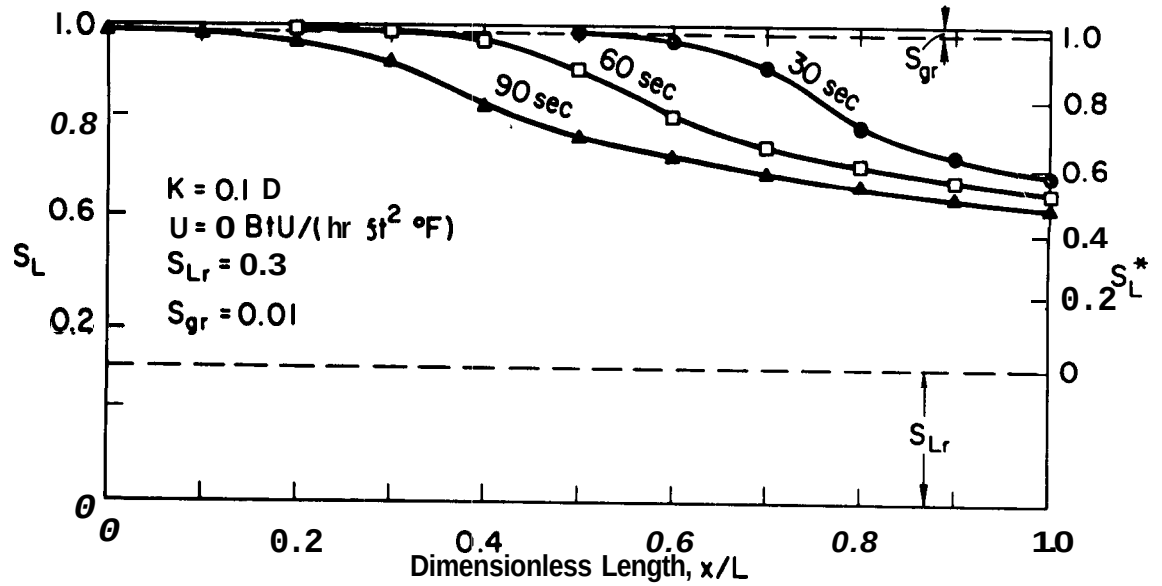

Figure 52. Simulation No. 3 of Saturation History.

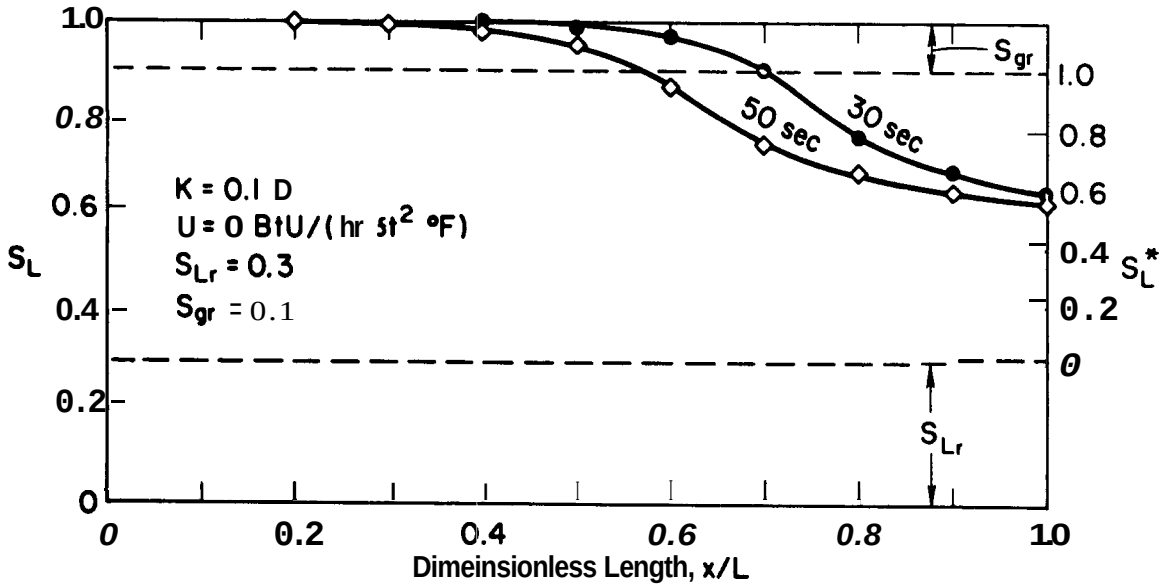

Figure 53. Simulation No. 4 of Saturation History.

saturation, S_L^*, is quite similar.

Further work remains to be done in the efforts to compare physical and calculated results. In particular it is important that the initial physical and simulated systems be more similar than was the case above. In addition, work is being done to make the numerical simulator more accurate, while at the same time allowing more rapid execution. The theoretical and programming aspects of flow regime changes (e.g., single-phase compressed liquid to two-phase saturated flow) are also being studied.

REFERENCES

Ames, W.F., Nonlinear Partial Differential Equations in Engineering, Academic Press, 1965.

Ames, W.F., Numerical Methods for Partial Differential Equations, Barnes & Noble, Inc., 1969.

Andrews, J.N. and Wood, D.F., Mechanism of Radon Release in Rock Matrices and Entry into Groundwaters, Inst. of Mining and Met. Trans./Section B 81:792, November 1972.

Baker, P.E., The Effect of Pressure and Rate on Steam Zone Development in Steam Flooding (SPE 4141), presented at the 47th Annual Fall Meeting of SPE of AIME, San Antonio, Texas, Oct. 8-11, 1972.

Belin, R.E., Radon in the New Zealand Geothermal Regions, Geochimica et Cosmochimica Acta 16:181-191, 1959.

Bunce, L.A. and Sattler, F.W., Radon-222 in Natural Gas, Radiological Health and Data Reports 7:441-444, 1966.

Cady, G.V., Model Studies of Geothermal Fluid. Production, Ph.D. Dissertation, Stanford University, Nov. 1969.

Cady, G.V.; Bilhartz, H.L.; and Ramey, H.J., Jr., Model Studies of Geothermal Steam Production, AIChE Symposium Series "Water," 1972.

Carslaw, H.S. and Jaeger, J.C., Conduction of Heat in Solids, Oxford University Press, 1947.

Chicoine, S., Study of Production of Geothermal Fluids from Consolidated Sandstones, Personal Communication, 1974.

Coats, K.H.; George, W.D.; Chu, Chieh; and Marcum, B.E., Three-Dimensional Simulation of Steamflooding (SPE 4500), presented at the 48th Annual Meeting of SPE of AIME, Las Vegas, Nevada, Sept. 29-Oct. 3, 1973.

Corey, A.T.; Rathjens, C.H.; Henderson, J.H.; and Wyllie, R.J., Three-phase Relative Permeability, Trans. AIME 207:349, 1956.

Crichlow, H.B., Heat Transfer in Hot Fluid Injection in Porous Media, Ph.D. Dissertation, Stanford University, May 1972.

Culham, W.E.; Farouq Ali, S.M.; and Stahl, C.D., Experimental and Numerical Simulation of Two-Phase Flow with Interphase Mass Transfer in One and Two Dimensions, Soc. Pet. Engr. J., 323-337, Sept. 1969.

Elkins, L.F. and Skov, A.M., Determination of Fracture Orientation fron Pressure Interference, Pet. Trans. Reprint Series No. 9, Pressure Analysis Methods, SPE of AIME, 97-100, 1967.

Ellis, A.J.; Mahon, W.A.J.; and Ritchie, J.A., Methods of Collection and Analysis of Geothermal Fluids, 2nd Ed., Chemistry Div., Dept. of Scientific and Industrial Research, New Zealand, July 1968.

Finlayson, J.B., The Collection and Analysis of Volcanic and Hydrothermal Gases, Geothermics, Special Issue 2, 1970.

Forsythe, G.E. and Moler, C.B., Computer Solution of Linear Algebraic Systems, Prentice-Hall Inc., 1967.

Isaacson, E. and Keller, H.B.; Analysis of Numerical Methods, John Wiley & Sons, 1966.

Jones, S.C., Senior Res. Engr. Marathon Oil Co., Denver Res. Center, Personal Communication.

Klinkenberg, L.J., The Permeability of Porous Media to Liquids and Gases, A.P.I. Drilling and Production Practice, 201-211, 1941.

Kreith, F., Principles of Heat Transfer, 2nd Ed., International Textbook Co., 1969.

Kruger, P. and Ramey, H.J., Jr., Stimulation of Geothermal Aquifers, Progress Report No. 1, to Advanced Technology Dept., RANN, National Science Foundation, Grant No. GI-34925, March 1973, 91 pp.

Kruger, P, and Ramey, H.J., Jr., Stimulation of Geothermal Aquifers, Progress Report No. 2, to Advanced Technology Dept., RANN, National Science Foundation, Grant No. GI-34925, Sept. 7, 1973, 2 pp.

Lauwerier, H.A., The Transport of Heat in an Oil Layer Caused by Injection of Hot Fluid, Appl. Sci. Res. Sec. A.5, 1955.

Lucas, H.F., Improved Low-Level Alpha-Scintillation Counter for Radon, Rev. Sci. Instr. 28:9, Sept. 1957.

Lucas, H.F., A Fast and Accurate Survey Technique for Both Radon-222 and Radium-226, in Adams, J.A.S. and Lowder, W.M., eds., The Natural Radiation Environment, University of Chicago Press, 1964.

Marx, J.W. and Langenheim, R.H., Reservoir Heating by Hot Fluid Injection, Trans. AIME 216, 1959.

Messmer, J.H. , Thermal Conductivity of Porous Media: Packing of Particles, Proc. Fourth Conf. on Thermal Conductivity, Paper C, Session III, 1964.

Meyer, C.A. ; McClintock, R.B. ; Silvestri, G.J.; and Spencer, R.C. , Jr., 1967 ASME Steam Tables, 2nd Ed., Am. Soc. Mech. Engrs., 1968.

Miller, F.G., Steady Flow of Two-Phase Single-Component Fluids through Porous Media, Trans. AIME 192:205-216, 1951.

Mitchell, A.R., Computational Methods in Partial Differential Equations, John Wiley & Sons, 1969.

Muskat, M., Wyckoff, R.D. , Botset, H.G.; and Meres, M.W. , Flow of Gas-Liquid Mixtures through Sands, Trans. AIME 123:69-96, 1937.

Poston, S.W. ; Ysrael, S. ; Hossain, A.K.M. S. ; Montgomery, E.F. , IV; and Ramey, H.J., Jr., The Effect of Tenperature on Irreducible Water Saturation and Relative Permeability of Unconsolidated Sands, Soc. Pet. Engr. J., 171-180, June 1970.

Ramey, H.J., Jr., A Reservoir Engineering Study of the Geysers Geothermal Field, 1963, submitted as evidence, Reich and Reich: Petitioners vs. Commissioner of Internal Revenue, 1969 Tax Court of the U.S., 52 T.C. No. 74, 1970.

Richtmyer, R.D. and Morton, K.W., Difference Methods for Initial Value Problems, Interscience Publishers, Interscience Tracts in Pure and Applied Mathematics, No. 4, 2nd Ed., 1967.

Sakakura, A.Y.; Lindberg, C.; and Faul, H., Equation of Continuity in Geolopy with Application to the Transport of Radioactive Gas, USGS Bulletin 1052-1, 1959.

Sass, J.H. and Lachenbruch, A.H., Thermal Conductivity of Rocks fron Measurements on Fragments and Its Application to Heat-Flow Determinations, J. Geoph. Res. 76:339, 1971.

Scott, R.C., The Question of Radon-222 and Lead-210 Environmental Pollution from Development of Geothermal Resources, USEPA, presented at Geothermal Resources Research Conference, Batelle Seattle Research Center, Sept. 1972.

Shutler, N.D., Numerical Three-phase Simulation of the Linear Steamflood Process, Trans. AIME 246:232-246, 1969.

Shutler, N.D., Numerical Three-phase Model of the Two-Dimensional Steamflood Process, Trans. AIME 249, 1970.

Smith, G.D., Numerical Solution of Partial Differential Equations, Oxford University Press, 1965.

Strobel, C.J., Model Studies of Geothermal Fluids Production from Consolidated Porous Media, Engineers Thesis, Stanford University, July 1973.

Tanner, A.B., Physical and Chemical Controls on Distribution of Radium-226 and Radon-222 in Groundwater near Great Salt Lake, Utah, in Adams, J.A. S. and Lowder, W.M., eds., The Natural Radiation Environment, University of Chicago Press!, 1964.

Tokarev, A.N. and Shcherbakov, A.V., Radiohydrogeology, translated from the Russian as AEC-tr-4100, 1960.

Walsh, J.B., Effect of Pressure and Saturating Fluid on the Thermal Conductivity of Compact Rock, J. Geoph. Res. 71:3053, 1966.

Weinbrandt, R.M., The Effect of Temperature on Relative Permeability, Ph.D. Dissertation, Stanford University, May 1972.

Weinbrandt, R.M.; Ramey, H.J., Jr.; and Casse, F., The Effect of Temperature of Relative Permeability of Consolidated Rocks (SPE 4505), presented at the 47th Annual SPE Fall Meeting, San Antonio, Texas, Oct. 8-11, 1973.

White, D.E.; Muffler, P.; Truesdell, A.; and Donaldson, I., Personal Communication.

Whiting, R.L. and Ramey, H.J., Jr., Application of Material and Energy Balances to Geothermal Steam Production, J. Pet. Tech., 893-900, May 1969.

Wollenberg, H.A., Radioactivity of Nevada Hot-Spring Systems, Lawrence Berkeley Laboratory (LBL-2482), Jan. 1974.

Woodside, W. and Messmer, J.H., Thermal Conductivity of Porous Media, 11. Consolidated Rocks, J. Appl. Phys. 32, No. 2:1699, 1961.

ACKNOWLEDGEMENT

This work was supported by the National Science Foundation. In keeping with the objectives of the RANN program, communications were maintained with many academic, industrial, and government agencies. Acknowledgement is made for the advice and cooperation given us by these several agencies.

APPENDIX A

EFFECTIVE THERMAL CONDUCTIVITY OF FRACTURED ROCK

1. Series Model:

$$- \frac{k_s k_f}{\phi k_f + (1-\phi)k_s}$$

where: $k_{eff.}$ = effective thermal conductivity of porous solid
k_s = thermal conductivity of solid
k_f = thermal conductivity of fluid
ϕ = porosity (fractional)

2. Parallel Model:

$$k_{eff.} = \phi k_f + (1-\phi)k_s$$

3. Geometric Mean Model:

$$k_{eff.} = (k_f)^{\phi}(k_s)^{1-\phi}$$

4. Combination of Series and Parallel Model:

$$k_{eff.} - \frac{ak_s k_f}{k_s(1-d) + dk_f} + bk_s + ck_f$$

where: $ad + b = (1-\phi)$

$$b = \frac{k_{vac}}{k_s}$$

$$c = \frac{k}{k_f}$$

k_{vac} = thermal conductivity of unit volume of porous solid if the thermal conductivity of pore space is zero

k = thermal conductivity of: unit volume of porous solid if the thermal conductivity of the solid is zero

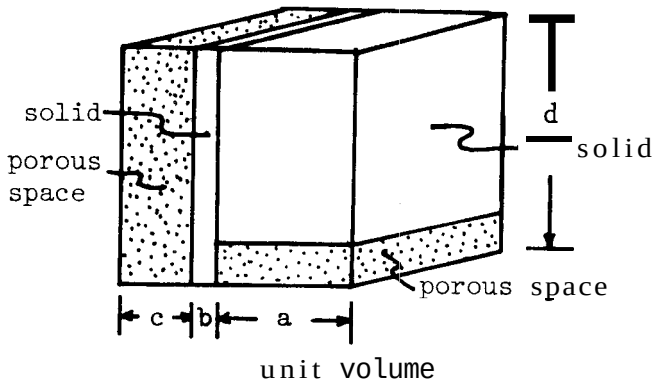

5. Electric Analog:

(Random distribution of cracks)

$$\frac{k_s - k_{eff.}}{k_{eff.} - k_f} = R\left(\frac{\phi}{3(\frac{k_f}{k_s})}\right)$$

where: R = function of crack density and the ratio of crack length to crack width

APPENDIX B

MATHEMATICAL FORMULATION OF LINEAR TWO-PHASE BOILING SINGLE-COMPONENT FLOW IN A DIPPING, POROUS MEDIUM

We apply the basic principles of mass and energy conservation to an elemental volume of uniform cross-sectional area, A, and length, δx. The system is defined to include both the fluids and rock matrix.

Conservation of Mass

$$\text{Mass' Out} - \text{Mass' In} + \text{Storage} = 0 \qquad \text{(B-1)}$$

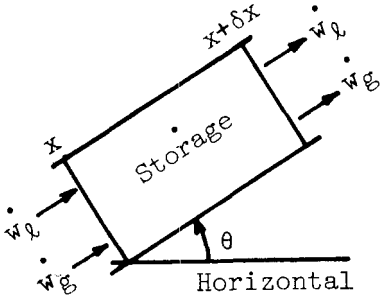

where: w = mass flowrate

θ = angle of inclination from horizontal

subscript: ℓ = liquid

g = gas

$$(\dot{w}_\ell + \dot{w}_g)_{x+\delta x} - (\dot{w}_\ell + \dot{w}_g)_x + \frac{\partial}{\partial t}(\text{Total Mass in Volume}) = 0 \qquad \text{(B-2)}$$

Assuming that the total mass of rock in the elemental volume does not change, we have:

$$\frac{\partial}{\partial t}(\text{Total Mass in Volume}) = \frac{\partial}{\partial t}\left[A\phi\delta x(\rho_\ell S_L + (1-S_L)\rho_{st})\right] \qquad \text{(B-3)}$$

where: ϕ = fractional porosity of the medium

S_L = fractional liquid saturation in the pore space

$(1-S_L) = S_g$ = the fractional steam saturation in the pore space

ρ_ℓ = the density of' the liquid

ρ_g = the density of' the steam

Taking the limit as δx goes to zero, the mass balance in differential form becomes:

$$\frac{\partial}{\partial x}\left(\dot{w}_\ell + \dot{w}_g\right) + \frac{\partial}{\partial t}\left(A\phi(\rho_g + S_L(\rho_\ell - \rho_g)\right) = 0, 0<x<L,\ t>0 \qquad \text{(B-4)}$$

Conservation of Energy

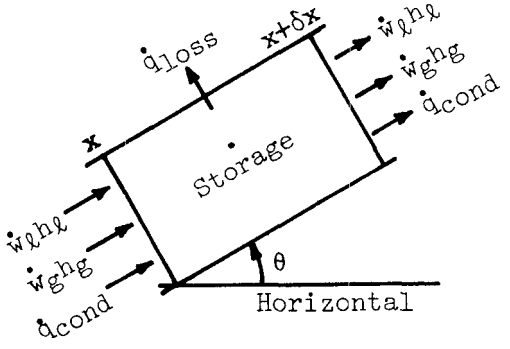

Neglecting energy changes in the system due to kinetic energy and gravitational potential effects:

$$\dot{\text{Energy}}\ \text{Out} - \dot{\text{Energy}}\ \text{In} + \frac{\partial}{\partial t}[\text{Energy Storage}] = 0 \qquad \text{(B-5)}$$

$$[\dot{w}_\ell h_e + \dot{w}_g h_g + \dot{q}_{cond}]_{x+\delta x} + \text{'losses}$$

$$- [\dot{w}_\ell h_e + \dot{w}_g h_g + q_{cond}]_x + \frac{\partial}{\partial t}[\text{Energy Storge}] = 0 \qquad \text{(B-6)}$$

where: h = specific enthalpy

q_{cond} = the heat conduction rate in the direction of flow

'losses = the heat loss rate out the side of the volume

Considering the energy storage in the system to be the total enthalpy of rock and fluids as measured above some datum temperature T_o, and taking the limit as δx goes to zero, the energy balance in differential form becomes :

$$\frac{\partial}{\partial x}[\dot{w}_\ell h_\ell + \dot{w}_g h_g + \dot{q}_{cond}] + \frac{\partial}{\partial t}[A(1-\phi)\rho_r h_r + A\phi(\rho_\ell h_\ell S_L + (1-S_L)\rho_g h_g)]$$

$$+ \dot{q}'_{losses} = 0;\ 0<x<L;\ t>0 \qquad \text{(B-7)}$$

where: q'_{loss} = the heat loss per unit length

Rate Equations

Fluid flow: We hypothesize that Darcy's law for isothermal dipping fluid flow can be generalized to nonisothermal flow:

$$\vec{v}_i = - \frac{K_i(P,T,S_L)}{\mu_i} \frac{\partial}{\partial x}\left(P_i + \rho_i \frac{g}{g_c} z\right) \qquad \text{(B-8)}$$

where: $K_i(P,T,S_L)$ = the effective permeability to phase i, and is in general a :function of pressure, P, temperature, T, and volumetric liquid saturation, S_L

μ_i = the viscosity of phase i

$(\frac{g}{g_c})$ converts from mass units to force units

z = distance above some datum

For a constant angle of slope: $\frac{dz}{dx} = \sin\theta$. If there are no capillary pressure forces, then the local pressures of each phase are the same. Thus, the rate equations for the two phases become:

$$\dot{w}_\ell = \vec{v}_\ell A\rho_\ell = - \frac{K_\ell A}{\mu_\ell}\left(\frac{dp}{dx} + \rho_\ell \frac{g}{g_c}\sin\theta\right)\rho_\ell \qquad \text{(B-9)}$$

$$\dot{w}_g = \vec{v}_g A\rho_g = - \frac{K_g A}{\mu_g}\left(\frac{dp}{dx} + \rho_g \frac{g}{g_c}\sin\theta\right)\rho_g \qquad \text{(B-10)}$$

Heat Conduction: Applying Fourier's Law::

$$q_{cond} = -\kappa A \frac{\partial T}{\partial x} \qquad \text{(B-11)}$$

where κ = the effective thermal conductivity of the composite medium, and in general is a function of temperature, T, volumetric liquid saturation, S_L, and also the mass flowrates through the system

Heat Losses out the Side:

$$\dot{q}'_{loss} = \frac{UA}{\partial x}(T_{local} - T_{\infty}) \qquad \text{(B-12)}$$

where: U = the overall heat transfer coefficient between the fluid-core system and the surrounding environment

T = the local temperature of the core, and is a function of location x, and time, t

T_{∞} = the temperature of the environment surrounding the core

Statement of Local Thermodynamic Equilibrium and Resulting Equations of State

The assumption is made that locally the fluids and rock are all at the same temperature. Thus, it is necessary to specify only one temperature as a function of distance, x, along the system. As a result of this assumption, the presence of two fluid phases implies that their properties are thermodynamically specified as being at saturation conditions. Hence, for flat surface interfaces, temperature, T, density, ρ, enthalpy, h, and viscosity, μ, are all single-valued functions of pressure, p, only. These functional relationships are given in standard handbooks on the thermodynamic properties of steam and water (see, e.g., Meyer et al.).

In the more general case, where low liquid saturations in the pore volume causes surface effects to become important, it may be necessary to specify temperature in particular as a function of both pressure and saturation: $T(P,S_L)$. However, this is not being done at the present time.

As a result of specifying saturation conditions when two phases are locally present, the Clausius-Clapeyron equation can be used to convert temperature gradients, $\left.\frac{dT}{dx}\right|_{saturated}$, into pressure gradients, $\left.\frac{dp}{dx}\right|_{saturated}$.

$$\left.\frac{dT}{dx}\right|_{saturated} = \left.\frac{dT}{dp}\right|_{saturated} \left.\frac{dp}{dx}\right|_{saturated}$$

$$= \left(\frac{T_{absolute}\, v_{fg}}{h_{fg}}\right) \left.\frac{dp}{dx}\right|_{saturated} \qquad \text{(B-13)}$$

where: $T_{absolute}$ = absolute temperature

v_{fg} = change in specific volume as the liquid evaporates to the vapor state

h_{fg} = change in specific enthalpy as the liquid evaporates.

Resulting Flow Equations for Two-Phase Saturated Flow

Applying the preceding to the mass balance expression:

$$\frac{\partial}{\partial x}\left[\left(\frac{K_\ell(P,S_L)\rho_\ell(p)}{\mu_\ell(P)} + \frac{K_g(P,S_L)\rho_g(p)}{\mu_g(P)}\right)\frac{\partial p}{\partial x} + \frac{g}{g_c}\sin\theta\left(\frac{K_\ell(P,S_L)\rho_\ell(p)^2}{\mu_\ell(p)} + \frac{K_g(P,S_L)\rho_g(p)^2}{\mu_g(p)}\right)\right]$$

$$= \frac{\partial}{at}\left[\phi\left(\rho_g(P)+S_L\left(\rho_\ell(P)-\rho_g(p)\right)\right)\right] \quad 0<x<L, t>0, P>0, 0<x<1 \qquad \text{(B-14)}$$

This can be expressed as:

$$\frac{\partial}{\partial x}\left[\left(K_\ell(P,S_L)\alpha_1 + K_g(P,S_L)\alpha_2\right)\frac{\partial p}{\partial x} + \frac{g}{g_c}\sin\theta\left(K_\ell(P,S_L)\alpha_3 + K_g(P,S_L)\alpha_4\right)\right]$$

$$= \frac{\partial}{\partial t}\left[\phi\left(\alpha_5 + S_L\alpha_6\right)\right] \qquad \text{(B-15)}$$

where the a_i are functions of pressure only and are defined in Appendix C. (B-15) can be made more compact:

$$\frac{\partial}{\partial x}\left(\gamma_1(P,S_L)\frac{\partial p}{\partial x} + \gamma_2(P,S_L)\right) = \frac{\partial \gamma_3}{\partial t} \qquad \text{(B-16)}$$

Similarly, the energy balance becomes:

$$\frac{\partial}{\partial x}\left[\left(\frac{K_\ell \rho_\ell h_\ell}{\mu_\ell} + \frac{K_{gt}\rho_g h_g}{\mu_g} + \frac{\kappa\, T_{absolute}\, v_{fg}}{h_{fg}}\right)\frac{\partial p}{\partial x}\right.$$

$$\left. + \frac{g}{g_c}\sin\theta\left(\frac{K_\ell h_\ell \rho_\ell^2}{\mu_\ell} + \frac{K_g h_g \rho_g^2}{\mu_g}\right)\right]$$

$$= \frac{\partial}{\partial t}\left[(1-\phi)\rho_r c_p (T-T_o) + \phi\left(\rho_g h_g + S_L(\rho_\ell h_\ell - \rho_g h_g)\right)\right]$$

$$+ \dot{q}'''_{losses};\ 0<x<L;\ t>0;\ p>0;\ 0<S_L<1 \qquad \text{(B-17)}$$

where c_P = specific heat of the rock matrix

ρ_r = density of the rock matrix

T_o = datum temperature

$\dot{q}'''$ = heat loss per unit foot of length per unit of exposed surface area.

This can he expressed as:

$$\frac{\partial}{\partial x}\left[\left(K_\ell \beta_1 + K_g \beta_2 + \kappa\beta_7\right)\frac{\partial p}{\partial x} + \frac{g}{g_c}\sin\theta\left(K_\ell \beta_3 + K_g \beta_4\right)\right]$$

$$= \frac{\partial}{\partial t}\left[(1-\phi)\rho_r c_p (T-T_o) + \phi\left(\beta_5 + S_L \beta_6\right)\right] + \dot{q}'''_{losses} \qquad \text{(B-18)}$$

where the β_i are functions of pressure only and are defined in Appendix C.

This equation can be made even more compact:

$$\frac{\partial}{\partial x}\left(\gamma_4(P,S_L)\frac{\partial p}{\partial x} + \gamma_5(P,S_L)\right) = \frac{\partial \gamma_6}{\partial t} + \dot{q}'''_{losses} \qquad \text{(B-19)}$$

APPENDIX C

NUMERICAL EVALUATION AND COMPARISON OF NONLINEAR COEFFICIENTS IN THE FLOW EQUATIONS

For purposes of understanding the behavior and structure of the governing flow equations, it is useful to examine the nonlinear coefficients in them. This can lead to valuable physical insight into the flow problem, which in turn is useful for finding a solution of the problem. This appendix examines the nonlinear coefficients and their contribution to physical interpretation of the flow equations.

Dimensional Considerations

A definition of the nonlinear coefficients and standard units used for them is given below.

Dependent Variables:

p = pressure, psia

S_L = volumetric liquid saturation, $\frac{\text{volume liquid in pore space}}{\text{volume pore space}}$

Independent Variables:

x = distance, ft

t = time, sec

Specified Functional Relationships:

k_ℓ, k_g = effective permeability to the phase, Darcy (note that elsewhere in this report, permeability is represented as upper case K)

$$\alpha_1 \triangleq \rho_\ell/\mu_\ell, \ \frac{lb_m}{ft^3 cp}$$

$$\alpha_2 \triangleq \rho_g/\mu_g, \ \frac{lb_m}{ft^3 cp}$$

$$\alpha_3 \triangleq \rho_\ell^2/\mu_\ell, \ \frac{lb_m^2}{ft^6 cp}$$

$$\alpha_4 \triangleq \rho_g^2/\mu_g, \quad \frac{lb_m^2}{ft^6 cp}$$

$$\alpha_5 \triangleq \rho_g, \quad \frac{lb_m}{ft^3}$$

$$\alpha_6 \triangleq \rho_\ell - \rho_g, \quad \frac{lb_m}{ft^3}$$

$$\beta_1 \triangleq \frac{\rho_\ell h_\ell}{\mu_\ell}, \quad \frac{Btu}{ft^3 cp}$$

$$\beta_2 \triangleq \frac{\rho_g h_g}{\mu_g}, \quad \frac{Btu}{ft^3 cp}$$

$$\beta_3 \triangleq \frac{\rho_\ell^2 h_\ell}{\mu_\ell}, \quad \frac{Btu\ lb_m}{ft^6 cp}$$

$$\beta_4 \triangleq \frac{\rho_g^2 h_g}{\mu_g}, \quad \frac{Btu\ lb_m}{ft^6 cp}$$

$$\beta_5 \triangleq \rho_g h_g, \quad \frac{Btu}{ft^3}$$

$$\beta_6 \triangleq \rho_\ell h_\ell - \rho_g h_\ell, \quad \frac{Btu}{ft^3}$$

$$\beta_7 \equiv \frac{T_{abs}\, v_{fg}}{h_{fg}}, \quad \frac{{}^\circ R\ ft^3}{Btu}$$

where: ρ = density

μ = viscosity

h = specific enthalpy

T_{abs} = absolute temperature

v = specific volume

T = temperature, °F

subscripts: ℓ = liquid phase

g = gas phase

fg = change in going from liquid to gas

o = base value

constants: $\left(\frac{g}{g_c}\right) = \frac{lb_f}{lb_m}$

ϕ = fractional porosity, $\frac{\text{volume pore space}}{\text{bulk volume of medium}}$

κ = effective thermal conductivity, $\frac{Btu}{hr\ ft\ ^\circ F}$

$(C_{pr}\rho_r)$ = specific heat content of matrix rock on a volume basis, $\frac{Btu}{ft^3\ ^\circ F}$

Nonlinear Coefficient

$q'''_{loss}(x,t)$ = local heat loss rate from sides of core on a unit volume basis, = $\frac{h\{T(x,t) - T_\infty\}}{L}$ in $\frac{Btu}{hr\ ft^3}$

h = convective heat loss coefficient, $\frac{Btu}{hr\ ft^2\ ^\circ F}$

In order to make the units given above dimensionally consistent in the governing flow equations, it is necessary to .makethe following conversions:

a) Convert permeability, k(darcies) to (cp ft2/sec psia) by multiplying by (1/1.3656 x 10^4);

b) Convert thermal conductivity, $\kappa\left(\frac{Btu}{hr\ ft\ ^\circ R}\right)$ to $\left(\frac{Btu}{ft^4\ ^\circ R\ sec\ psia}\right)$ by multiplying by $\left(\frac{1}{1.9454 \times 10^4}\right)$;

c) Convert effective convective heat transfer coefficient for heat losses to the surrounding medium, h $\left(\frac{Btu}{hr\ ft^2\ ^\circ R}\right)$ to $\left(\frac{Btu}{sec\ ft^2\ ^\circ R}\right)$ by multiplying by $\frac{1}{3600}$;

d) Convert α_3 and α_4, $\left(\frac{lb_m^2}{ft^6 cp}\right)$ to $\left[\frac{lb_m^2}{ft^4\ in^2 cp}\right]$ by multiplying by $\left(\frac{1}{144}\right)$;

e) Convert β_3 and β_4, $\left(\frac{\text{Btu lb}_m}{\text{ft}^6\text{cp}}\right)$ to $\left[\frac{\text{Btu lb}_m}{\text{ft in}^2\text{cp}}\right]$ by multiplying by $\left(\frac{1}{144}\right)$.

Components ~~of the~~ Nonlinear Coefficients

It is convenient to express the two governing flow equations:

$$\frac{\partial}{\partial x}\left(\gamma_1 \frac{\partial p}{\partial x} + \gamma_2\right) = \frac{\partial \gamma_3}{\partial t} \qquad \text{(C-1)}$$

$$\frac{\partial}{\partial x}\left(\gamma_4 \frac{\partial p}{\partial x} + \gamma_5\right) = \frac{\partial \gamma_6}{\partial t} + \dot{q}'''_{loss} \qquad \text{(C-2)}$$

where the $\gamma_{i,i=1,6}$ are defined below. We also wish to evaluate the a_i and β_i as a function of pressure. This was done at pressures of 100 and 1000 psia, and the results are expressed below in Table C-1 in units consistent;with the rest,of the equation.

Table C-1

Values of a_i and β_i at p = 100 and 1000 psia

(These values are dimensionally consistent with the governing equations)

Function	p = 100	p = 1000	Function	p = 100	p = 1000
α_1	344	492	β_1	1×10^5	3×10^5
α_2	16	120	β_2	2×10^4	1.5×10^5
α_3	140	160	β_3	4×10^5	9×10^4
α_4	.02	1.8	β_4	29.2	2180
α_5	.23	2.2	β_5	268	2675
α_6	56.2	44.1	β_6	1.6×10^4	2.2×10^4
			β_7	3.9	0.6

In the discussion below it should be remembered that permeability

to each phase may range from zero to k_{max} [darcies]/(1.36 x 104), where the resulting numerical value is dimensionally consistent with the equations.

For $\gamma_1 \triangleq k_\ell \alpha_1 + k_g a_2$, we see that the contribution to mass flow of the gas is small, but not negligible unless effective gas permeability is much smaller than effective liquid permeability.

For $a_2 \triangleq \left(k_\ell \alpha_3 + k_g \alpha_4\right)\frac{g}{g_c}\sin\theta$, we see that unless the effective permeability to gas is much greater than that to liquid, then liquid characteristics dominate the dipping flow term. However, at low liquid saturations when the system begins to dry up locally, we do find extremely large effective k_g/k_ℓ ratios. Thus, as a dry zone begins to form, the gas characteristics will dominate the gravity segregation behavior.

For $\gamma_3 \triangleq \phi(\alpha_5 + S_L \alpha_6)$ we see that a_5 is smaller than α_6, but not necessarily negligible compared to it. In addition, a_5 has a much stronger dependence on pressure. Thus, although most of the mass storage in the pore volume is in the liquid phase (except at low liquid saturations), the mass present as gas should probably be considered.

The term $\gamma_4 \triangleq k_\ell \beta_1 + k_g \beta_2 + \kappa\beta_7$ indicates, energy transfer. We first wish to examine the contribution to the term given by $\kappa\beta_7$ (energy transfer by conduction). Considering a relatively large effective thermal conductivity for rock of 10 Btu/hr ft °F, and using the larger value of $\beta_7(p)$, we find a dimensionally consistent value of $\kappa\beta_7 = 2.5 \times 10^{-3}$. For a tight porous medium of low maximum permeability 10^{-3} darcy (1 millidarcy), we find that the term $k_\ell \beta_1$ (p = 1000 psia) has a dimensionally consistent value of 2×10^{-2}:

$$\kappa\beta_7 \simeq \left(\frac{10}{2 \times 10^4}\ \frac{\text{Btu}}{\text{ft}^4\,^\circ\text{R sec psia}}\right) \times \left(4\ \frac{^\circ\text{R ft}^3}{\text{Btu}}\right) = 2 \times 10^{-3}\ \frac{\text{Btu}}{\text{ft sec psia}}$$

$$k_\ell \beta_1 \simeq \left(\frac{10^{-3}}{1.5 \times 10^4}\ \frac{\text{cp ft}^2}{\text{sec psia}^2}\right) \times \left(3 \times 10^5\ \frac{\text{Btu}}{\text{ft}^3\,\text{cp}}\right) = 2 \times 10^{-2}\ \frac{\text{Btu}}{\text{ft sec psia}}$$

Thus, under adverse physical conditions, it can be seen that thermal conduction does contribute significantly to energy transfer in the system. For more permeable systems of 0.1 darcy or 1 darcy the conduction contribution would be smaller. Since β_1 and β_2 are of roughly the same order of magnitude, their contribution to γ_4 will depend on the relative values of k_ℓ and k_g, which of course depend on the liquid saturation, S_L.

The term $\gamma_5 \triangleq k_\ell\beta_3 + k_g\beta_4$ indicates tne contribution to vertical segregation in the energy balance. Since β_3 is somewhat larger than β_4, the $k_\ell\beta_3$ term will dominate the γ_5 value unless $k_\ell << k_g$ at lower liquid saturations.

Finally, the term $\gamma_6 \triangleq (1-\phi)(C_{pr}\rho_r)(T-T_0) + \phi(\beta_5 + S_L\beta_6)$. This term gives the energy stored in the composite rock and fluid system. It is not immediately possible to compare rock and fluid contributions to the value of γ_6, because such a comparison is sensitive to the choice of datum temperature T_0. However, we are really interested in the contribution to $d\gamma_6$ caused by a change in the temperature (or pressure) of the system. If the contributions to $\frac{d\gamma_6}{dT}$ or $\frac{d\gamma_6}{dp}$ from the rock and fluids are examined at various values of pressure and for realistic physical parameters, it will be seen that much of the heat comes from the rock. However, the heat from both fluid phases does contribute enough to need consideration. Only at extreme values of liquid saturation can the contribution from one of the two fluid phases be neglected.